SPECKLE INTERFEROMETRY USING A HARDWIRED AUTOCORRELATOR

By

Jeremy Charles Hebden, B.Sc.

May 1984

A thesis submitted for the degree of Doctor of Philosophy of the University of London and for the Diploma of Membership of the Imperial College of Science and Technology.

Astronomy Group,
Blackett Laboratory,
Imperial College,
London SW7 2BZ.

I wish to dedicate this thesis to my parents,
who deserve it, and to Tottenham Hotspur
Football Club, who too often don't.

Acknowledgements

I wish to extend my thanks to my supervisor, Dr Brian L. Morgan, and to Mr Harry Vine for their generous help and guidance. Sincere thanks also to numerous other members of the group both past and present who have helped to make life so interesting and enjoyable during the course of this research.

I am very grateful to the Science and Engineering Research Council for the provision of an SERC Research Studentship.

Finally I would like to thank Dr Tony Cañas for his advice and assistance in the formatting and printing of this thesis.

This thesis was produced using the Format-80 word processor.

Abstract

Stellar speckle interferometry is a technique which enables diffraction limited information to be obtained from large telescopes despite the presence of atmospheric turbulence which normally limits resolution to about one arcsecond or worse. The information is retained in quasi-instantaneous images whose exposure times are short in comparison with the lifetime of the atmospheric perturbations on the wavefront of light from a star. Such images have a speckled appearance.

This thesis describes research concerning real-time digital analysis of speckle images using a hardwired autocorrelator. A device called a speckle interferometer was built which is designed to produce high magnification bandwidth limited images of low light level stellar objects using large telescopes. The images are focussed from the output phosphor of a four stage image intensifier onto the tube of a television camera. They are then recorded onto video tape and may be processed in real-time at a rate of twenty five frames per second. The hardwired autocorrelator produces a two-dimensional spatial autocorrelation which is stored in an 8K by 20 bit integrating memory.

A microcomputer based data reduction system has been developed which enables data to be displayed in numerous forms and stored on magnetic disc. In addition several calculations such as azimuthal averaging may be performed. A system of data analysis has also been developed which involves the calculation of computer generated models.

System development has been complemented by a very active programme of observations. Recent published work includes the results obtained from observations of the Seyfert nucleus of NGC 1068, the extremely compact object R136a, the bright and variable star Eta Carinae and the binary star in the centre of the Red Rectangle nebula. Additionally results of binary star observations as part of the Hipparcos project have been published and a number of asteroid observations have been made.

Speckle Interferometry Using A Hardwired Autocorrelator

Contents

Chapter Four : Data Reduction Procedure

Chapter Five : Data Analysis

Chapter Six : Astronomical Results

Chapter Seven : Conclusions And Future Work

List of Figures

Chapter One

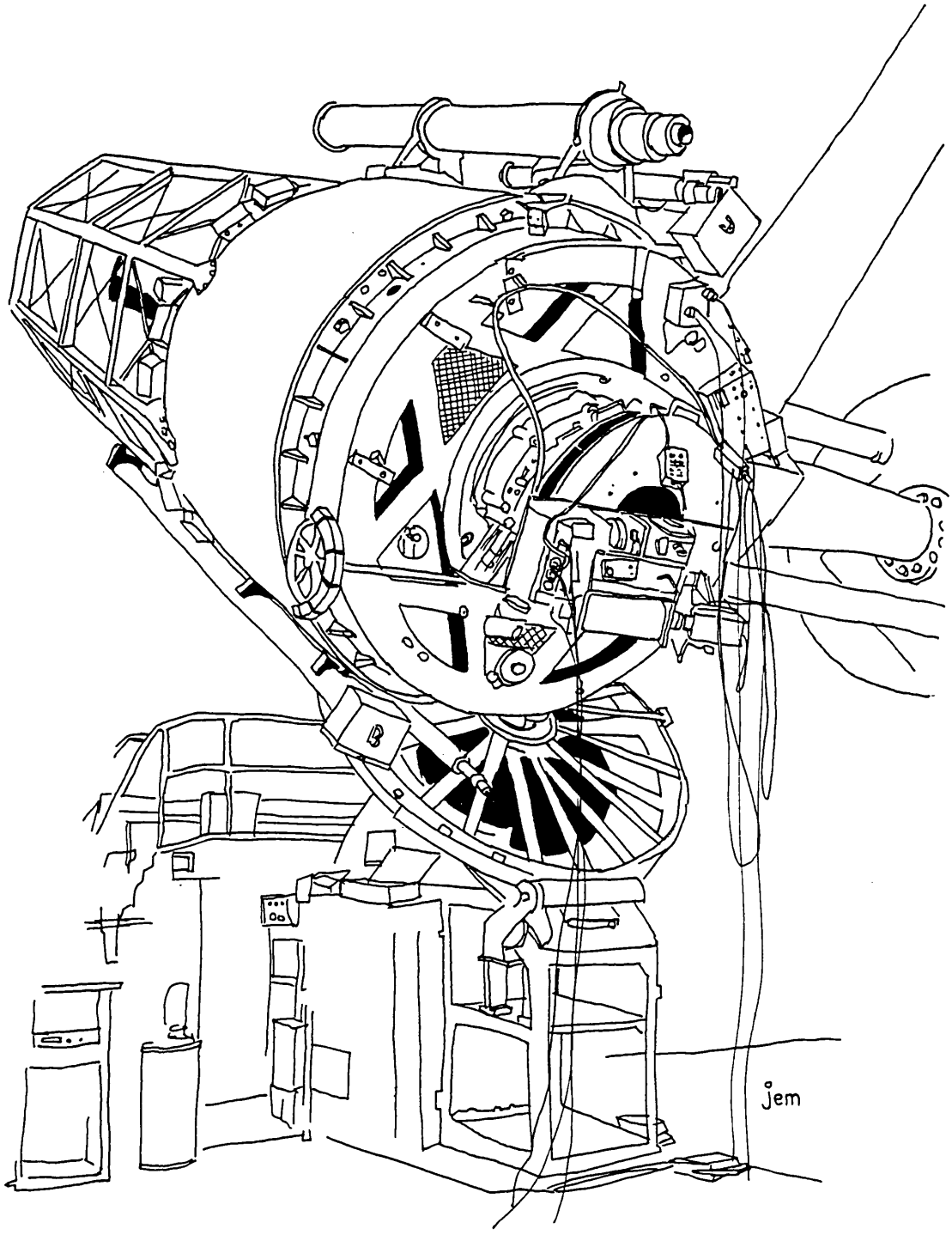

Chapter One : Introduction

1-1 High resolution optical astronomy

The angular resolution of large telescopes at visible wavelengths is drastically reduced by the effects of atmospheric turbulence. The image of a star, usually called the seeing disc, has an angular diameter which varies approximately from 0.5 arcseconds, during periods of good seeing, to 10 arcseconds or more, depending on the atmospheric conditions. A seeing disc diameter of one arcsecond is equivalent to the resolution limit at visible wavelengths of a telescope with an aperture of 12cm in diameter. Hence even at the time of Newton and Herschel telescopes were being built whose resolution was limited by the atmosphere rather than by telescope optics.

The desire to overcome the atmospheric degradation of stellar images has resulted in the introduction of the Space Telescope, a 2.4m aperture instrument which is due to be placed in orbit around the Earth in 1986. However, a few enterprising physicists have succeeded in developing techniques which can, to some degree, avoid the damaging effects of atmospheric turbulence on ground based observations. The idea of using optical interferometry to determine the structure of stellar objects was first suggested by Fizeau [66] in 1868. Several years later this suggestion was brilliantly applied by Michelson [67], resulting in the development of a single telescope synthetic aperture system. In 1921 this was developed still further by Michelson and Pease [80] into the long baseline interferometer (see section 1-3). A twenty foot baseline interferometer, mounted on the 100-inch telescope at Mount Wilson, enabled Michelson and Pease to determine the angular diameter of Betelgeuse. During the following ten years Pease [73] reported measurements of several other bright red giants and supergiants whose angular diameters lay in the range from 0.02 to 0.05 arcseconds. However, as mentioned by Hanbury Brown [84], a critical assessment of the accuracy of the results was never published. Nevertheless, these were the first ever measurements of stellar angular diameters. A fifty foot baseline instrument was also constructed but due to practical difficulties it never yielded reliable results.

Few further advancements were made in optical high resolution techniques until Hanbury Brown and Twiss [68] proposed the intensity interferometry method in 1958. Despite the inherent low sensitivity of the method, it enabled the angular diameters of the 32 brightest southern stars to be measured remarkably accurately. A resolution of the order of one milli-arcsecond was obtained [69].

The greatest breakthrough so far came in 1970 when Labeyrie [1] invented the technique of stellar speckle interferometry. Labeyrie suggested that diffraction limited information is contained within short exposure images. Such images have a speckled appearance. Stellar speckle interferometry is the technique on which the research reported here is based. A review of the basic principles involved and a description of how they are implemented are given in chapter two.

The area of astronomy in which speckle interferometry made its first significant contribution is the measurement of binary star separations and position angles. Binary star observations enable accurate estimates of stellar masses and absolute distances to be made. If a given system is a double-lined spectroscopic binary (i.e. the radial velocities of both components are known), one measurement of its position angle and separation will yield both the masses of each component and the absolute distance. For a single-lined spectroscopic binary the masses and distances cannot be derived. However, if masses are assumed from the given spectral type of the stars, distances may be calculated. This method has been applied to the binaries in the Hyades cluster by Morgan et al. [52] and McAlister [70] using speckle interferometry. They found that the stars have a normal mass-luminosity relationship if the distance of the cluster is considered to be approximately 10 percent greater than previous techniques have indicated.

Before the introduction of speckle interferometry measurements of binary stars whose separations were less than the typical seeing disc diameter were made by conventional visual observation. Observers estimated the relative position of the two stars during brief (< second) intermittent periods of good seeing. The reported accuracy in such measurements of separations is typically between 0.1 and 0.01

arcseconds. Beddoes [14] describes the impact of the speckle technique on the field of binary star measurement.

As will be shown, speckle interferometry is not confined to observation of binary stars but may be used to obtain the angular diameters of objects whose sizes are less than that of the seeing disc. Measurements have been made of the diameters of nearby giant stars such as Betelgeuse [31],[9] and of asteroids [20]. Recent improvement in data reduction methods and instrumentation has enabled much fainter objects to be observed. Two of the most widely known results concern the triple quasar PG 1115+08, which was resolved by Hege et al. [50], and the Seyfert nucleus of the galaxy NGC 1068, observed in the visible by our group at Imperial College [71] and at 2.2 μm by McCarthy et al. [72] (see chapter six).

It has recently become apparent that speckle interferometric techniques enable useful information to be derived from almost all types of visible and near-infrared objects in the sky. Many of the recent observations made in association with this work have been of relatively faint (m_v >10) objects. Some of these objects, R136a and the nucleus of NGC 1068 for example, are known to be very distant, yet their brightness implies that they are extremely luminous; millions of times more so than the sun. Speckle observations have been able to establish whether such luminosity is due to a group of separate stars, a single compact (unresolved) object or possibly an extended source. The consequences of such observations are vital to the understanding of the nature of stars and galaxies at various stages of their evolution and thus of the origins of the universe itself.

The introduction of the Space Telescope will inevitably stimulate interest in high resolution optical astronomy. A simple universal method of yielding unambiguous reconstructed images from speckle observations has not yet been developed. Several techniques have been proposed and implemented (see section 2-7) though no particular method appears to offer an ideal solution. Should, as seems possible, ground based diffraction limited imaging become a reality for all classes of optical objects, the advantages of having large and expensive optical telescopes in orbit will be severely reduced.

1-2 Hardwired data processing

Speckle interferometry involves the processing of large numbers (sometimes tens of thousands) of individual short exposure stellar images. Following the initial results obtained using the technique, progress in the technology of sensors produced considerable gains in both the sensitivity of instruments and the accuracy of data reduction.

Naturally, one of the most important criteria involved in developing a system required to process vast amounts of data is speed. The work presented here concerns a method of processing data by performing two dimensional spatial autocorrelations of large numbers of stellar images contained on television frames. The facility to perform such calculations in real time, while not absolutely necessary, is undoubtedly extremely useful, particularly when requiring an initial confirmation of the suitability of the data.

All current real-time TV processing is performed using hardwired packages. Even large computer systems that offer real-time processing facilities make use of hardwired units which are controlled through software. Thus it was decided to construct a hardwired real-time autocorrelator, which became operational in late 1979. The design requirements and operation of the device are described in chapter three.

Current technological developments indicate that processing speeds will continue to increase over the next decade. This is due to higher levels of integration (i.e. more devices situated on a single chip) as well as improvements in circuit design. In the near future, however, the introduction of computers containing parallel processors will perhaps enable far greater processing speeds to be achieved using software.

1-3 Related techniques

The research described in the following chapters is concerned with the technique of stellar speckle interferometry as proposed by Labeyrie [1]. In addition to the earlier interferometric methods mentioned in section 1-1, several modified versions of speckle interferometry have

been proposed. Though these do not directly concern the work presented here, they indicate the extent to which the basic principles, described in chapter two, have been applied. Many of the physicists involved have not confined research to just one aspect of the technique.

Labeyrie has investigated the advantages of long baseline interferometry [74] at the Observatoire de Paris. The method enables very high resolution to be obtained from the coherent interference of light from separate apertures (i.e. separate telescopes). The configuration for the technique may be considered as two independent telescopes having a common coudé focus. A two-telescope interferometer has been built in southern France which consists of two 25cm telescopes with a separation variable up to 20m. Blazit et al. [76] have used this instrument to resolve the stellar discs of Capella A and B with an accuracy of about 0.002 arcseconds. However, because of the relatively small apertures involved, observations are limited to bright stars only.

Differential speckle interferometry, as proposed by Beckers [75], is a method of obtaining a resolution at visible wavelengths greater than the diffraction limit of the telescope. The technique uses variations in the spectrum across astronomical objects to obtain information on the object on the scale of milli-arcseconds. By using the Doppler shift associated with spectroscopic binary stars, the technique may enable sub-milli-arcsecond measurement of separations using 4m telescopes.

All current applications of speckle interferometry involve the processing of spatial, or angular, information contained in short exposure images (see chapter two). No use is made of the fact that photons detected within a given exposure arrive at separate times. Photons detected at the end of one exposure relate to the same intantaneous image distribution as those detected at the beginning of the following exposure. Space-time speckle interferometry, as discussed briefly by Dainty [2], includes the determination of correlations in the time domain as well as the spatial domain. Dainty concludes, however, that such a technique has few advantages to make its implementation worthwhile.

Since efficient two-dimensional array detectors operating in the

infrared are not yet readily available, near-infrared (2-5 μm) speckle interferometry is restricted to analysis in one dimension. At visible wavelengths, say 0.5 μm, the diffraction limit of a 4m telescope is about 0.03 arcseconds. At a wavelength of 5 μm, however, the diffraction limit is about 0.3 arcseconds. Since a seeing disc diameter of one arcsecond in the visible (assuming good seeing) corresponds to about a diameter of 0.64 arcseconds at 5 μm (see Dainty [2]), the gain in resolution at 5 μm is only about a factor of 2 compared with about a factor of 33 at visible wavelengths. Nevertheless, due to the great number of large (i.e. potentially resolvable) bright infrared objects in the sky the technique is very valuable. A review of the technique is given by Sibille et al. [77]. The method requires careful calibration of the effects of infrared emission from the sky background and the telescope itself. Notable results achieved with this technique include the measurement of the triple nature of MonR2-IRS3 by McCarthy [78] and the image reconstruction, via the Knox-Thompson algorithm (see section 2-7), of the very bright infrared source Eta Carinae by Chelli et al. [79].

Chapter Two

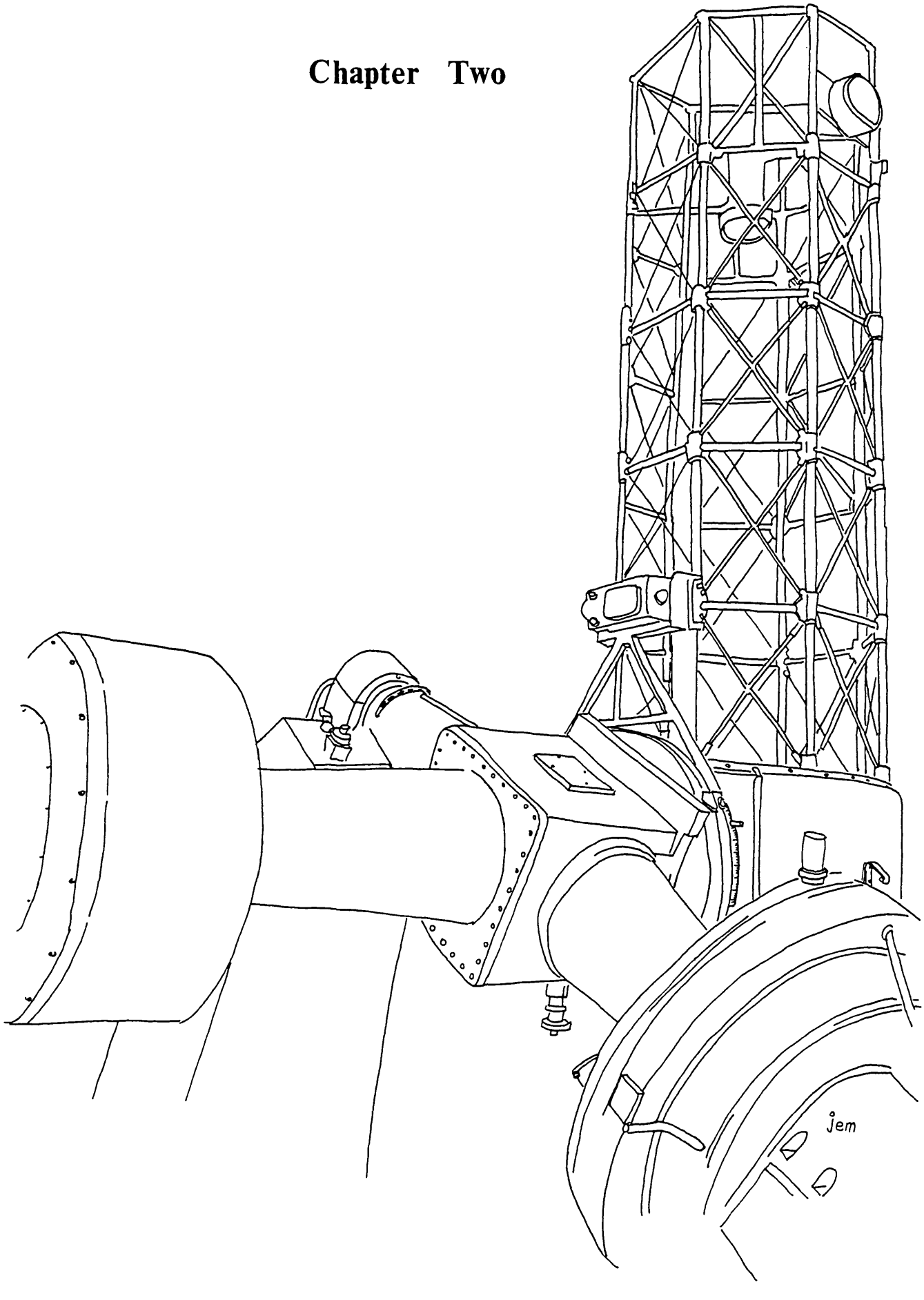

Chapter Two : Theoretical Review

2-1 Introduction

The diffraction limited resolution of a 4m telescope at a wavelength of 500nm is approximately 0.03 arcseconds. Atmospheric turbulence, however, normally limits the resolution to about one arcsecond or worse. Astronomers have known for some time that a short exposure stellar image of a few milliseconds in duration has a speckled appearance. In 1970 Labeyrie [1] showed that it should be possible to obtain diffraction limited information from the fine structure exhibited in such an image. Labeyrie proposed that information at spatial frequencies of up to that corresponding to the diffraction limit of the telescope aperture is retained in the power spectrum of a short exposure image. The technique by which this information may be obtained is known as stellar speckle interferometry. Reviews of the technique may be found in Dainty [2] and Worden [3].

Figure 2.1 shows a typical short exposure image of an unresolved star which is composed of a random pattern of speckles enclosed in the seeing disc. Extensive study of atmospheric turbulence, as reviewed by Labeyrie [4], has shown that disturbances in the optical path are produced by a variety of mechanisms. Refractive index variations in the Earth's atmosphere impose random phase and amplitude fluctuations on the wavefront of light from a star. The coherent addition of light from regions of the atmosphere over the whole aperture produce a single diffraction limited image, or speckle. Regions over which part of the wavefront can be considered uniform are known as "seeing cells" and they are typically about 10cm in diameter (see section 2-3). To obtain a well contrasted short exposure image the exposure time must be within the lifetime of the seeing cells. Thus the atmospheric turbulence can be considered as effectively "frozen". Roddier and Roddier [5] have investigated the effect of exposure time on the image power spectrum of a point source for different telescope apertures and various seeing conditions. Their results suggest that under typical observing conditions for a 2.5m telescope a 10ms exposure is sufficiently short to ensure little attenuation of higher spatial frequencies though the power spectrum is negligibly affected by exposure times of up to 20ms. Dainty

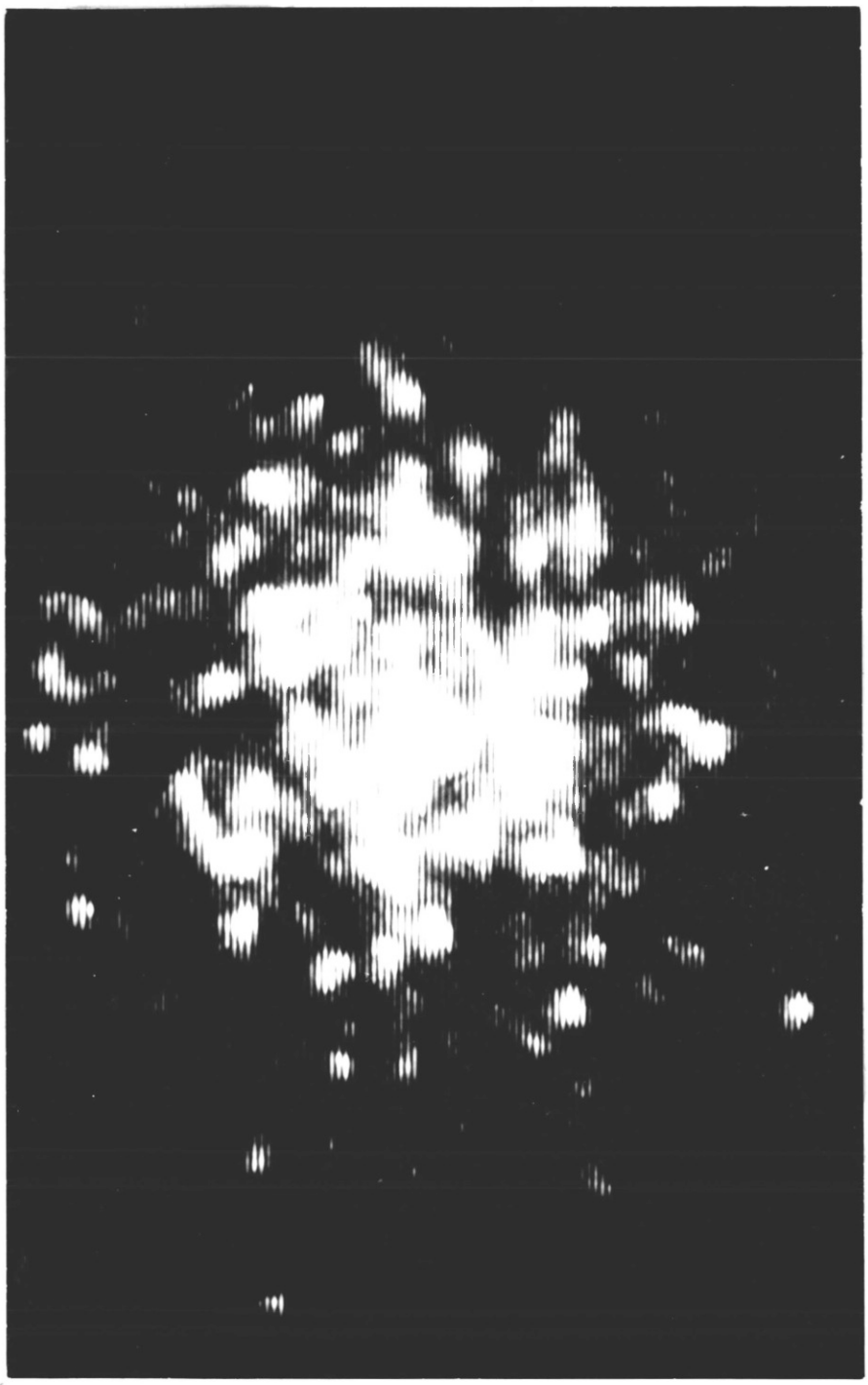

Figure 2.1 : A short exposure image of an unresolved star

(TV frame; exposure duration = 40ms)

[2] has noted that to maximise the signal-to-noise ratio of stellar speckle interferometry the exposure time should be as long as possible consistent with "freezing" the atmosphere.

Scaddan and Walker [6] have investigated the temporal coherence of speckle behaviour and have examined the effect of optical bandwidth and wavelength on speckle contrast. Their experiments suggest that exposure times should be no longer than 10ms and, while temporal coherence is not significantly dependent on bandwidth, high spatial frequency information becomes degraded with increasing wavelength. The necessary bandwidth ($\Delta\lambda$) required to avoid this has been discussed by Dainty [7] and Korff [8] and is given by

$$\Delta\lambda \leqslant w.<\lambda>/D \qquad (2.1)$$

where w = diameter of Airy disc,
$<\lambda>$ = mean wavelength,
and D = diameter of seeing disc.

In practice the technique of stellar speckle interferometry involves the statistical analysis of large numbers of quasi-instantaneous images obtained using large telescopes. The first successful results were obtained by Gezari et al. [9] in 1972 on the 5m Hale telescope at Mount Palomar. This initial attempt involved the recording of individual speckle images using a camera equipped with a motorized photographic film transport and shutter. Beddoes et al. [10] and Worden [3] have subsequently used cine film as a means by which a large number of images are recorded consecutively. Current work at Imperial College is primarily concerned with real-time digital analysis where speckle images are recorded on video tape (see chapter 3).

2-2 Theoretical outline

For an exposure short enough to be effectively instantaneous, the following quasi-monochromatic incoherent imaging equation can be applied ([11] p421):

$$I(x,y) = O(x,y) * P(x,y) \qquad (2.2)$$

where $I(x,y)$ = instantaneous image intensity,
$O(x,y)$ = object intensity,
$P(x,y)$ = instantaneous point spread function of the system,
and * is the symbol which denotes convolution.

Analysis of this data may be carried out in two equivalent ways. One method involves finding the Wiener or power spectrum of the image intensity. This is defined as the mean squared modulus of the Fourier transform in the spatial frequency domain ([11] p415) and may be written

$$W(u,v) = \langle |i(u,v)|^2 \rangle = |o(u,v)|^2 \langle |T(u,v)|^2 \rangle \qquad (2.3)$$

where $i(u,v)$ = Fourier transform of the image intensity,
$o(u,v)$ = Fourier transform of the object intensity,
and $T(u,v)$ = Fourier transform of $P(x,y)$ and is called the "instantaneous transfer function".

It can be shown (for a comprehensive description see Dainty [12]) that whereas in the long exposure case the resolution obtained is governed by the form of the average transfer function $\langle T(u,v) \rangle$, by taking the squared modulus and then averaging $\langle |T(u,v)|^2 \rangle$, the high frequency components can be retained.

A photographic record of a speckle pattern represents the instantaneous image intensity. The optical diffraction pattern produced from such a record is equivalent to the squared modulus of the Fourier transform of that image. If coherent light is passed through a series of short exposure images of a binary star a set of cosine fringes is produced, where separation and position angle of the binary system may be derived from the fringe separation and orientation respectively. The magnitude difference, too, may be deduced from the depth of modulation [9]. Thus diffraction limited information can be recovered via the diffraction pattern ($\equiv$ Fourier transform) of speckle images without having to remove the mean square transfer function. This is exactly the method employed by Morgan et al. [13] at Imperial College prior to present digital techniques. (see also Beddoes [14])

The second equivalent method involves the calculation of the ensemble average autocorrelation in the spatial domain. This may be written as follows :

$$C(x,y) = \langle I(x,y) \bigstar I(x,y) \rangle$$
$$= \langle [O(x,y) * P(x,y)] \bigstar [O(x,y) * P(x,y)] \rangle \qquad (2.4)$$

or equivalently

$$= [O(x,y) \bigstar O(x,y)] * [\langle P(x,y) \bigstar P(x,y) \rangle] \qquad (2.5)$$

where $\bigstar$ denotes space autocorrelation.

The two expressions 2.3 and 2.5 are related by the Wiener-Khintchine theorem ([11] p416), W(u,v) and C(x,y) being Fourier transform pairs. Whereas the power spectrum method is more conveniently applicable to coherent optical analysis, the spatial autocorrelation method is best exploited using digital techniques.

The basic principles involved in spatial autocorrelation and the reasons for its suitability to fast digital analysis of speckle images are discussed in sections 2-4 and 2-5.

2-3 Signal to noise ratio

Dainty [12] uses the spatial domain to derive an expression for the overall signal-to-noise ratio for speckle interferometric observations of binary stars which is written below :

$$Q = \langle N_{ph} \rangle . \sqrt{(N_p / 2 \langle N_s \rangle)} . f/(1+2f+f^2) \qquad (2.6)$$

where $\langle N_{ph} \rangle$ = average number of photons/image,
N_p = total number of images,
$\langle N_s \rangle$ = average number of speckle cells/image,
and f is related to the magnitude difference Δm by $f = (2.5)^{-\Delta m}$.

The average number of speckle cells (speckle "cells" since a speckle may contain zero photons) contained within a single instantaneous image is given by the expression:

$$\langle N_s \rangle = (D/r_o) \qquad (2.7)$$

where D = aperture of telescope,
and r_o = diameter of a "seeing cell".

The parameter r_o , as defined by Fried [54], is the "seeing cell" diameter which is equivalent to the diameter of a diffraction limited telescope having an Airy disc with the same angular subtense as the seeing disc. Equating λ/r_o to a typical seeing disc diameter of one arcsecond produces a value of r_o equal to about 10cm at a wavelength of 500nm. The number of speckle cells per quasi-instantaneous image with a 4m telescope is therefore about 1600.

Dainty [2] also derives an expression for the limiting magnitude for detection of an equal magnitude binary star:

$$m_v = 17.3 + 2.5\log(\Delta t.\Delta\lambda.QE) - 2.5\log(SNR)_M + 1.25\log M + 2.5\log D + 2.5\log r_o \qquad (2.8)$$

where Δt = exposure time of each image (seconds),
$\Delta\lambda$ = optical bandwidth of observation (nm),
QE = quantum efficiency of the detector,
M = total number of images,
$(SNR)_M$ = overall signal-to-noise ratio for M images,
D = aperture of telescope (m),
and r_o = diameter of a "seeing cell" (m).

Using this expression Dainty [2] suggests that binary stars of magnitude $m_v \simeq 17.6$ should be detectable using 10^5 images obtained from observations with a 4m telescope and using the parameters $\Delta t = 0.02$ seconds, $\Delta\lambda = 25$nm and a detector with a quantum efficiency of ten percent. In section 4-7 an estimate is made of the likely practical limiting magnitude of the Imperial College speckle system. Speckle observations of the triple quasar PG1115+08 (brightest component $m_v = 16.2$) by Hege et al. [50] resolved two components from 2×10^4 images using an effective bandwidth of 2000Å. This result was obtained using the central mirror of the Multiple Mirror Telescope, Arizona.

Beddoes [14] describes how in practice the magnitude limit appears

significantly reduced if the two components of a binary star have a large magnitude difference.

Walker [47] has investigated the accuracy with which the diameter of an object can be estimated by speckle interferometry assuming a known limb darkening profile. For a one percent error in the diameter whose value is 0.5 arcseconds, the limiting magnitude is calculated to be approximately $m_v=16$.

2-4 Autocorrelation

The two dimensional spatial autocorrelation of a function f(x,y) is represented mathematically by the expression

$$A(X,Y) = \iint_{-\infty}^{\infty} f(x,y)f^*(x-X,y-Y)dxdy \qquad (2.9)$$

where * denotes the complex conjugate of the function ([11] p416).

Spatial autocorrelation may be considered as a means of measuring the distance over which a function is coherent. For example, a two dimensional distribution which contains pairs of points whose relative separation and orientation occur frequently will produce an autocorrelation which contains a high signal at a point corresponding to that separation and orientation.

One way to visualise the process of spatial autocorrelation is to consider it as the product of the overlapping regions between a distribution and a displaced version of that distribution as a function of their relative displacement. This is illustrated in figure 2.2 for the one dimensional case where the distribution is a simple top-hat. The autocorrelation produced is triangular. For this and other examples see Hecht and Zajac ([11] p403).

Whereas this example could be considered as an analogue visualisation of autocorrelation, a second equivalent approach could be regarded as a digital description. Autocorrelation of a function described by any number of discrete equally weighted points may be defined as the distribution of vectors between each point and every

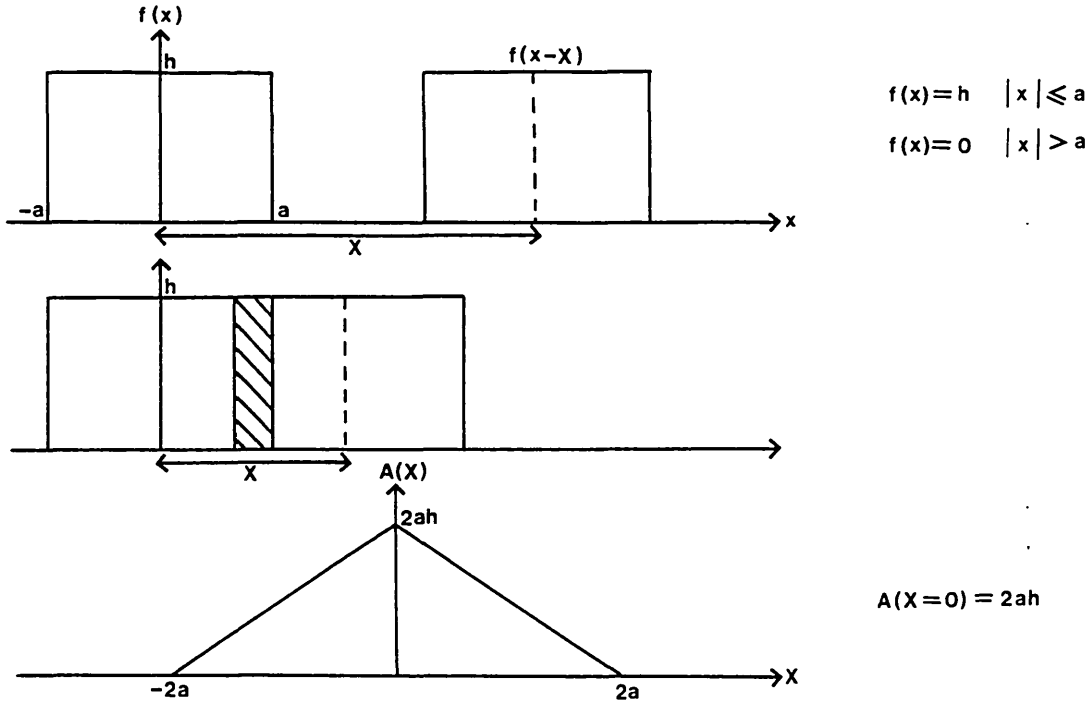

Figure 2.2 : Autocorrelation by area overlap

other point within the function. In order to show the validity of this statement it is necessary for demonstration purposes to impose a finite "sampling cell" so that the density of vectors (i.e. the number of vectors between cells) is finite.

Consider again the top-hat function; this time divided into a four by four array of cells as shown in figure 2.3. The one dimensional autocorrelation of the top-hat may be considered as the distribution of vectors between each cell centre and all other cell centres that lie in the ±x direction. Figure 2.3 shows that there are 16 vectors of zero length (i.e. 16 cells), 12 of length a/2 in the +x direction and so on. The vector distribution (i.e. the digitised autocorrelation) shown in figure 2.3 has the same envelope as that of A(X) shown in figure 2.2. The digital representation becomes totally equivalent to that defined in equation 2.9 as the sampling cell size tends to zero.

2-5 Autocorrelation of speckle images

A typical short exposure image of a star comprises a large number of

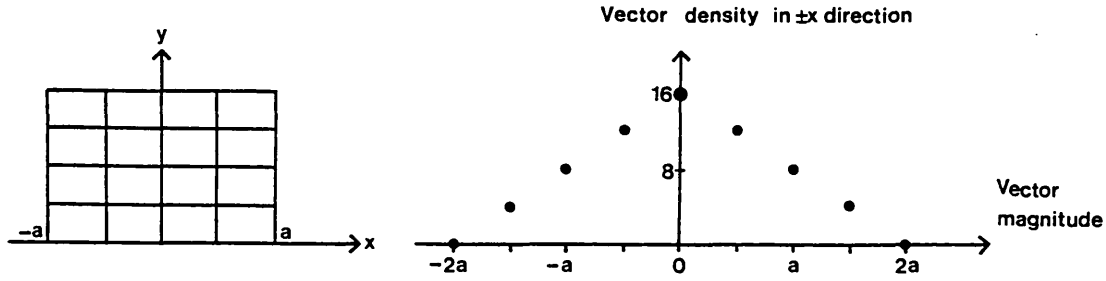

Figure 2.3 : Autocorrelation by vector distribution

speckles randomly distributed over the seeing disc. Speckles are confined to the optical axis of the telescope with an overall envelope of approximately Gaussian form (Parry et al. [16], Woolf [17]; see section 5-3). Each speckle may be considered as a statistical distribution of one or more photon events.

For an image consisting of discrete point-like photon events ("point-like" implies a detector of infinite resolution) the autocorrelation of that image is equivalent to the distribution of vectors between each event and all other events within that image. Vectors between events that occurred in separate speckles contribute to a distribution equivalent to the autocorrelation of the long exposure seeing limited envelope and, since the autocorrelation of a Gaussian is another Gaussian, it closely resembles the seeing disc. However, events occurring within the same speckle contribute to a component equivalent to the autocorrelation of the diffraction limited image. Thus, as previously stated in section 2-2, the autocorrelation of short exposure stellar images contains diffraction limited information.

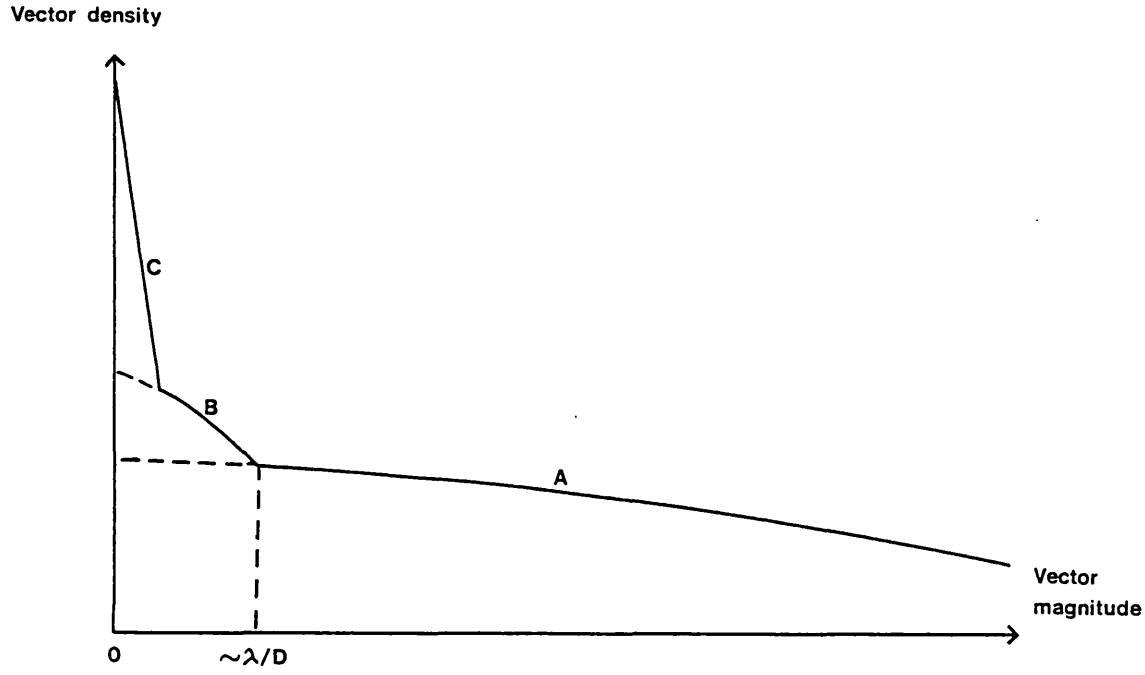

Figure 2.4 : An autocorrelation profile

It is often the case in practice that photon events appear neither point-like nor discrete. In chapter three a description is given of a system comprising a TV camera and image intensifier which produce speckle images which are digitised by a hardwired autocorrelator. It is an artefact of the system that photon events are typically two or three times larger in diameter than the digital sampling cell of the autocorrelator. As a consequence, autocorrelations of speckle images contain a third component produced by vectors between sampling cells (the "cells" are "picture elements" or "pixels") within isolated photon events. This single event component or "photon spike" dominates the central region of an autocorrelation.

Figure 2.4 shows the form of a typical profile of the centro-symmetric autocorrelation of a single unresolved star obtained by integrating the autocorrelations of many short exposure images containing discrete, but not point-like, photon events. The broad base (A) is the seeing component or "seeing pedestal" which is dependent on the atmospheric transfer function. The speckle component (B) produces a sharp deviation from the smooth seeing distribution at the point

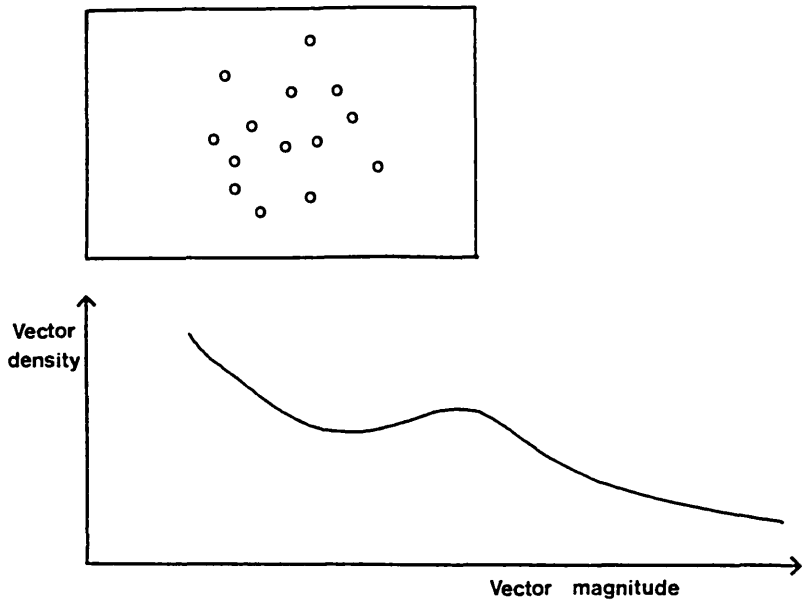

Figure 2.5 :

a) Idealised speckle image of a binary star

b) A secondary peak situated within an autocorrelation profile

corresponding to a vector separation approximately equal to the diffraction limit of the telescope. The central region contains the photon spike (C), which is a wholly instrumental effect. The central point of a two dimensional autocorrelation contains the number of zero length vectors which is, of course, equal to the total number of pixels which had contained all or part of a photon event.

The requirement for detection of single discrete photon events is not always necessary and sometimes not even desirable. The "isoplanatic patch" is defined as the area of sky over which all light from that area entering the telescope aperture is refracted in an identical fashion by the turbulent atmosphere. It is typically 2 or 3 arcseconds across [18] though partial coherence might extend out to around 20 arcseconds. A short exposure image of a bright equal magnitude binary star whose two components are situated within the same isoplanatic patch will appear as two slightly displaced identical speckle patterns; i.e. each speckle has a double nature as simplistically represented in figure 2.5.

The autocorrelation of such an image will exhibit an anomaly, or a

"secondary peak", corresponding to the vector describing the binary system's separation and position angle, as also shown in figure 2.5. Not only does this method of investigation of binary or multiple point objects not require the necessary detection of discrete single photon events, i.e. photometric data, but it is to the advantage of the technique to utilise images which consist of very bright multi-event speckles which ensure a good signal-to-noise ratio. This alternative to the "photon counting mode", but where the modulation of the image intensity is still considered as either bright or dark (i.e. no grey levels), is known as the "clipping mode".

The autocorrelation of a function f(x,y) as defined by equation 2.9 is a symmetric distribution. A two dimensional autocorrelation has a 180° rotational symmetry about its origin. In other words, for each pair of image pixels there are two vectors of identical magnitude but opposite direction. It is therefore only necessary in practice to compute and record one half of an autocorrelation (see chapter three).

2-6 Crosscorrelation

The crosscorrelation of the functions f(x,y) and h(x,y) is represented by the expression :

$$C(x,y) = \iint_{-\infty}^{\infty} f^{*}(x,y)h(x+X,y+Y)dxdy \qquad (2.10)$$

The two dimensional crosscorrelation of two patterns can be regarded as a measure of the degree of correlation between their relative spatial distribution, or, analogously to autocorrelation, as the distribution of vectors describing each point within one function with respect to all points in another.

In section 2-1 it was mentioned that speckle interferometry requires quasi-instantaneous images and that exposure times of about 10ms are necessary to achieve this. Over timescales significantly larger than this random refractive index fluctuations in the turbulent atmosphere cause the distribution of speckles to become totally uncorrelated with respect to their initial distribution. Thus the digital cross-correlation between two stellar images sufficiently well separated in

time will only exhibit vectors associated with the positions of speckles in one image with respect to speckle positions in the other which are each wholly random within the Gaussian-like envelope.

Provided there is negligible macroscopic image movement the crosscorrelation produced from speckle images separated by about one second in time, a period long enough to ensure thorough decorrelation, has a mean intensity which is a good approximation to the form of the autocorrelation seeing component. Significant image movement due to large scale phase variations across the telescope pupil and/or small telescope movements broadens a crosscorrelation which slightly reduces the effectiveness of a comparison. Analysis of data by using such a comparison was first proposed by Welter and Worden [19]. The assumptions on which the method is based are discussed in more detail in chapter five.

The approximation becomes less accurate as the mean number of events per image decreases. For example, when there is only one photon per image the autocorrelation obviously contains no "seeing" vectors yet the crosscorrelation is not zero. Arnold et al. [21] and Worden et al. [20] have successfully used this method to isolate the diffraction limited component from autocorrelated speckle data of Pluto and the asteroid Vesta respectively.

2-7 Phase retrieval

The methods described so far have shown how diffraction limited information about an object may be obtained from the squared modulus of the Fourier transform or, equivalently, the autocorrelation of the object intensity. To achieve actual image reconstruction it is necessary to recover the "phase" of the object transform or the object intensity $O(x,y)$ by some form of analysis different from that suggested by equations 2.3 and 2.5. One can consider the problem in autocorrelation space as arising from the 180° rotationally symmetric properties mentioned in section 2-5. Each vector has a 180° ambiguity such that reconstruction of an object from autocorrelation alone becomes virtually impossible. Not even the object distribution of an unequal magnitude binary star can be uniquely determined unless individual

double speckles can be visually identified and the comparative intensity of each component detected.

Without phase information the method appears to be restricted to use for binary and centro-symmetric objects. In chapter five it is described how computer generated models can be employed to investigate objects with centro-symmetric intensities.

Since the technique of speckle interferometry was first invented a number of numerical and other phase retrieving methods have been proposed and several have been pursued with varying degrees of success. Reviews of some of these image reconstruction techniques have been made by Worden [3], Dainty [2] and Walker [22].

One of the first highly successful methods is that of speckle holography as investigated by Liu and Lohmann [23], Bates et al. [24], Gough and Bates [25] and Weigelt [28]. The concept of the method, as described by Dainty [2], relies on the fact that the autocorrelation of an object in combination with a point source contains a component which represents the exact object intensity distribution. Unfortunately this method is only applicable to objects which contain a point source within the same isoplanatic region, i.e. within a few arcseconds. This could be of particular use for imaging of outer planets as they approach occultation of bright stars.

A numerical method proposed by Knox and Thompson [27] involves finding the average autocorrelation of the Fourier transform of the images. This consists of computing the phase differences in the spatial frequency domain between all pairs of adjacent points. The phase of the Fourier transform of the object intensity at a particular point in the transform plane is then given by the sum of the phase differences from the origin to that point. This method is highly susceptible to noise, particularly if the seeing is poor [2],[30]. A form of the Knox-Thompson algorithm has been successfully applied to image reconstruction of solar features [26] where, of course, photon noise [29] is not a problem!

The technique developed by Lynds et al. [31] supposes that short

exposure images of a point source consist of a few widely separated bright speckles. Each individual bright speckle, considered as a photon noise limited image of the object, can be superimposed, with the aid of a digital microdensitometer and computer, to form a high signal-to-noise ratio diffraction limited image. Unfortunately there is doubt whether speckle patterns of point sources can be considered to consist often of widely separated bright speckles. The technique is restricted to objects which are just resolved by the telescope, such as Betelgeuse, which was measured by Lynds et al. [31], and other supergiants [32]. The method has been developed by Bates and Cady [33] into that known as shift-and-add. (See also Hunt et al. [34]).

The technique known as speckle masking, developed by Weigelt [35], enables images of a restricted class of objects, particularly double stars, to be reconstructed. Non-linear image processing of speckle photographs yields a distribution which is essentially the instantaneous point spread function. These new photographs, representing that of a synthetic point source, are then used in the same way the reference star is used in speckle holography. Weigelt and Wirnitzer [36] present results of close spectroscopic double star observations obtained using speckle masking.

One of the first numerical image reconstruction techniques to show evidence of some tolerance to noise was that proposed by Fienup [37]. It is suggested that the phase may be found by an iteration involving successive Fourier and inverse Fourier transforms with the solution being constrained to the observed object modulus in Fourier space and known object parameters in image space. The single doubt concerning this technique is that the iteration will not necessarily converge to the correct solution. Fienup shows that, for one dimensional simulations at least, there could be a very large number of solutions. However, the problem appears to be less severe in two dimensions.

Walker [38] has proposed a technique known as the "exponential filter method". Walker shows that the modulus of the Fourier transform of the object intensity (as usually measured in stellar speckle interferometry), together with the modulus of the Fourier transform of the product of the object intensity and an exponential, contain all the

information necessary to retrieve uniquely the phase of the object Fourier transform and thus to deduce the form of the object. One suggested iteration process (there are several alternatives) is similar to that of Fienup except that the iterative loop includes a second stage where the object intensity is multiplied by an exponential distribution which is then Fourier transformed and inverse Fourier transformed with similar constraints placed on the form of the produced moduli according to the observed parameters. Computer simulations [22] indicate that the technique may be applicable to astronomical objects as faint as 11th magnitude.

Chapter Three

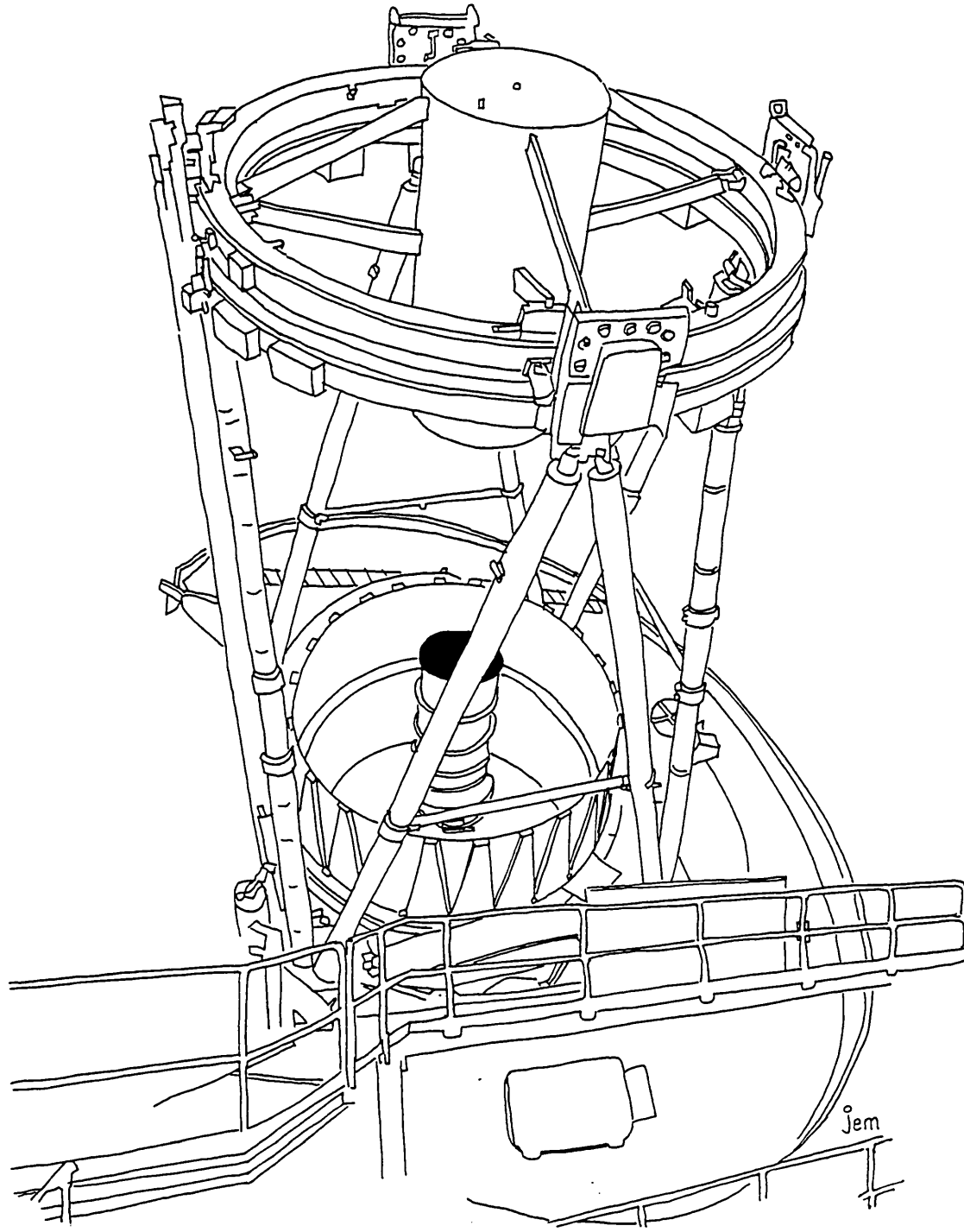

Chapter Three : The Imaging System And Digital Analysis Hardware

3-1 The speckle interferometer

The Imperial College speckle interferometer is designed to produce high magnification bandwidth limited images of low light level stellar objects using large telescopes. It was initially constructed to accommodate a cine camera system, as described by Beddoes et al. [10]. The cine camera has now been replaced with a television camera which enables data to be recorded onto video tape or processed in real time.

Figure 3.1 shows a schematic diagram of the interferometer. Light from the telescope enters the system through a circular hole in the baseplate where it is either viewed through an eyepiece or is reflected down the optical axis of the interferometer. The wide field eyepiece, which has an illuminated crosswire, facilitates fine adjustment of the image position onto the optical axis. A rotating sector shutter, placed at the position approximately corresponding to the focal point of the telescope, enables the exposure time of the image to be controlled (see section 3-4). Microscope objectives of various focal lengths determine the overall magnification of the system which is usually such that the field of view on the TV camera is of the order of the seeing disc diameter. The light which has been collimated by the microscope objective passes through a pair of rotatable double prisms which are used to compensate for atmospheric dispersion. The first set of prisms made for the system were designed for operation at visible wavelengths. In section 3-2 the theory associated with dispersion correction is reviewed and the design requirements for the second set of prisms, which now permit observations at near ultra-violet wavelengths, are discussed. The next element in the optical train is a filter which restricts the range of transmitted wavelengths. This ensures temporal coherence according to the formula given by equation 2.1. In practice the largest allowable bandwidth is used unless the observation requires a specific narrow bandwidth corresponding to a particular emission line. A neutral density filter may also be included here either to reduce the light level should there be a requirement for photon counting and the image is considered too bright (see section 2-5), or to match the brightness of a comparison star to that of an object (see chapter four). A relay lens

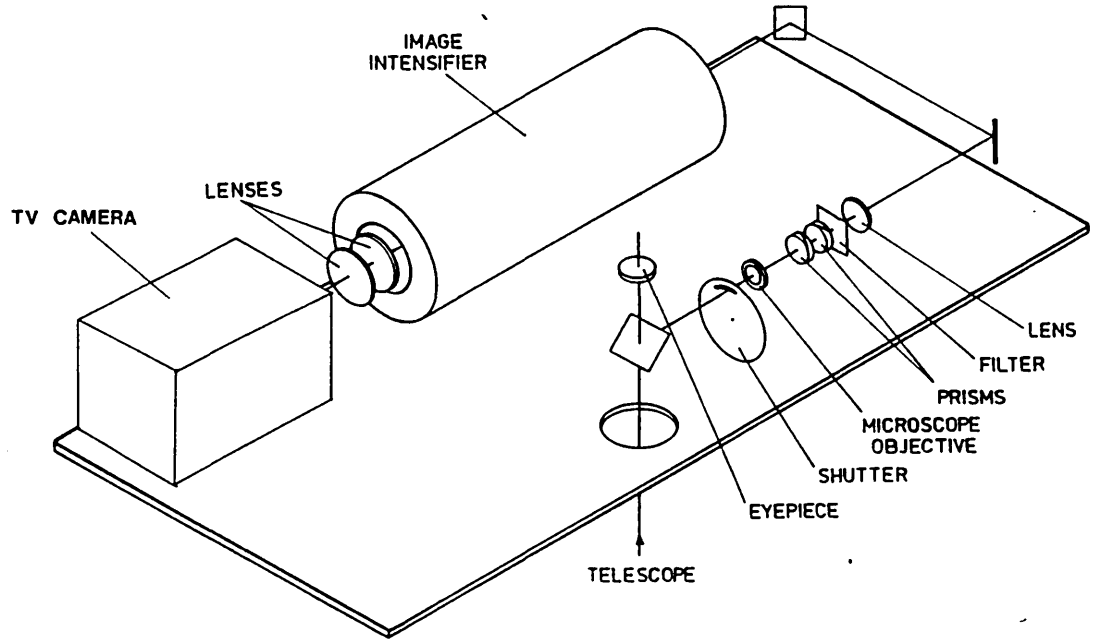

Figure 3.1 : The speckle interferometer

of 600mm focal length then focuses the light onto the photocathode of the image intensifier. Two plane mirrors are inserted to keep the system compact. A sliding shutter in front of the photocathode serves to protect the tube from accidental exposure to bright sources between observations. The microscope objective and relay lens provide a magnification approximately equal to the ratio of their nominal focal lengths which is typically about 12. An experimental investigation of the magnification produced by the interferometer has been performed which is described in section 3-5.

The image intensifier, required because of the very low light levels involved as a consequence of short exposure time and limited bandwidth, is magnetically focussed within a specially designed water cooled solenoid. A description of the two EMI four stage cascade tubes used and their performance is given in section 3-3. The image on the output phosphor screen is re-imaged onto the faceplate of a Plumbicon tube TV camera via two f/1.2 lenses of 55mm focal length. Several LED's situated between the camera and the lens provide a bias illumination which greatly enhances the contrast of the TV images (see section 3-3).

3-2 The atmospheric dispersion compensation prisms

When the sky is viewed through a telescope away from the zenith the atmosphere acts as a prism wedge across the pupil such that the light from a star suffers transverse chromatic aberration. Most astronomical imaging systems have relatively low magnification and consequently atmospheric dispersion is not a serious problem. Stellar speckle interferometry, however, relies on very high magnification and without dispersion correction speckles appear elongated.

Schneiderman and Karo [39] and Labeyrie [4] have investigated the employment of diffraction gratings for atmospheric dispersion correction.

In 1870 Airy [15] proposed that correction to a first order could be made using a single wedge of glass but since air has dispersion characteristics very different from any glass, correction over any significant bandwidth is impossible. A double prism system, however, provides a perfectly adequate solution. Two identical double wedge prisms, each comprised of two different types of glass, may be designed to provide an equal and opposite dispersion to that imposed on the light by the atmosphere and yet retain a net zero deviation at an optimum wavelength. Each prism need only have half the total dispersive power required and by rotating one pair with respect to the other a measured amount of compensating dispersion may be provided. (See Breckinridge et al. [40].)

Consider the atmosphere as a uniform layer of air. An incident ray is refracted as shown in figure 3.2. By differentiation of Snell's law it can be shown that for a small net deviation D the dispersion, usually defined in units of radians per 100nm, is given by

$$\frac{dD}{d\lambda} = \frac{dn}{d\lambda} \tan z \qquad (3.1)$$

where n = wavelength dependent refractive index of air,
and z = zenith angle.

It can also be shown that the atmospheric dispersion at the prism

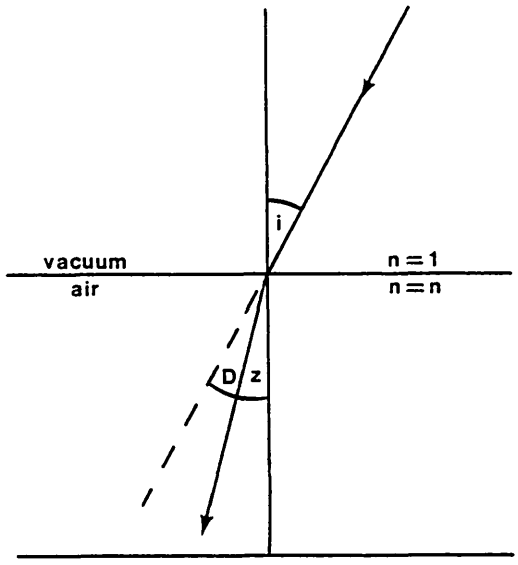

i = angle of incidence
z = zenith angle
D = deviation = i - z

Figure 3.2 : Refraction by the atmosphere

plane is a factor of F/f larger than that at the telescope pupil, where F and f are the focal lengths of the telescope and the microscope objective respectively. Thus the compensating dispersion required per double prism is given by

$$\frac{dD}{d\lambda} = \frac{1}{2}\left[\frac{dD}{d\lambda}\right]_{\lambda_o} \tan z . F/f . 3600 . 180/\pi \qquad \text{arcsec/100nm} \qquad (3.2)$$

where $\left[\frac{dD}{d\lambda}\right]_{\lambda_o}$ = atmospheric dispersion in rad./100nm at wavelength λ_o.

Consider two wedge prisms arranged as shown in figure 3.3. Their axes are normal to the page and the incident ray is normal to the face of the first prism.

From Snell's Law $n_1 \sin A_1 = n_2 \sin B_1$ and $n_2 \sin B_2 = \sin B_3$

$\Rightarrow$ $B_1 = \sin^{-1}(n_1/n_2 . \sin A_1)$

$\Rightarrow$ $B_2 = B_1 - A_2$

and $B_3 = \sin^{-1}(n_2 \sin B_2)$

The deviation is given by $D = (A_1 - B_1) - (B_3 - B_2) = A_1 - A_2 - B_3$

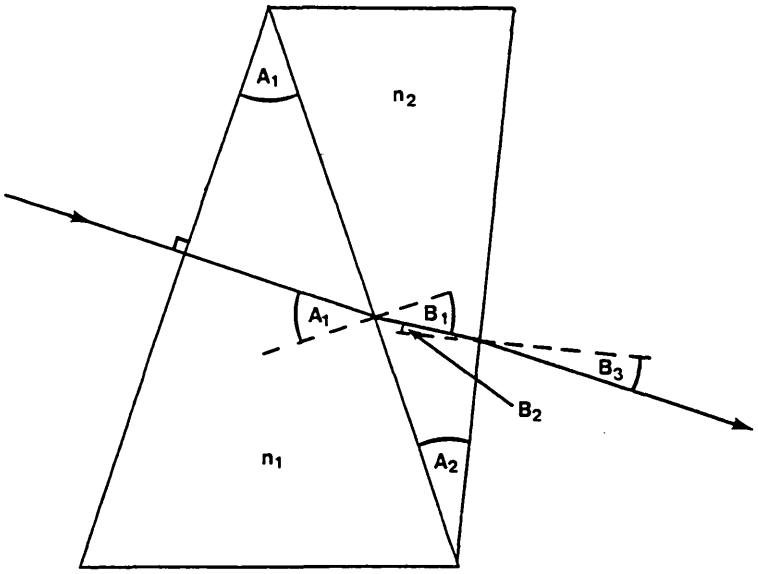

A_1 = wedge angle of prism 1
A_2 = wedge angle of prism 2
n_1 = refractive index of prism 1
n_2 = refractive index of prism 2

$n_2 > n_1$

Figure 3.3 : Light path through a double prism

The dispersion is given by $\frac{dD}{d\lambda} = -\frac{dB_3}{d\lambda} = -\frac{d}{d\lambda}[\sin^{-1}(n_2 \sin B_2)]$

Let $a = n_2 \sin B_2$

$$\Rightarrow \quad \frac{dD}{d\lambda} = -\frac{d}{d\lambda}\sin^{-1}a = -(1-a^2)^{-\frac{1}{2}}\frac{da}{d\lambda} \qquad \text{where } |\sin^{-1}a| < \frac{\pi}{2}$$

$$= -(1-a^2)^{-\frac{1}{2}}[\frac{dn_2}{d\lambda}\sin B_2 + n_2 \cos B_2 \frac{dB_2}{d\lambda}]$$

Let $b = n_1/n_2 . \sin A_1$

$$\Rightarrow \quad B_2 = \sin^{-1}b - A_2$$

$$\Rightarrow \quad \frac{dD}{d\lambda} = -(1-a^2)^{-\frac{1}{2}}[\frac{dn_2}{d\lambda}\sin B_2 + n_2(1-b^2)^{-\frac{1}{2}}\cos B_2 \frac{db}{d\lambda}] \text{ where } |\sin^{-1}b| < \frac{\pi}{2}$$

$$= -(1-a^2)^{-\frac{1}{2}}[\frac{dn_2}{d\lambda}\sin B_2 + (1-b^2)^{-\frac{1}{2}}\cos B_2 \sin A_1 (\frac{dn_1}{d\lambda} - n_1/n_2 . \frac{dn_2}{d\lambda})]$$

For zero deviation $B_3 = A_1 - A_2$

$$\Rightarrow \quad B_2 = \sin^{-1}[1/n_2 . \sin(A_1 - A_2)]$$

$$\Rightarrow \quad a = \sin(A_1 - A_2)$$

and $\quad b = \sin(B_2 + A_2)$

Therefore the dispersion produced by the doublet when the outgoing ray has suffered a net zero deviation is given by

$$\frac{dD}{d\lambda} = -[\frac{dn_2}{d\lambda}\sin(A_1 - A_2) + (n_2\frac{dn_1}{d\lambda} - n_1\frac{dn_2}{d\lambda})\cos B_2 \sin A_1 / \cos(A_2 + B_2)] / n_2 \cos(A_1 - A_2) \qquad (3.3)$$

where $\quad B_2 = \sin^{-1}[1/n_2 . \sin(A_1 - A_2)]$.

$\frac{dn_1}{d\lambda}$ and $\frac{dn_2}{d\lambda}$ are the gradients of the refractive index versus wavelength characteristics for each material. By equating expressions 3.2 and 3.3 the prism parameters required to correct for atmospheric dispersion at any wavelength and maximum zenith angle may be calculated.

The first set of prisms made for the Imperial College speckle interferometer were designed to operate at an optimum wavelength of 486nm on the 2.5m Isaac Newton Telescope for zenith angles of up to $\tan^{-1}2$ using a microscope objective of 50mm focal length. The required compensating dispersion is 408 arcsec./100nm per double prism. A detailed description of their performance is given by Beddoes [14].

A second set of prisms have been made in order to facilitate observations at an optimum wavelength of 360nm on the 3.9m Anglo-Australian Telescope (AAT). The two types of glass were selected for their low absorption at that wavelength and are specified below.

1. LiF: Refractive index (360nm) = 1.4017 $\frac{dn}{d\lambda}$(360nm) = 0.00872 $(100nm)^{-1}$

2. SiO: Refractive index (360nm) = 1.4753 $\frac{dn}{d\lambda}$(360nm) = 0.0148 $(100nm)^{-1}$

AAT observations at zenith angles of up to $\tan^{-1}2$ with a 50mm objective at 360nm require a compensating dispersion of 1799 arcsec./100nm per double prism. Prisms made of the above glasses would require wedge angles of 74° and 50° which is highly impractical. Restricting observations to maximum zenith angles of $\tan^{-1}1$ and to the use of an 80mm objective (i.e. reduced magnification) enables the use of prisms having more realistic wedge angles of 36° and 30°. Such prisms have been manufactured and successfully employed.

Each double prism is set inside an aluminium wheel which is graduated in one degree intervals around its circumference. The relative orientation of the two wheels determines the amount of compensating dispersion imposed on the light passing through. Numerical calculations by Simon [41] enable prism settings as a function of hour-angle and declination to be pre-computed and displayed in sets of tables.

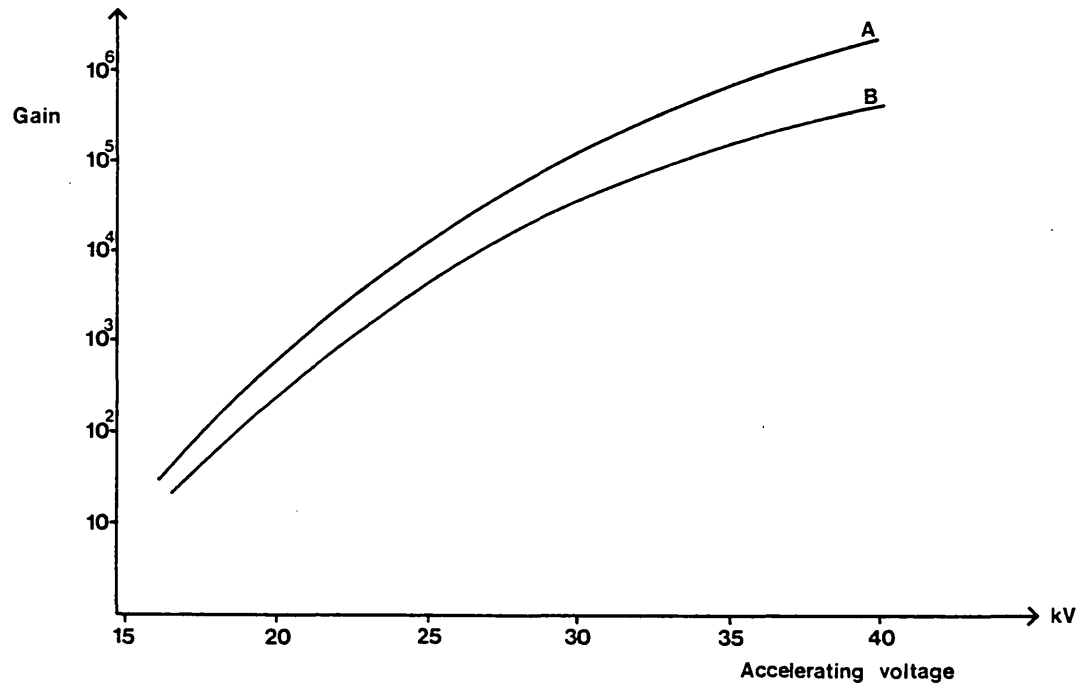

Figure 3.4 : Gain curves of the A and B image intensifiers

3-3 The sensor system

The two image intensifiers currently used for speckle observations are EMI four stage cascade tubes, type 9912, with bi-alkali photocathodes. The gain of both intensifiers, as measured in the laboratory, is illustrated as a function of accelerating voltage in figure 3.4. The diagram indicates that tube A, the older of the two, has a significantly higher gain than the newer tube B at the optimum running voltage of 40kV. They are equipped with blue (P11) and green (Yttrium Aluminate) output phosphors respectively. The overall decay rate on both output phosphors is of the order of a millisecond which is significantly faster than the typical exposure period of the processed images. A full specification of both intensifiers is published by EMI Ltd. [42]. The EHT voltage is provided by a Miles Hivolt TH50 transistorised supply and is connected via an EMI C152B EHT divider chain. The divider enables the voltage across each individual stage of the tube to be controlled and thus facilitates fine focussing.

The magnetic focussing is provided by the water-cooled solenoid

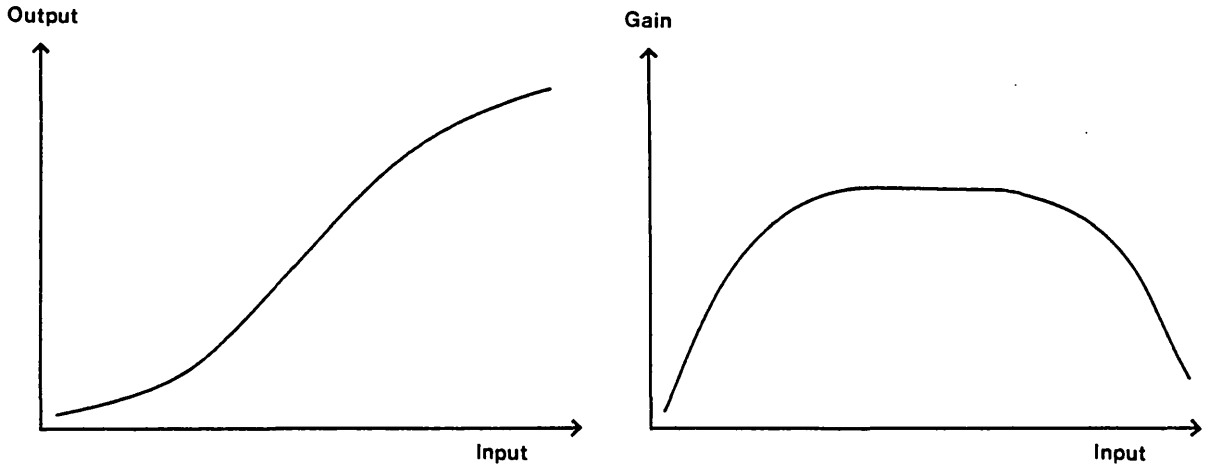

Figure 3.5 : Output and gain of the TV camera plumbicon tube

which is powered by a 60 volt (8 amp max.) Lambda Electronics LES-EE-04-OV power supply. The photo-electrons are accelerated by the electric field in a direction parallel to the axis of the tube. The magnetic field, however, introduces a circular motion in the plane perpendicular to the axis. If the current is such that the electrons have described an exact integral number of circular loops during each stage, then the random transverse momentum imparted on the electrons at emission at each cathode has zero effect on the transverse position of the electrons at each interface. Thus the final image will be in focus. Increasing the current produces an increase in the number of loops per unit length and causes the electrons to describe tighter orbits in the transverse plane. This results in a decrease in the residual positional error at the output phosphor and hence a further improvement in image quality. In practice, solenoid heating effect considerations restrict the current to "two-loop focus" which corresponds to about 5 amps and therefore a dissipation of about 300 watts.

Beddoes [14] noted that the image intensifier used with the cine camera system produced a net rotation of the image of about 2.3° . In

chapter four it is described how, using the image processing hardware, rotation effects can be calibrated.

The television camera, a type 109A manufactured by Link Electronics Ltd., has a one inch Plumbicon tube, type XQ1070B [43]. The camera is coupled to the output phosphor of the image intensifier by means of a Nikon f/1.2 55mm lens and the f/1.2 55mm camera lens.

The response of the camera is not linearly related to the intensity of the input signal. The output and the gain of the Plumbicon tube as a function of input signal intensity are illustrated in figure 3.5. Weak and very strong signals have a compressed output. Compression of very weak signals may be overcome by means of a bias illumination. This adds a uniform intensity level to the input signal so that weak signals register in the linear region. Photon events appear at the output phosphor of the image tube having an approximately Poissonian pulse height distribution. The addition of a bias illumination has enabled the detection of the fainter events, ensuring a better signal-to-noise ratio for observations of faint objects. This was achieved by placing six small LEDs between the camera lens and the faceplate of the Plumbicon tube. They are powered by a small 10 volt supply.

The television images are recorded on Sony V-62 video tapes using a Sony AV-3620CE video tape recorder.

3-4 The shutter

In chapter two it was described how speckle interferometry requires atmospheric perturbations to be effectively frozen over the exposure period of individual speckle images. It was also mentioned that experiments show that an exposure time of about 10 ms is necessary to achieve this condition. A standard 50Hz 625 line TV picture is composed of two fields. Each field is scanned on alternate lines, the second being between the lines of the first. There are twenty five new pictures per second such that the exposure time of each TV field is 40ms. Though experience has shown that even this comparatively large period is sufficient to give good binary star results under most observing conditions, it is usual practice nevertheless to insert a

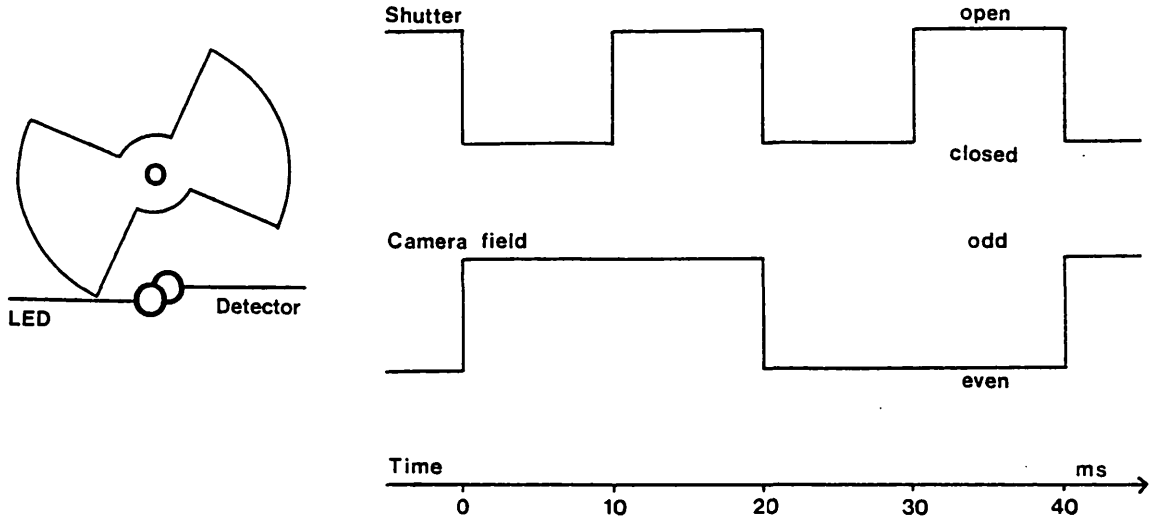

Figure 3.6 : The shutter

rotating sector shutter in front of the microscope objective in order to reduce the exposure time to 20ms or 10ms.

The Rofin shutter, type 7513, is shown schematically in figure 3.6. It consists of two 90° sectors which rotate between an LED and a photo-detector arranged on the outer edge of the shutter. The detector provides a signal to a Rofin frequency-programmable microchopper unit which compares the rotation rate to the synchronisation signal from the TV camera. The device then adjusts the shutter speed such that it is opened and closed exactly once during each scan of the TV field. The TV camera synchronisation signal is processed by pulse shaping and phase shifting circuitry to ensure compatibility with the control unit. The synchronisation cycle is illustrated in figure 3.6. Every point on a TV field is effectively exposed from the moment it is scanned by the camera until it is scanned again, providing that the shutter is open, which is a duration of 20ms. Note however that the period between the beginning and ending of exposure of a field is only reduced to 30ms. The exposure time can be reduced further to 10ms by masking off one of the open sectors, while ensuring that the photo-detector is not shut off from the

LED on that side.

3-5 Magnification and image scale

The magnification produced by the interferometer is approximately equal to the ratio of the focal lengths of the relay lens and the microscope objective. Thus, if the image size were unaffected by the cascade tube, and the image tube output phosphor is coupled to the camera one-to-one, a 50mm objective should produce a magnification equal to a factor of 12. The actual magnification of the interferometer in conjunction with the cine camera system was measured experimentally by Beddoes [14]. An objective of 50mm focal length produced a magnification of 11.52 when the image intensifier was run at 36kV. The coupling of the TV camera is identical to that used for the cine camera and thus the overall magnification of the present system is the same.

The effective resolution of the TV system is equal to the width of the field line spacing. A determination has been made, which is now described, of the image scale produced by the interferometer expressed in arcseconds per resolution element for any telescope platescale and microscope objective.

The separation of a standard line grating was determined using a travelling microscope. The grating was then placed at the focus of the interferometer which is situated just in front of the shutter (see figure 3.1). A 50mm objective was inserted. The image intensifier was run at 40kV and the grating was imaged by applying a faint background illumination. The focusing solenoid was run at two-loop focus. The grating was arranged so that it appeared parallel to the TV scan lines. A tape recording was then made of the TV images of the grating and the mean number of TV field lines per grating interval was calculated. This was performed for both image intensifiers. Hence from a calculation of the number of field lines per millimetre of grating the size of the effective resolution element, or "resel", of the system incorporating an objective of focal length f(mm) and for a telescope platescale p(arcsec/mm) was found to be given by the expression

$$\text{resel} = p(\text{arcsec/mm}) \times f(\text{mm}) \times 6.76 \times 10^{-5} \quad \text{arcseconds} \qquad (3.4)$$

for all observations made with either image tube run at 40kV, using two-loop magnetic focus.

As mentioned in section 2-5, photon events appear with a diameter typically two or three times greater than the sampling cell ($\equiv$ resel) of the system. However, the magnification is chosen such that the diffraction limit of the telescope is equivalent to a diameter several times greater than the typical photon event diameter (see section 5-4).

3-6 Design requirements of a hardwired real-time autocorrelator

The purpose of a hardwired digital autocorrelator for stellar speckle interferometry is to produce two dimensional autocorrelations of short exposure stellar images. The first such device to be built is that described by Blazit et al. [44], [45] and another has been constructed at Kitt Peak National Observatory [46]. The design requirements of a hardwired autocorrelator at Imperial College were initially discussed in 1977. It was decided that the proposed autocorrelator should be capable of processing television pictures in real-time and of displaying immediate on-site results.

The standard British TV system generates pictures at a rate of 25 per second, composed of two interlaced fields each containing 293 lines of image information. To significantly reduce project costs only alternate fields are processed. Though the effective resolution is reduced, in practice photon events appear significantly larger than the spacing between successive field lines so negligible information is lost.

The Imperial College hardwired real-time autocorrelator divides the central 256 lines of the TV field into a 256 by 256 square and examines each picture element, or pixel, within the square for the presence of photon events. Thus each pixel is registered as having one of two states indicating the presence or absence of signal above an adjustable detection threshold. The x,y locations of each pixel containing part of a photon event, up to a maximum number of M, is stored in a memory. Using two identical memories enables coordinates to be stored in one while the locations already stored in the other are being processed.

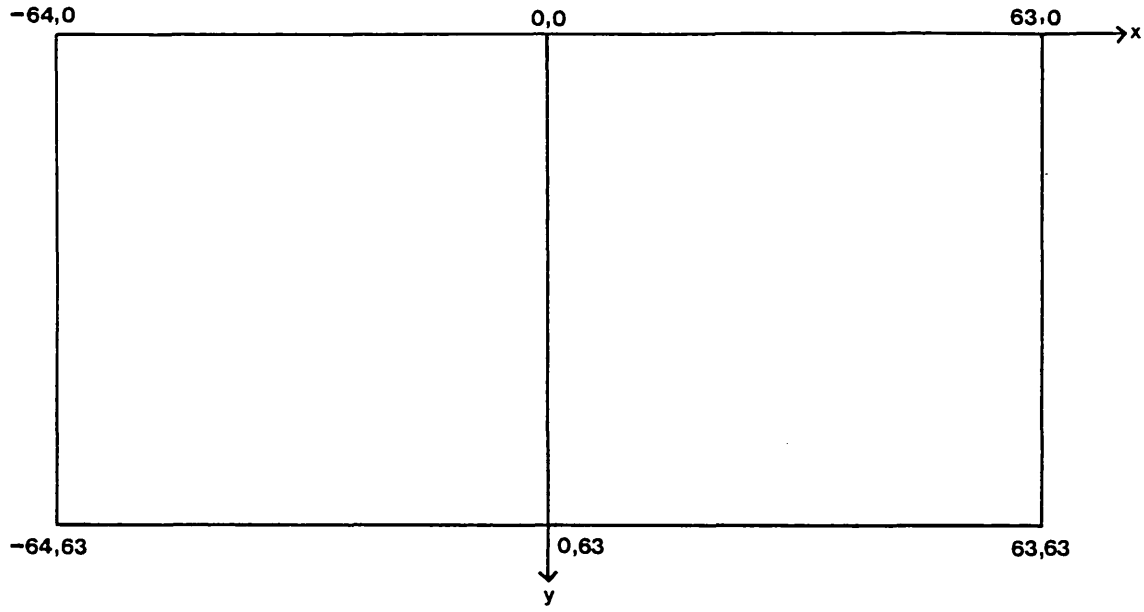

Figure 3.7 : Autocorrelation vector window

Thus for the processing to be achieved in real time all the necessary calculations must be carried out in 40ms.

The number of vectors calculated from M pixel coordinates, assuming no 180° redundancy, is equal to $(M^2 - M)/2$ or, for $M >> 1$, $M^2/2$ "operations". One operation, as is explained in section 3-7, consists of two eight bit subtractions and the increment of a 20 bit memory. If the operation time is t then it is required that

$$M^2 \, t/2 < 40\text{ms} \qquad (3.5)$$

The technological limit within the available budget in 1977 limited t to a minimum of about 300ns. As a consequence M, the maximum number of "occupied" pixels per frame, was chosen to be 512. Further decrease in operation time could only be achieved for a disproportionate increase in costs. Incidentally, 1984 technology could improve the operation speed by at least a factor of two within the original financial limitations.

Most of the 293 field lines are examined and generally the optical magnification is chosen such that the seeing disc occupies most of this area. Making the image much larger in order to increase resolution introduces serious telescope tracking problems. A great saving in memory costs is made by storing only those vectors calculated that lie within a 64 by 128 pixel window, as shown schematically in figure 3.7. The range of binary separations or object extensions detectable will depend on the magnification used.

3-7 Operation of the hardwired real-time autocorrelator

The autocorrelator samples each of the 256 lines at regular intervals such that the line is divided into 256 pixels of width equal to the field line spacing. If the signal exceeds 1.1 volts then the X and Y coordinates of that pixel are stored as 2 x 8 bits in one of two 512 x 16 bit memories. A DC voltage (called the video level) is added to the video signal and thus facilitates an adjustable detection threshold. Conventionally the X direction is defined as along each line as scanned by the camera, and the Y direction as orthogonal to this, vertically down the feild.

While the image coordinates from a field are being stored in one memory, digital autocorrelation is performed on the coordinates previously stored in the other memory. This process involves subtracting the coordinates of the ith pixel from those of the jth pixel where $j \geqslant i$. Providing that the result of the X subtraction is $\geqslant -64$ and $\leqslant 63$ and that the result of the Y subtraction is $\leqslant 63$, then a location in a large integrating memory is incremented whose address is given by the result of the subtraction. Otherwise the result is ignored. If the Y subtraction does exceed 63, then, since all subsequent Y differences will also do so, the current j incrementation is terminated and the next value of i considered. In this way the autocorrelation is stored in a 128 x 64 x 20 bit integrating memory consisting of forty 4K MOS static RAM chips arranged in 20 pairs. The number contained at the location corresponding to an array element (x,y) represents the number of times that the difference between two image pixels was x in the X direction and y in the Y direction. The vectors (-x,-y) in the negative Y direction are identical in number, contain no

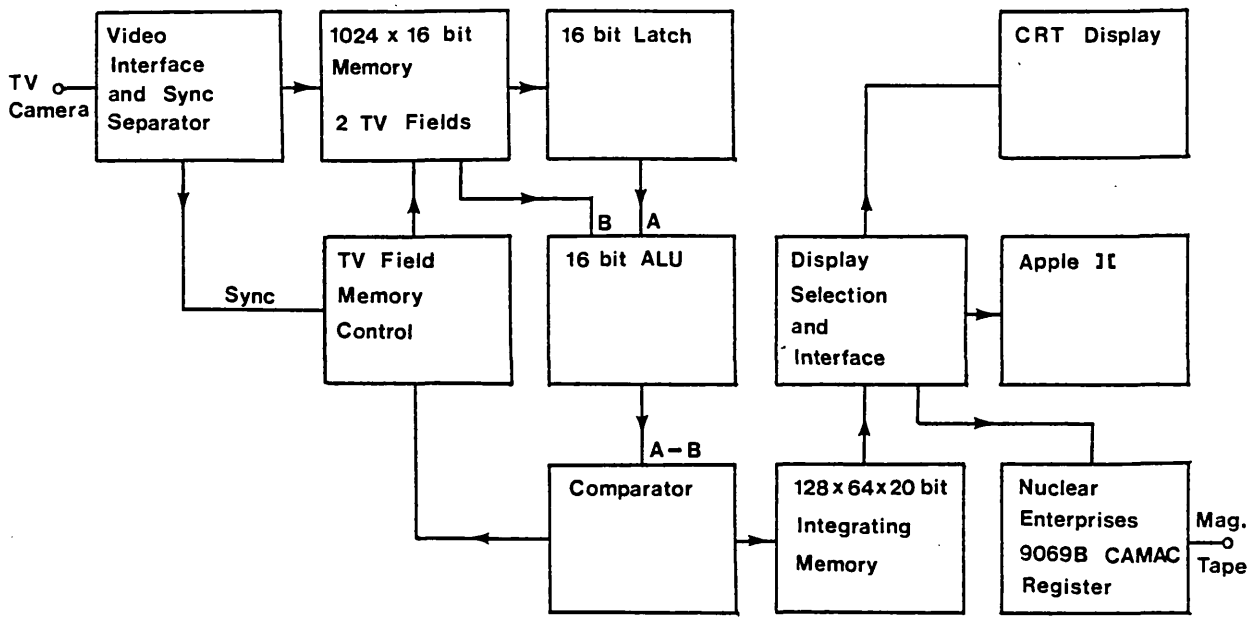

Figure 3.8 : Operation of the hardwired real-time autocorrelator

new information and therefore are not recorded.

Figure 3.8 shows a schematic diagram which illustrates the operation of the autocorrelator. It shows the video signal applied at the input where the TV synchronisation signal is used to drive the TV field memory control which acts as an address counter and a read/write mode selector. As mentioned earlier, whilst the pixel locations of a TV field are loaded into one of the 512 x 16 bit memories, the data previously stored in the other memory are processed. The coordinates of the first occupied pixel are stored in the 16 bit latch memory and are subtracted from those of all the other occupied pixels in turn by the arithmetic logic unit. All the coordinates except those of the first are then re-written into the buffer memory and the coordinates of the second occupied pixel are stored in the latch memory and subtracted from the remaining coordinates and so on. The comparator unit distinguishes when X or Y limits are exceeded and increments the appropriate address counter. Otherwise the corresponding memory location of the integrating memory is incremented. The contents of this memory may be periodically displayed as described later.

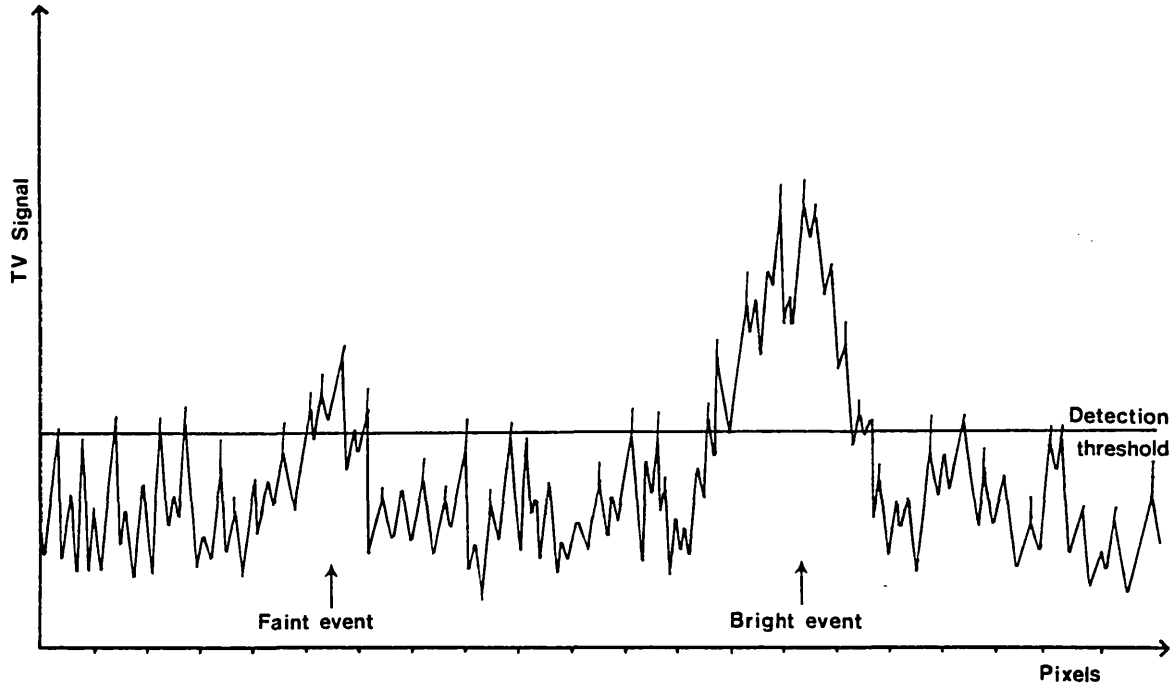

Figure 3.9 : A TV line containing faint and bright events (schematic)

3-8 System developments

The Imperial College hardwired real-time autocorrelator, shown in figure 3.10, first became operational in late 1979 when it was used for a programme of binary star observations on the AAT. Work on binary stars prompted the proposal for a device which would enable the autocorrelator to sample just one pixel per speckle by some form of speckle centering. Such a facility would enable more speckles per frame to be sampled without requiring a decrease in the detection threshold, and would produce a better defined secondary peak in the autocorrelation. Calculating the central pixel within each speckle requires moderately complex circuitry. Consequently a much less complex circuit was designed which detects the top right-hand pixel of each speckle. The device has enabled a significant improvement in the identification of bright binary stars. However, since most recent observations have been of faint objects which produce images consisting of individual events (i.e. not solid bright speckles), the device is rarely used. The speckle centering circuitry would not be useful in the investigation of single objects because of the consequent loss of many speckle component

Figure 3.10 : The hardwired autocorrelator

vectors near the centre of the autocorrelation.

Experience of faint and extended object observation has prompted several other additions to the circuitry which are all associated with overcoming various manifestations of noise in the system. It was mentioned in section 3-3 that photon events appear on the output phosphor of the image intensifier with a range of intensities. Observation of faint objects requires the detection of every event possible, even the very faintest. Figure 3.9 represents the voltage distribution along a typical TV line containing a section through a faint event and a bright event. The detection threshold is shown such that the autocorrelator detects the faint event as having a width of one or two pixels. Under these conditions the high frequency background noise from the camera tends to be detected. To enable the autocorrelator to distinguish between the effects of the camera noise spikes, which persist for less than the pixel scan time, and the faint photon events, which are typically several pixels across, a high frequency discriminator has been built which discounts any signal persisting over less than about eighty percent of the pixel scan time.

Another possible source of noise is that produced by on-site interference between the video camera/recorder system and any other electronic equipment in the vicinity, which can cause bright hum bars to appear on the tape records. This problem has been partly alleviated for AAT observations by the use of an aluminium cradle designed to enable the tape recorder to be installed in the cassegrain cage and yet remain horizontal to ensure correct functioning. Thus the co-axial cable connecting the camera to the recorder is now very much shorter and hence less liable to suffer interference. Slight tape damage or signal drop-out can also produce bright lines on a video tape record. Autocorrelations of such records naturally exhibit a spurious horizontal broadening. An electronic addition to the autocorrelator facilitates the rejection of any signal which persists over a scan time corresponding to about twenty two consecutive pixels. The low frequency discriminator, as it is known, rejects the entire TV line on which such a signal is registered.

One fairly common source of noise that has not yet been mentioned is

that due to the occurrence of "ion-events" in the image intensifier. Electron bombardment desorption, mainly from the aluminium backing of the phosphor, introduces a variety of heavy, organic and metal, negative ions which produce very bright random events on the output phosphor of the tube. The older of the two tubes used for speckle observations, tube A as described in section 3-3, is particularly liable to exhibit occasional intense ion-event activity. A circuit has been added to the autocorrelator which facilitates the establishment of an adjustable upper detection threshold above which a signal may be rejected. The device, known as the video limiter, substantially reduces the damaging effects of ion-events on the records of faint objects. Both discriminators and the video limiter may be switched out if not considered desirable or necessary.

In section 3-4 it was described how every standard TV picture is composed of two interlaced fields. For the benefit of commercial TV receivers the synchronisation signal associated with a particular field contains a pulse which indicates to the receiver that the field is either to be scanned across the "odd" or the "even" lines of the TV screen. The autocorrelator is capable of processing only alternate fields (see section 3-6). Originally the autocorrelator was designed to begin operation on the first "acceptable" field and if rejection of a field was necessary, perhaps due to a noisy synchronisation signal, it examines the following field. Another hardwired modification enables the autocorrelator to distinguish "odd" and "even" fields so that either type of field may be exclusively examined. Two distinct records become available from the same tape recording such that no acceptable field need remain unprocessed. Hence recorded data yields twice the number of frames obtained from direct on-site processing from the same observation (see section 4-7). This device also facilitates the identification of spuriae due to transients such as ion-events which occur in individual frames.

3-9 The hardwired crosscorrelator

In chapter two it was mentioned that the mean intensity of the crosscorrelation of pairs of speckle images sufficiently well separated in time is a good approximation to the form of the autocorrelation

seeing component. It was also described how crosscorrelation could therefore be used to isolate the diffraction limited information from autocorrelated speckle data. Subsequently, after the Imperial College hardwired autocorrelator began operation, the building of a device designed to produce crosscorrelations of TV images was initiated.

In order to crosscorrelate between fields separated by about one second's duration at a processing rate equivalent to that of the autocorrelator, it is necessary that the image pixel coordinates from many frames are held in memory at one time. The proposed design provides storage for twenty five frames. Alternate odd or even fields, occurring at 40ms intervals, are sampled and up to 512 image pixel coordinates per field are registered in one of twenty five 512 x 16 bit memories. These memories are continuously replenished in a cyclic manner. As a new set of coordinates is being loaded into memory the field stored most recently is crosscorrelated with the field which has been held the longest. Thus, for example, while the 25th field is being stored the 24th is crosscorrelated with the first. The temporal separation between crosscorrelated pairs is therefore equal to twenty three field periods, or 920ms, which should comfortably ensure that the images are uncorrelated. After the 25th is stored the next is loaded into the memory which had contained the first field while the second is crosscorrelated with the freshly stored 25th and so on.

Crosscorrelation is performed in an identical fashion to the autocorrelation process described in section 3-7 except that the pairs of coordinates that are subtracted occur in separate fields. Identical X and Y limits are imposed such that there exists a similar vector "window" to that produced by the autocorrelator (see figure 3.7). The crosscorrelation is stored in another 8K by 20bit integrating memory. Apart from the use of twenty five memories instead of just two, the logic and arithmetic operation is otherwise the same as that of the autocorrelator.

Whilst this design is in the process of being realised, however, a working interim crosscorrelator has been constructed which is essentially the same as that described above except that it stores just two frames at one time. It is designed to store any two odd or even

fields separated by any desired interval from ten fields (400ms) to infinity. After crosscorrelation has been performed two more fields separated by the same interval are stored and so on. The frames occurring during this interval remain unprocessed. Thus, to achieve the same signal-to-noise ratio as that of the autocorrelation produced from the same record, the interim crosscorrelator must examine data in real-time for the same period multiplied by a factor given by the crosscorrelation interval expressed in numbers of odd or even fields.

The interim crosscorrelator has provided the opportunity to investigate the temporal correlation properties of the atmosphere. Experiments are being performed which demonstrate the effects of the interval between stored frames on the form of the crosscorrelation and on the effectiveness of comparison with the autocorrelation seeing component. Valuable information is being obtained on the necessary interval required for complete decorrelation for different atmospheric seeing conditions.

The practical arrangement of the crosscorrelator is very simple. The device has no independent detection threshold or noise discriminators but is supplied the coordinates of image pixels direct from the autocorrelator. This arrangement ensures that the crosscorrelator and autocorrelator effectively process the same data, sampled in an identical manner. Thus the devices may run in unison, each storing data in separate integrating memories, enabling a comparison to be made in software.

3-10 Image monitoring and data display

The highest priority during observation is to obtain the best possible video tape records of the speckle images in accordance with the necessary intensity, image scale and other requirements. To reduce the possible effects of noise from other sources the tape recorder is supplied with its own direct line from the television camera. A second independent output from the camera is usually divided between a TV monitor, the hardwired autocorrelator and possibly an oscilloscope.

The Sony CVM100 UK monitor enables the observer to ensure that the

images are properly centred on the screen at a suitable image scale and that the atmospheric dispersion is properly corrected. If the detection of single photon events is required then the monitor indicates when it may be necessary to insert neutral density filters in the interferometer. TV monitoring also assists fine adjustment in the telescope guidance.

The autocorrelator is equipped with the facility to provide an immediate on-site display of the data held in its integrating memory. The 64 x 128 array memory is continuously scanned and outputed as a 64 line signal modulated by the contents at each memory location. A Tektronix 607A storage monitor is used to display the contents of the vector window, as shown schematically in figure 3.7, where the larger the number contained in a memory location the brighter the corresponding point of light on the storage monitor's green phosphor screen. The dynamic range of the display may be adjusted by means of the "display gain" control on the autocorrelator.

Whenever speckle data is processed a Tektronix 465B oscilloscope is employed to ensure that the detection threshold is at a suitable level and that no significant amount of noise is being sampled. It was mentioned in section 3-7 that the video signal has added to it an adjustable DC bias (the "video level") which is detected by the autocorrelator whenever it exceeds 1.1 volts above ground. By monitoring the TV image, or perhaps individual TV lines, on the oscilloscope the nature of the signal above and below this threshold can be observed. It is important, for instance, to ensure that the camera noise (see section 3-8) is kept below the sampling level at all times if possible.

A facility exists to monitor the number of arithmetic "operations" (which, as mentioned in section 3-6, is approximately proportional to the square of the number of detected pixels) per field. By connecting the oscilloscope to the output of the arithmetic logic unit, a band of pulses may be exhibited where each pulse corresponds to one vector calculation or "operation". The autocorrelator can process a maximum number of 512 image pixels per frame. If the number of pixels above the detection threshold exceeds 512 then all those occuring after the 512th

are ignored. When this condition exists an autocorrelation is produced that contains statistically fewer high Y value vectors than high X value vectors. To avoid this distortion the video level must be kept sufficiently low so that the observed band of pulses never reaches its saturation point.

3-11 Operational procedure

The facility to obtain on-site autocorrelations is generally only used as an opportunity for a first look and a check on the suitability of the data. On occasions it has been decided not to include the autocorrelator on an observing trip abroad. Keeping the device in the laboratory avoids the risk of damage during transportation and enables reduction of previous data to continue during the period of eight weeks or so it would otherwise have been away.

Setting up all the equipment before an observing session generally takes two or three hours. The interferometer is usually bolted to the Cassegrain mounting plate, and, in the case of the AAT, all other apparatus is secured within the Cassegrain cage. The 3.9m Anglo-Australian Telescope is shown in figure 3.11. The image intensifier is slowly run up to its optimum operating voltage of 40kV and the water supply for the solenoid is connected. With a suitable filter and objective in place the system is optically and magnetically focussed while observing a bright star. A minimum of two observers is required. While one operates the interferometer and tape recorder (i.e. from within the cage), the other, possibly with the help of a night-assistant, operates the telescope, provides the settings of the dispersion prism wheels (which are corrected for every new object or typically every twenty minutes during observation of any given object) and keeps a written log of all observations.

Each video tape may contain records of 60 minutes total duration. The length of each observation depends on the brightness of the object, the effects of noise in the system and the seeing conditions (including cloud). Typical observations range between 2 and 50 minutes each.

During autocorrelation of a video record, which is initiated by

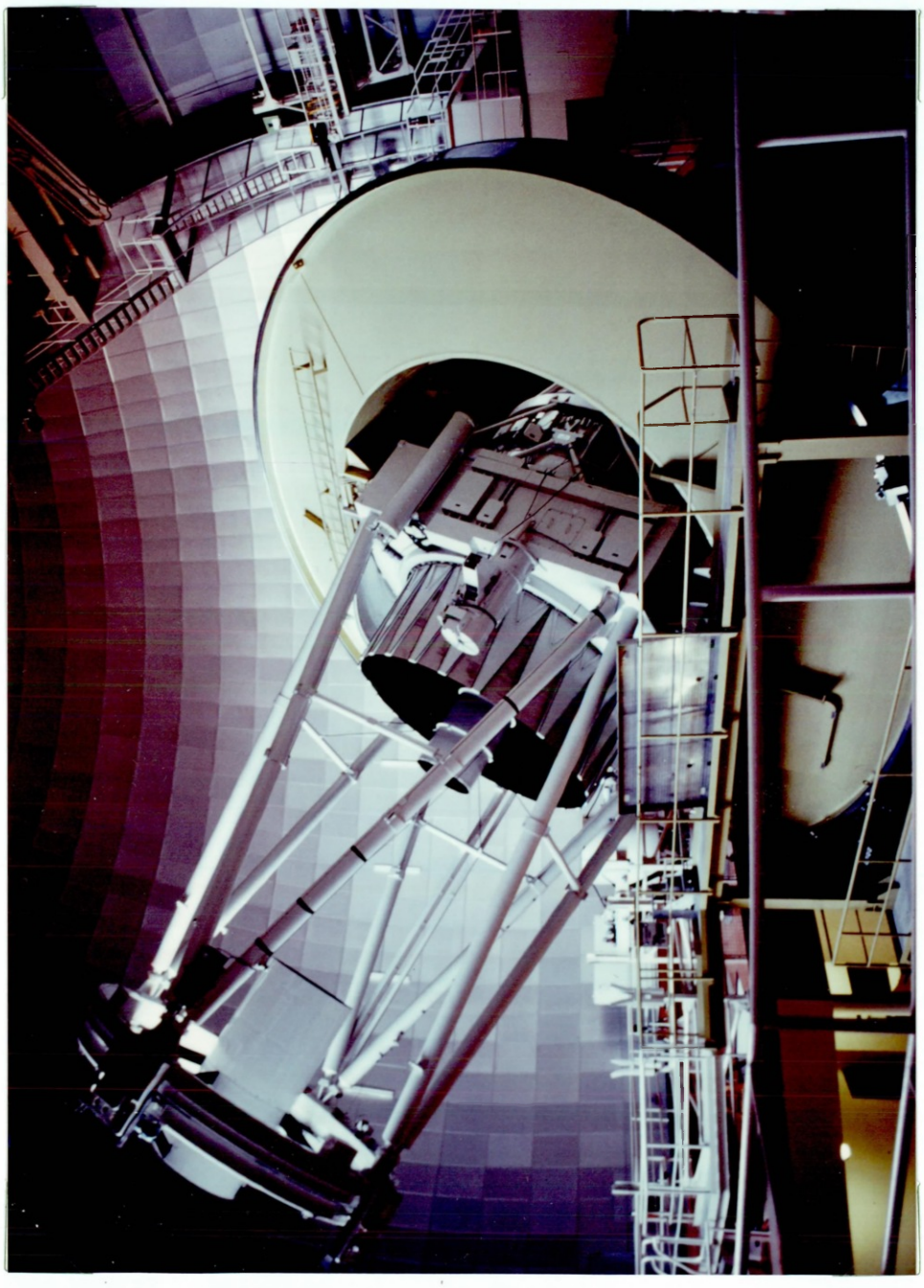

Figure 3.11 : The Anglo-Australian Telescope, Siding Spring

pressing the "start" button on the front panel, an array of LEDs indicate (in binary notation) the on-going total number of image pixels detected or, equivalently, the number contained in the central X=0,Y=0 pixel of the autocorrelation. When the "display" button is pressed autocorrelation is halted and the storage monitor displays the contents of the integrating memory. Autocorrelation is restarted without loss of the memory contents by pressing the "continue" button. Pressing the "start" button at any time causes the autocorrelator to restart processing with the memory cleared. The crosscorrelator operates in an identical fashion.

While using all the monitoring facilities described in section 3-10 data is processed using the noise discriminators when considered necessary. The overall signal-to-noise ratio is optimised by co-adding the autocorrelations obtained from odd and even fields of a video recording. The immediate product of this exercise is eight thousand, one hundred and ninety eight twenty bit numbers contained in 8Kx20bit RAM plus a low density qualitative display of its contents. The means designed to analyse the data are described in chapter four.

Chapter Four

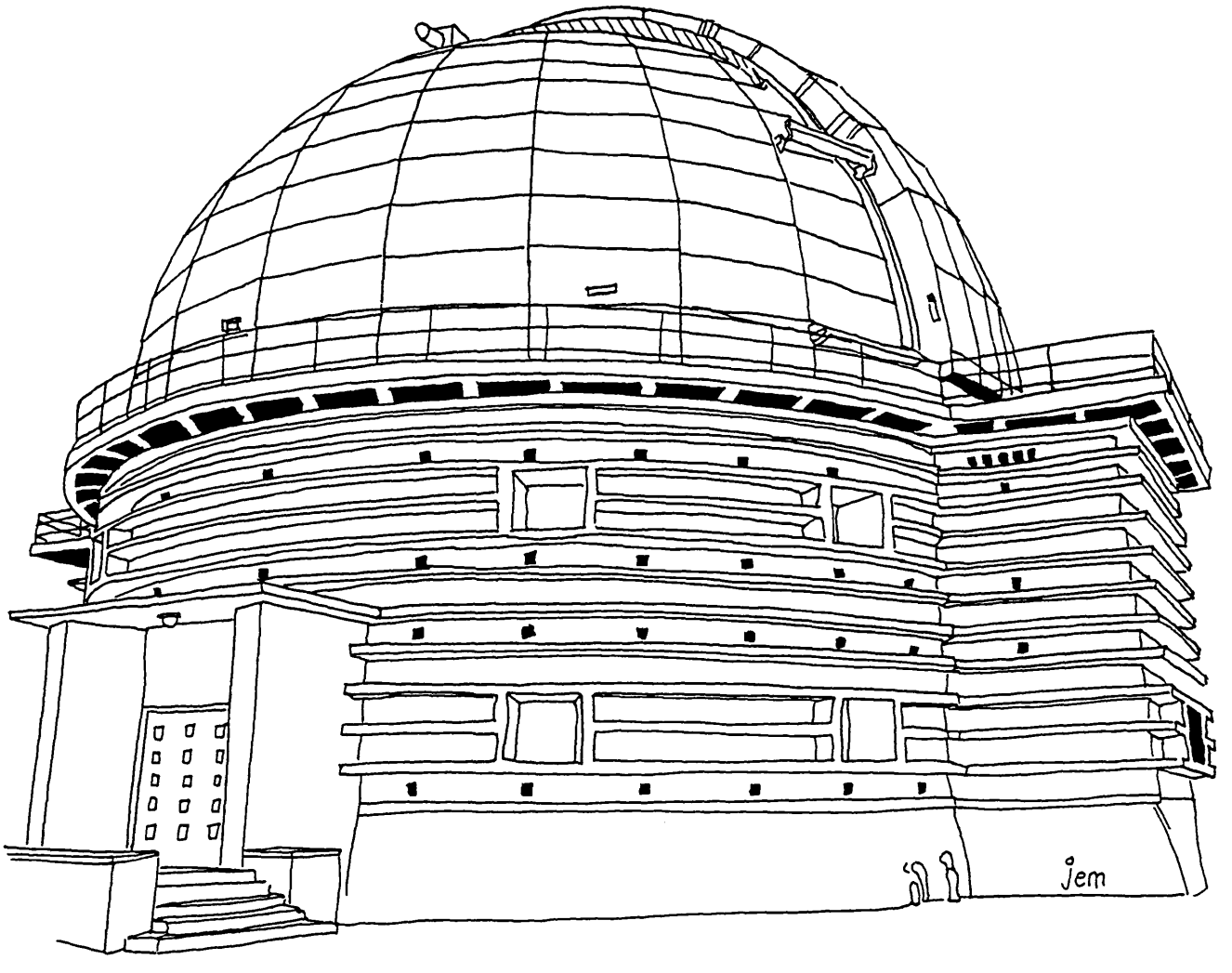

Chapter Four : Data Reduction Procedure

4-1 The profile selector

The storage monitor, as described in chapter three, is only of significant use when required to detect secondary peaks within an autocorrelation. The investigation of extended objects requires study of the autocorrelation speckle component (see section 2-5). Soon after the autocorrelator became operational a device was built which was designed to provide a temporary facility for such study while more efficient methods were being investigated. The device is known as the profile selector. In section 3-11 a description is given of an LED array which is employed to monitor the rate at which image pixels are detected. The LED array consists of three 7 segment alpha-numeric displays. The binary value corresponding to each segment is illustrated in figure 4.1. The profile selector enables the LEDs to display particular values contained in the autocorrelation memory corresponding to eight radial sections through the data. Note that "sections" are often referred to as being "profiles" of the autocorrelation. During autocorrelation of video data the profile selector knob on the front panel of the autocorrelator is set on the "autoc." position. In order to examine a section through an autocorrelation the knob is set at a position corresponding to one of the eight directions A to H as shown in figure 4.1. As a switch is toggled successive pixel values along the profile are indicated on the LED display. Translation of the numbers from binary notation to decimal enables a profile to be plotted by hand. In chapter five it is described how autocorrelation profiles are used to determine the extent of the object.

The profile selector is, of course, a very crude device which makes very inefficient use of the data stored in memory. A secondary peak produced from a binary star observation could only be detected in this way if it should lie within one of the eight profiles. Means of providing superior methods of data reduction are described in the following sections.

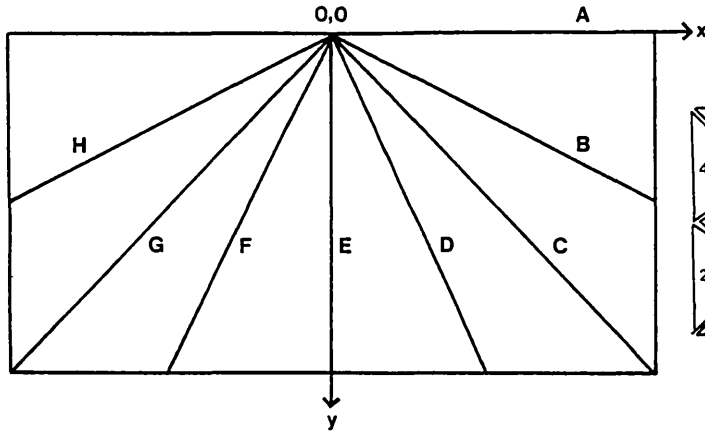

Figure 4.1 :

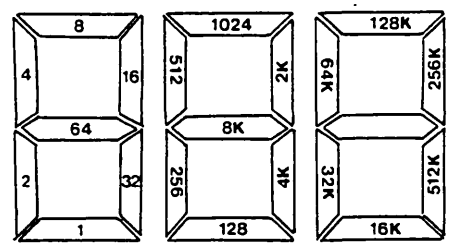

a) Selected profiles

b) The LED display

4-2 Mainframe computer systems

One of the initial requirements of the Imperial College real-time autocorrelator was that it should include the facility to transfer the contents of its memory to large computers such as the minicomputers existing at most large telescopes. Thus the autocorrelator was equipped with a CAMAC interface. CAMAC (Computer Automated Measurement And Control) is an internationally recognised system designed to provide a standardization of interface instrumentation linking large computers to other instruments. The autocorrelator's parallel port interface consists of twenty data lines, a data ready line and a data received line. By generating a data ready signal the autocorrelator informs the computer that it has a twenty bit number ready to send. The data received line enables the computer to tell the autocorrelator that it has read and stored the number and is ready to receive another. Thus the 8192 twenty bit numbers in the autocorrelator integrating memory may be transferred to a computer for immediate analysis or for storing on magnetic tape or disc.

The autocorrelator was used for the first time in late 1979 for a programme of binary star observations on the AAT. The autocorrelations obtained on site were successfully transferred to the AAT minicomputer and were displayed in the form of a two dimensional contour map. Polaroid photographs of the monitor screen provided hard copy of the display. The autocorrelations were also stored on magnetic tape and later examined using the Imperial College mainframe computer.

Recently data obtained on-site has been examined using the Manchester node of STARLINK. STARLINK is the name given to the system which links a large number of computers worldwide, enabling users to share software and data and to communicate efficiently and inexpensively.

In order to carry out examination of video recordings in the laboratory a link was established between the autocorrelator and the Imperial College Astronomy Group PDP-11 minicomputer. The autocorrelator was connected to the PDP-11 via a Nuclear Enterprises' parallel input register Type 9069 which is inserted in the PDP-11's CAMAC crate. This device provides the handshaking as performed in software by the PDP-11 and enables the data to be loaded into the computer memory. However, the PDP-11 CAMAC system exhibited a series of major hardware malfunctions. After repeated failure of the system to function correctly, alternative means of data reduction were considered.

4-3 Requirements of a permanent data reduction system

The use of mini or mainframe computers has several obvious advantages compared to the employment of smaller machines. There is often much readily available software, speed is high and memory capacity enormous. However there are significant disadvantages. The Astronomy Group PDP-11 is used by many persons and is thus only available for speckle data reduction for about one or two days per week on average. The autocorrelator may be linked to the PDP-11 either directly, which involves installing a large amount of equipment next to the computer, or via a long cable link to the speckle laboratory. Difficulties caused by operating both computer and speckle apparatus simultaneously makes using the cable link a very cumbersome process. If a system is required that

is dedicated to a particular task then smaller computers must be considered.

The amount of memory required to store a single autocorrelation or crosscorrelation is 8K by twenty bits. Thus if each number is stored as three bytes (24bits) the total memory needed is 24K, well within the capacity of many microcomputers. A data reduction system requires provision for high resolution graphics display and subsequent hard copy of autocorrelation contour maps, profiles and so on. A microcomputer-based system inevitably requires purpose written software and programming is usually limited to BASIC and machine code. The requirement for a suitable parallel port interface is a major consideration. Many microcomputers have no facility for twenty bit interfacing. Most current microcomputers use either audio tape or magnetic "floppy" discs for storage purposes. The use of discs, however, enables far quicker access to data and programs.

4-4 The Apple][and peripheral devices

The microcomputer chosen as the basis of a permanent laboratory data reduction system is the Apple][Europlus manufactured by Apple Computers Inc.. At the time the machine was acquired in early 1982 the Apple][was considered the most suitable mainly because of its peripheral card slot system. It is designed to enable up to eight peripheral devices or extension cards to be connected directly on to the main board inside the case. Two Rockwell 6522 Versatile Interface Adapters, inserted in two of the eight slots, provide a twenty four bit bidirectional port interface to the autocorrelator. The Apple contains 48K of memory and can be programmed using machine code and floating point or integer BASIC. In order to store programs of substantial length as well as an autocorrelation or crosscorrelation, additional RAM is necessary. This is supplied by a Ramex 16K memory extension card manufactured by Vergecourt Limited. Another slot is occupied by a disc controller card which links the Apple to a pair of Siemens disc drive units. These enable data and programs to be stored on 5-inch minidisks (Verbatim Datalife). The Apple is equipped with a green screen Transtec 1200 display monitor.

Permanent copies of computer generated graphics are produced using an Epson MX-80F/T Type II dot matrix printer. This is linked to the Apple by means of a Grappler interface card (Orange Micro Inc.). The printer is particularly useful for obtaining program listings and tables of raw data. High quality graphics are produced using a Hewlett Packard 7470A graphics plotter connected via an RS-232 serial interface card (C/WP).

Finally, a recent addition to the system is an Accelerator II card manufactured by Saturn Systems Inc.. This device replaces the Apple's (1 MHz) 6502 processor and memory with a new (3.6 MHz) processor and fast memory which enables the computer to perform all calculations nearly four times faster.

4-5 Data reduction software

A simple machine code program was written which enables data to be loaded into the Apple memory. It provides the necessary handshaking, reads each twenty bit number and stores it as three bytes. The 24K of RAM occupied includes space normally reserved for one of the two high resolution graphics screens and additional memory supplied by the RAM extension card. An autocorrelation or crosscorrelation is stored in memory locations 16384 to 40960 which correspond to the points from the top left hand position of the data as represented by figure 4.2 to the bottom right hand position, scanning horizontally. The data loading routine required a small amount of initial adjustment to establish the fastest baud rate compatible with error free transfer.

The main body of the data reduction software is written in BASIC. The initial requirement was the production of a single program which enables data to be loaded, stored on disc and displayed in suitable forms.

The program written to accomplish this exists in three versions known collectively as APLOT. The features common to each version include facilities to load and store data and to display any defined radial section through the data. One minidisk can contain up to five complete autocorrelations or crosscorrelations. Data can be transferred

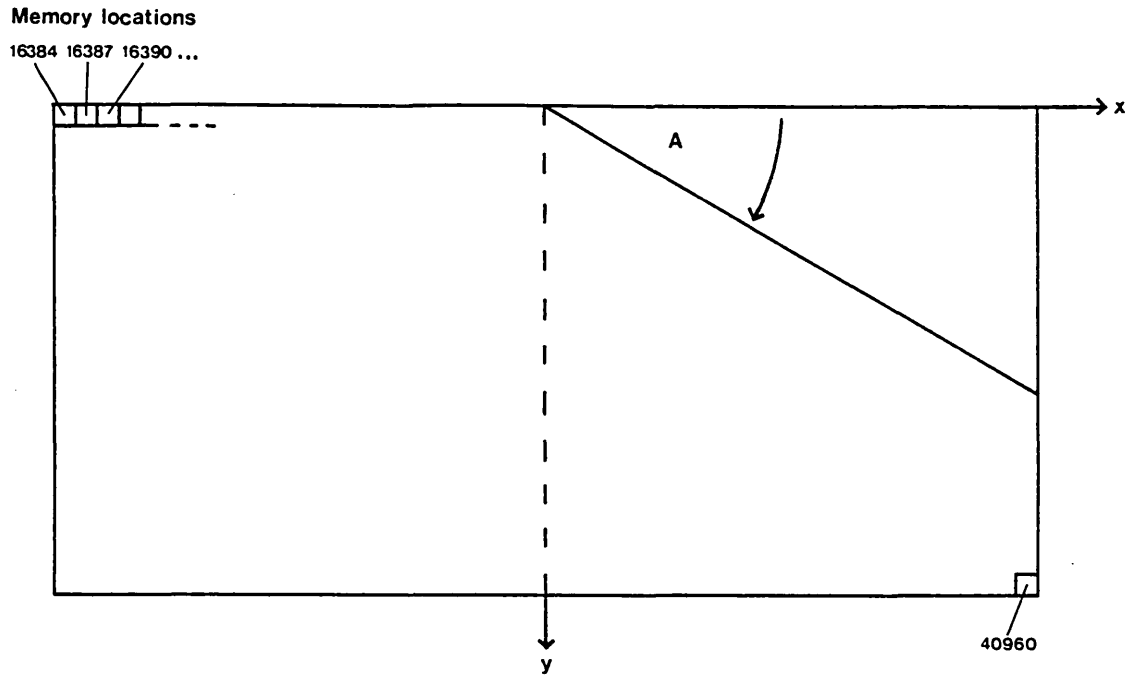

Figure 4.2 : Autocorrelation array and profile angle

to or from disc and loaded direct from the autocorrelator. Similarly, high resolution graphics displays can be saved on or loaded from disc.

The profile option featured on all versions of APLOT enables all or part of any radial section of the data to be plotted on the video screen. The profile is selected by defining the desired angle with respect to the horizontal axis, A, as indicated in figure 4.2. The displayed data is normalised between adjustable upper and lower limits and the axes are automatically scaled.

The first data reduction program, known as APLOT-1, includes additional options which enable data to be displayed in the form of a three dimensional distribution and a two dimensional contour map. It also facilitates the transfer of screen graphics and lists of raw data to the dot matrix printer.

A simple algorithm translates the coordinates and value of each element of data to an X,Y position on the graphics screen such that the whole autocorrelation or crosscorrelation is represented in three

dimensions, viewed with perspective from any given azimuthal angle and elevation angle. By defining suitable vertical and horizontal scales particular areas of the data can be examined in greater detail.

The contour display option represents each pixel of data as a square of colour within a two dimensional map. The entire autocorrelation or crosscorrelation can be displayed, or alternatively just the central 40 x 20 pixels represented on a larger scale. The representative colour (on a monochrome monitor this implies either black, white or "hatched") is dependent on the range of values selected to correspond to each colour. This form of display is similar to that obtained on the storage monitor except that the storage monitor can not indicate such fine detail in the distribution of the data.

Figure 4.3 shows an example of the three methods of data display mentioned so far produced using APLOT-1 and the dot matrix printer. The autocorrelation shown is that obtained from an AAT observation of the binary star ADS 1123. The visual magnitude of this star is 6.7 and the magnitude difference between its two components is 0.2. The autocorrelation represents 100 seconds of odd and even frame data. Using the convention as illustrated in figure 4.2 one can see from the contour map (centre of figure 4.3) that a large secondary peak is situated at an angle A of about 159°. The top illustration is the profile obtained at $A=159^{\circ}$. The vertical axis has been normalised to the value located at a radius of about 8 pixels.

Features unique to the second version of the program, APLOT-2, include a facility to calculate and display an azimuthally averaged (centro-symmetric) profile. The mean profile will naturally have a far greater signal-to-noise ratio than that of any given single section and will thus contain a much clearer indication of the nature of the speckle component (see chapter five). The option uses every pixel of data out to a radius of 63 pixels. Each pixel sampled has its value stored in an array element having an index corresponding to the distance of that pixel from the origin expressed in the nearest number of half pixels. The mean profile is then calculated by dividing each array element by the number of times that a value was added to it. Hence a profile is plotted in steps of half pixels.

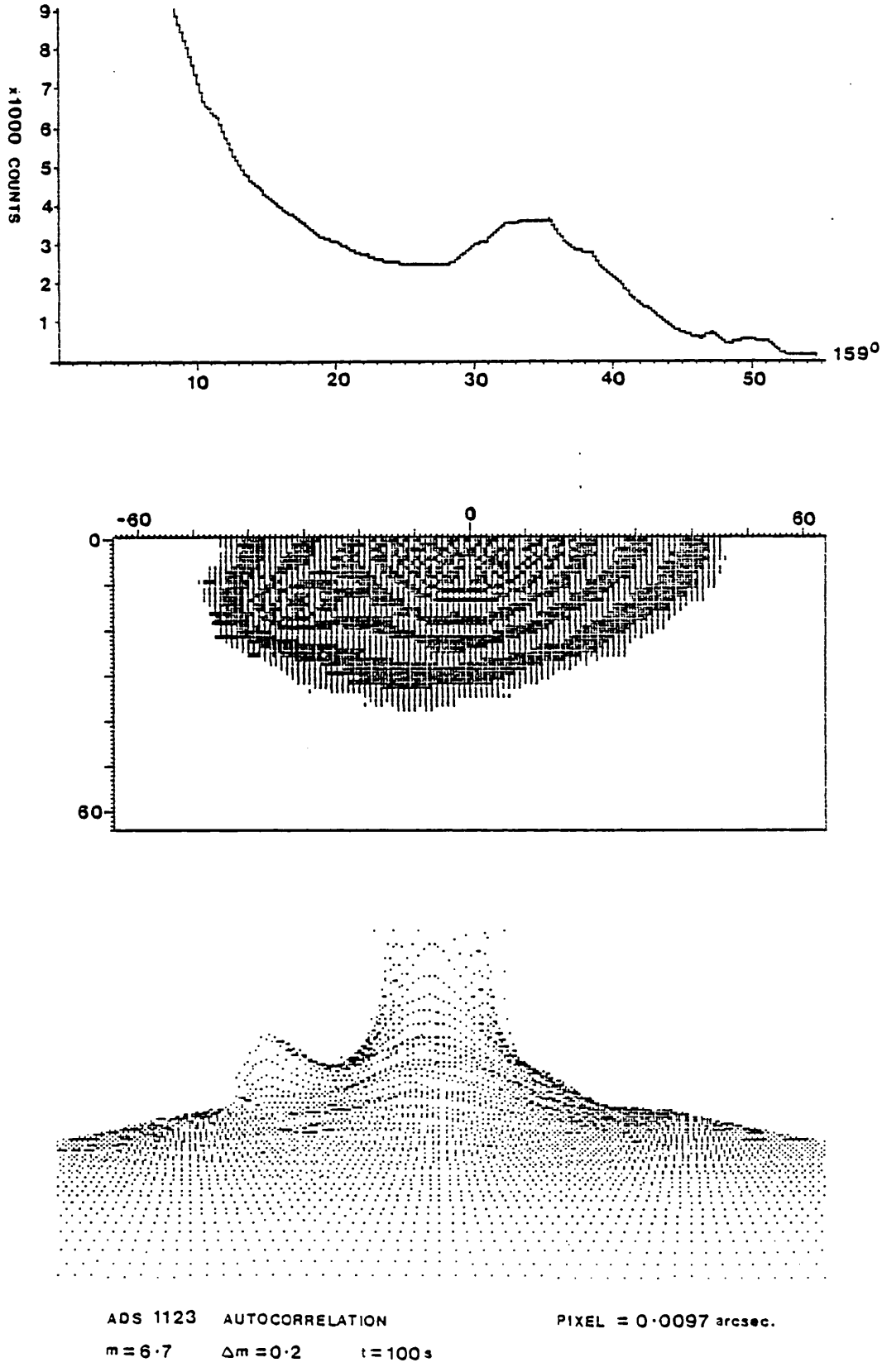

Figure 4.3 : Three displays of the autocorrelation of the binary star ADS 1123

Not all secondary peaks are as prominent as that indicated in figure 4.3. When the overall magnitude of a binary star is low and the magnitude difference between components is large (for example $m > 10$, $\Delta m > 3$) then it is likely that neither the three dimensional display or the contour map will exhibit obvious evidence of binary nature. A better method of detecting small secondary peaks (and note that a "peak" need not necessarily imply a reverse in the general gradient of a profile at any given point) is to examine the entire autocorrelation as a series of profiles. The APLOT-2 option which rapidly displays a series of profiles, sampled in steps of increasing profile angle A, is known for obvious reasons as the RADAR option. Profiles are displayed for a couple of seconds each, starting at $A=0^{\circ}$. The profile angle is continually incremented by a desired amount until $A \geqslant 180^{\circ}$. The profile corresponding to $A=180^{\circ}$ is, of course, equivalent to that corresponding to $A=0^{\circ}$.

The Apple's high resolution graphics screen is a 280 by 160 point grid. All the computer displays are confined to this area and however great the signal to noise ratio of the data, displays are restricted by the resolution of the screen. APLOT-3 enables data profiles and azimuthally averaged profiles to be plotted with far greater resolution using the Hewlett Packard graphics plotter. An A4 size graph can be produced with a resolution equivalent to approximately forty points per millimetre. The program contains a routine whereby the size of each axis is defined as a percentage of the paper dimensions. Incidentally, many of the figures shown in chapters five and six have been produced using APLOT-3.

Each version of APLOT is contained on a separate disc. When these discs are "booted" (i.e. when the system is switched on with the disc placed in the disc drive) a setting-up program is run. This establishes communication with the necessary extension cards and peripheral devices before loading and running APLOT.

Software is currently being developed which will automatically perform the subtraction of the seeing component of an autocorrelation by comparison to a crosscorrelation.

4-6 Operational procedure

Most observational records consist of frames containing discrete non-overlapping photon events. As explained in section 3-8, only for those records where the number of events per frame is very small is the detection threshold set very near the camera noise background level. As the detection threshold is increased the number of detected photon events increases due to the Poissonian pulse height distribution of the events appearing on the output phosphor of the image tube. Similarly, because of the peaked profile of the intensity distribution of a given event, the average number of detected pixels per event will also increase. For records containing a large number of discrete events the selection of the video sampling level is therefore a compromise between detecting as many events as possible and yet avoiding the 512 pixel per field saturation limit. Reaching this limit will result in a distortion in the data as described in section 3-10.

It was explained in section 2-5 that not all observations require photometric data. When investigating binary or multiple point objects it is to the advantage of the technique to utilise images which consist of very bright multi-event speckles. Such images are sampled by "clipping" each bright speckle at a video sampling level which is consistent with avoiding the saturation limit. Incidentally, since no single events are detected the autocorrelation of such a record does not strictly contain a "photon spike" but contains a highly distorted speckle component similar in shape to a typical single event component. This speckle component contains practically no information on the intensity distribution within a single speckle and is highly dependent on the detection threshold. The observer must ensure that the images are consistent with the type of information expected to be extracted from them. The determination of a suitable video level must therefore take account of the intensity of the image.

Autocorrelation of a given record is generally repeated using a range of video sampling levels and using discriminators if and when considered necessary. The odd and even field autocorrelations are co-added. Identical sampling parameters are used to produce crosscorrelations.

When the microcomputer system is booted the setting up and loading of APLOT takes about twenty seconds. A menu of options is displayed on the Apple's video monitor. One option on each version of APLOT enables data to be loaded from the digital hardware into the Apple's memory. Loading is initiated by toggling a switch on the front panel of the autocorrelator (or crosscorrelator) followed by the appropriate key on the computer keyboard. During the ten seconds it takes to load one autocorrelation (or crosscorrelation) a white spot scans vertically down the screen of the storage monitor indicating that data is being transferred correctly. When data has been loaded successfully the autocorrelation display returns to the storage monitor and the menu returns to the video monitor.

If after examination of the data the sampling parameters are considered reasonable for that record, the data is stored on a disc under a suitable filename. The stored data is registered in a log which contains a description of the section of video tape used, the video level, the state of the discriminators, the name of the object and the filename of the data.

The examination process depends, of course, on the type of information sought. For an object which has a completely unknown physical appearance it is usual to examine data initially using the three dimensional display and/or the contour map facility. These displays will indicate at once if there are one or more prominent secondary peaks and will show if there is a high degree of asymmetry due to a very irregular speckle component (i.e. the object is elongated).

A detailed search for less prominent peaks is accomplished using the RADAR option of APLOT-2. In order to sample every pixel out to a radius of, say, fifty pixels it is necessary that the angle of increment is no larger than one degree. In order to sample every pixel out to fifty pixels and yet examine data on a sufficiently large scale such that secondary peaks are clearly indicated, autocorrelations are often examined twice using RADAR: first data between radii of 0 and 46 pixels using an angle increment of 2.5° and then data between 17 and 63 pixels using an increment of 1°.

The radius to which the speckle component of an autocorrelation extends is often exhibited as a sharp deviation in gradient as described in section 2-5. If this component appears to extend to the same point in all directions, such as with an unresolved source, then a better indication of the nature of its distribution is obtained using the azimuthal averaging option of APLOT-2.

Useful data displays are printed out and the numbers which constitute a profile are often listed as well. The data reduction technique is described in chapter five.

4-7 Limiting magnitude

As explained in section 2-1 the technique of stellar speckle interferometry utilises a series of quasi-instantaneous images. A given image must contain a minimum of two photon events in order to derive useful information. If a sufficient amount of information is to be derived from a single observation of reasonable duration then this requirement implies a practical limiting magnitude for a given detector system. Observations of very large duration (in excess of one hour) are likely to experience large fluctuations in seeing conditions over that period. It is thus difficult to observe a reference star under similar conditions as the object. Very long observations are often impossible because of the necessity to observe the object sufficiently near to the zenith for atmospheric dispersion correction to be achieved (see section 3-2). The number of photons detected for a typical main sequence star using a 4m telescope is given by Pagel's "photon budget" formula:

$$\log N = 6.3 - 0.4m \qquad (4.1)$$

where N = number of photons detected per second per Å bandwidth,
and m = magnitude of the observed object.

Using the above formula the limiting magnitude for the Imperial College speckle system can be estimated. If the exposure time per field is 20ms and the optical bandwidth is 22nm (typical parameters) then in order to detect at least two events per image on average, Pagel's formula predicts that the object must be no fainter than about $m_v=16.6$.

Increasing the exposure time and bandwidth to 40ms and 200nm respectively suggests a magnitude limit of about $m_v = 20$.

However in practice the quantum efficiency of the detector is more likely to be of the order of one percent (this includes light lost at each reflection/transmission in the telescope/interferometer system). This reduces the estimated magnitude limit to 14.1 using the typical parameters, and to 17.3 using the larger exposure time and bandwidth. Recent observations of faint objects (see chapter six) indicate that the present system incorporating the image intensifier A, as described in section 3-3, has a performance as least as good as these latter figures predict.

The amount of information obtainable from an observation yielding a given number of events per field will naturally depend on the total number of processed images. In practice the length of time chosen for a particular observation is based mainly on experience gained from past observations of similar objects. For instance, using the typical parameters stated above the detection of a tenth magnitude binary star having components of equal brightness normally requires an observation with a minimum duration of about five minutes (using a 4m telescope). Using the relationship between the signal-to-noise ratio for binary star observations and the total number of events per frame and the total number of images, as defined by equation 2.6, the above result implies that the detection of a $m_v = 13$ equal magnitude component binary star requires an observation of no longer than 35 minutes.

Many recent observations have been of objects having quoted visible magnitudes of between 10 and 12. Estimates of surface brightness for extended objects however need to be related to the 3 to 4 square arcsecond area examined by the autocorrelator. In order to detect structure of these objects and be capable of detecting binary or multiple features with larger than zero magnitude differences the duration is typically not less than 40 minutes per observation.

4-8 System calibration

It was mentioned in section 3-3 that image intensifiers often

exhibit a net rotation of the image by a few degrees. This occurs because the electric and magnetic focussing fields are not exactly parallel. It is therefore usual practice to obtain a video record which indicates the precise orientation of the system with respect to the sky by recording the motion of a star across the TV image as the telescope is tracked from, say, east to west and north to south. The interferometer is usually mounted on the AAT such that the east to west direction approximately corresponds to the TV line scan direction. Crosscorrelations of the "star-trail" records exhibit an elongation in the direction of the star's apparent motion. This enables the exact orientation to be determined. The position angle of a binary star, defined as the orientation of the less bright component with respect to the brighter component measured from the north through east, is related to the autocorrelation profile angle for all AAT observations by the expression

$$P = A + 90^{\circ} \pm 180^{\circ} \qquad (4.2)$$

where P = position angle of the binary system,
and A = autocorrelation profile angle.

The only method of removing the 180° ambiguity without phase retrieval involves isolating individual double speckles on the video record and determining which component is the brighter of the two.

Once during each observation session, a brief (about 30 seconds) record is obtained of the camera signal while the camera cap is placed over the lens. By autocorrelating such a record, the video level at which camera background noise (and perhaps noise associated with electrical interference) is just detected may be determined. Thus, providing that there are a sufficient number of events detectable above this limit, these noise effects can be avoided.

If a record exhibits a low signal-to-noise ratio, processing of the data usually involves a series of autocorrelations. It may be established, for instance, whether features appearing in odd frames also appear in the even frames and whether the first half of the record indicates the same properties as the latter half. As described in section 4-9, comparison of data to that obtained from reference star

observations enables the elimination of many effects due to noise.

Additionally, a small amount of time is spent observing objects having well known parameters. Two examples of such observations are the binary star ADS 1123 and Europa, a moon of Jupiter which has a very well known diameter (see section 5-8). Beddoes [14] describes how artificially created binary stars enabled the performance of the cine camera system to be evaluated experimentally. These observations enable the actual performance of the system to be related to the predicted performance as described in section 4-7.

4-9 Reference star observations

Immediately after observation of every object of interest a record is obtained of an unresolved source in a neighbouring region of the sky. In order to be able to make a comparison of the data produced from the two observations, attempts are made to match the observing conditions as closely as possible. Often neutral density filters are placed in the optical path so that the intensity of the reference star image is equal to that of the object. Assuming negligible change in seeing conditions throughout both observations, if a star close in the sky to the object is chosen (Δ R.A. $\lesssim$ 5 minutes and Δ Dec. $\lesssim$ 3 degrees, but not necessarily in the same isoplanatic region), the seeing effects should be similar.

Data analysis is thus performed on both an object and reference star. Confidence in a result obtained for the object is much increased if, after removal of the seeing components from both sets of data by crosscorrelation subtraction or otherwise, the reference star indicates the result expected for a point source. Sometimes, however, the reference star may indicate evidence of being of binary or extended nature. Hence it is good practice to observe two or more reference stars per object.

Comparison to reference star data also assists the identification of spuriae due to various sources of noise which occur in both records.

Chapter Five

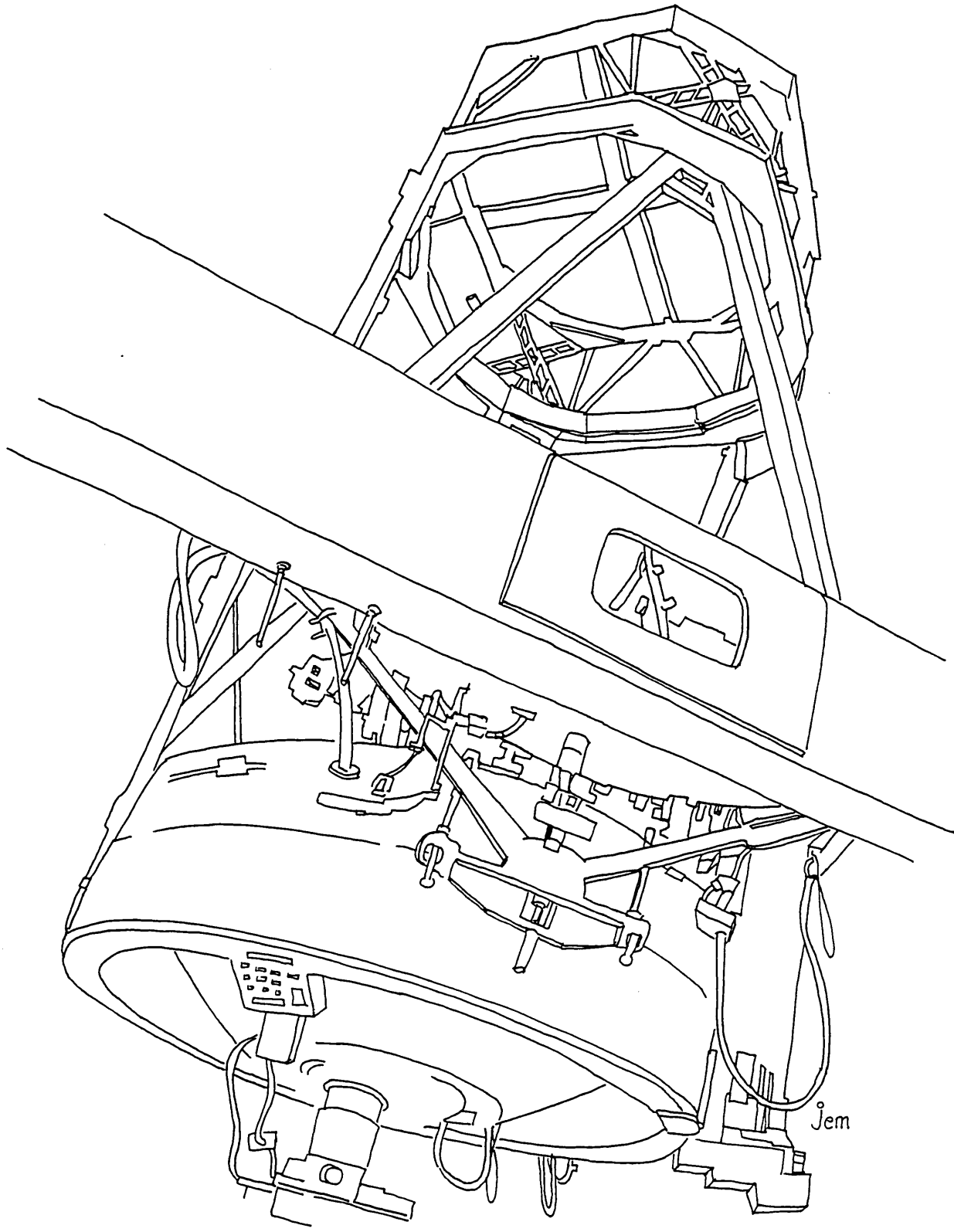

Chapter Five : Data Analysis

5-1 Introduction

The analysis of speckle data is based on the method proposed by Welter and Worden [19]. They suggest that the mean intensity of the crosscorrelation of pairs of speckle images sufficiently well separated in time may be subtracted from the average autocorrelation in order to obtain a result for the autocorrelated image that is unaffected by atmospheric turbulence (see section 2-6). However, as Dainty [2] shows, the procedure assumes Gaussian statistics for atmospheric wavefront perturbations which are known to be unrealistic (see section 5-3). Fante [65] and Bruck and Sodin [63] criticise the technique and from their calculations conclude that the method is particularly suspect when analysing images of objects whose angular extent are of the order of the size of the seeing disc. It has been suggested that the method could be improved by evaluating and subtracting the crosscorrelation of successive recentred images [55]. Dainty [2] also describes how the Welter and Worden method becomes entirely inappropriate for infrared speckle techniques.

Despite the unrealistic assumptions, the crosscorrelation subtraction method has been successfully implemented on several occasions [20],[21] and consequently a hardwired crosscorrelator, as described in section 3-9, has been built. During the period the device was being constructed seeing component subtraction was achieved using simplistic mathematical modelling. All the results presented in chapter six were obtained using this interim method. It is shown in section 5-3 that this elementary form of seeing component subtraction relies very strongly on the comparison of object and reference star autocorrelation profiles.

When the seeing component has been removed the information on the nature of the object intensity distribution is obtained by comparison of the residual data with speckle component profiles calculated for objects with known parameters (see section 5-6).

It was mentioned in section 2-7 that without phase information this

method is restricted to the investigation of binary and centro-symmetric objects. Objects with a high degree of asymmetry are often easily identified from an autocorrelation but, as described in section 5-7, obtaining a unique object intensity distribution from such data is impossible using the simple model comparison method. Problems associated with the contamination of the speckle component by the photon spike are discussed in section 5-4.

5-2 Binary star analysis

The determination of binary star position angles and angular separations are perhaps the simplest measurements made using stellar speckle interferometry. The technique has been very successful in this area. About two thousand speckle measurements of binary stars have been reported since the technique was first proposed in 1970, a large proportion of which have been made by McAlister [48],[49] from observations at Kitt Peak National Observatory. The astrophysical significance of binary star observations is briefly described in section 1-1.

The Imperial College speckle group has made a very large number of binary star observations using the interferometer in conjunction with the cine film system as described by Beddoes et al. [10]. Angular separations and position angles were obtained for many stars including some that were previously unresolved [13],[51],[52]. A few of the speckle observations of binary stars recorded on cine film were later imaged onto a CCD camera in order that data processing could be performed in software. These experiments, as described by Davies [53], enabled the CCD system to be tested and provided an opportunity to compare autocorrelation and Fourier transform methods.

Figure 4.3 shows an example of an autocorrelation obtained from the observation of a comparatively bright binary star (see section 4-5). As explained in chapter two the autocorrelation of such a record contains a secondary peak. This is generated by the vectors describing the relative displacement of the two components in each speckle image of the binary star. Usually the analysis of binary star autocorrelations involves the identification of secondary peaks and the precise

measurement of their position relative to the origin of the autocorrelation. If a secondary peak exists which is as conspicuous as that exhibited in figure 4.3, identification is extremely easy. However, binary stars with lower visual magnitudes and with greater magnitude differences will produce fewer vectors in the secondary peak (i.e. above the level of the seeing component) as a proportion of the total number of vectors in the entire autocorrelation. Identification thus becomes more difficult.

An autocorrelation pixel is equivalent in size to the resel as defined in section 3-5. The platescale at the Cassegrain focus of the AAT is 3.528 arcsec./mm and therefore, from equation 3.4, observations made using a microscope objective of 50mm focal length give rise to a pixel width of about 0.012 arcseconds. These parameters are typical for many observations. Calculations show (see section 5-5) that the Airy function of the AAT at a wavelength of 500nm has a distribution which is of significant amplitude over a diameter of more than 0.1 arcseconds. Thus, as will be shown in later sections, the speckle component of a point source autocorrelation typically extends to a radius of about ten pixels. Similarly secondary peaks produced in autocorrelations of binary stars extend over an appreciable number of pixels. Even very small secondary peaks (with, say, a peak height of only a few percent of the mean height of the seeing component) produce an anomaly in the general gradient of a radial profile which extends over at least five consecutive pixels. This enables them to be distinguished from random fluctuations (shot noise) in the data and systematic noise which occurs in isolated pixels or in lines of pixels (see section 3-8).

In order to establish the position angle ($\pm 180^{\circ}$) of an observed binary system the radial profile is found which appears to bisect the secondary peak. The autocorrelation angle of the profile, as defined in section 4-5, is then converted to a position angle using the relationship given by equation 4.2. The exact separation of the system is found by subtracting the seeing component from the profile and then measuring the radius corresponding to the centre of the peak. This is illustrated schematically in figure 5.1. Usually a very rough estimate of the form of the Gaussian-like seeing component below the peak is sufficient for this purpose. The angular separation is thus given by

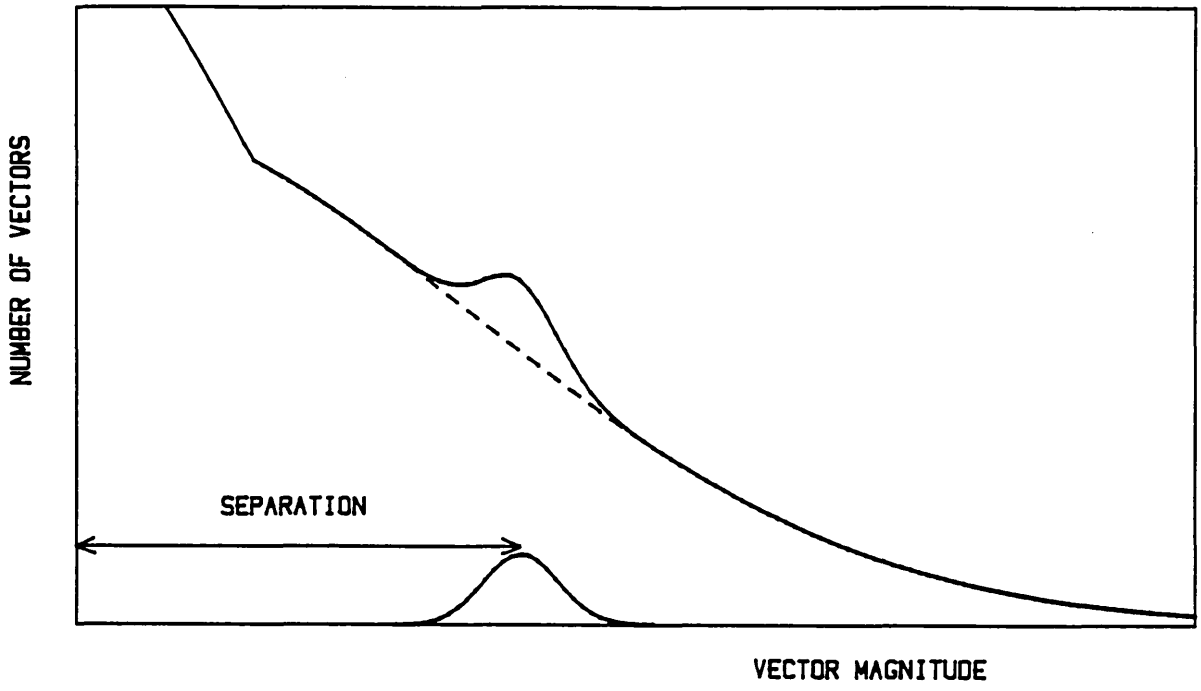

Figure 5.1 : Isolating a secondary peak

the radius in pixels at which the maximum of the peak occurred multiplied by the pixel width expressed in arcseconds.

It was mentioned in earlier chapters that the only method of removing the 180° ambiguity in the measurement of the position angle without phase retrieval involves isolating individual double speckles on the video record and determining which component is the brighter of the two. Using bright records where speckles on average contain a large number of events, this is perfectly feasible. Such records are favourable to binary star analysis. Unfortunately this method is almost impossible when applied to photometric data where speckles containing a number of events are few and are difficult to identify.

In principle the magnitude difference of the two components of a binary star can be obtained from analysis of the autocorrelation speckle component or, as proposed by Gezari et al. [9], by measurement of the fringe visibility of the Fourier transform. In practice, however, such analysis requires an extremely accurate calibration of the system using a reference star. Attempts by many observers to accurately determine

magnitude differences for binary stars using speckle interferometery have shown that such a measurement is, as Dainty [2] describes, "elusive".

Artificial binary stars corresponding to known magnitude differences have been created using a doubly-refracting calcite prism and a polarizer as described in section 5-8. Comparison of data with autocorrelations produced from such records enables a moderately accurate estimate of unknown magnitude differences to be made.

5-3 Seeing component modelling

Detailed analysis of diffraction limited information is achieved by subtraction of the seeing component from autocorrelated speckle data. As mentioned earlier, calculation of the mean crosscorrelation between pairs of speckle images separated by a sufficient period of time enables a reasonable subtraction to be made. While a hardwired crosscorrelator was being developed an interim method of subtraction by simplistic mathematical modelling was investigated.

Astronomers have often approximated the photometric profile of star images on long exposure photographs to a Gaussian distribution. Roddier [55] describes how, according to a theory of turbulence by Kolmogoroff (see Fried [54]), the atmospheric transfer function can be represented by the expression

$$T(u,v) = \exp -3.44\left(\lambda \sqrt{u^2 + v^2}\, / r_o\right)^{\frac{5}{3}} \qquad (5.1)$$

where u,v are spatial frequency coordinates,

λ = wavelength,

and r_o = the seeing cell diameter.

The long exposure stellar profile is given by the two dimensional Fourier transform of T(u,v). Roddier [55] states that, since the 5/3 exponent is nearly equal to 2, the transfer function and therefore its Fourier transform are nearly, but not exactly, Gaussian. King [59] found that a Gaussian curve fits observed stellar profiles reasonably well over the central one or two arcseconds. Woolf [17] compares a

Gaussian model with the above near-Gaussian model using the data obtained by King. Detailed experimental checks of the expression given by equation 5.1 have been performed by Roddier and Roddier [56], Kelsall [57] and Dainty and Scaddan [58]. Their results are consistent with the expected 5/3 exponential relationship.

The most satisfactory model for the complex amplitude of a wave propagated through the atmosphere is the log normal model in which the log amplitude and phase of the wave are each assumed to have Gaussian statistics (see Dainty [2]). The model has no simple analytic solution and requires extensive numerical calculations. Korff [8] has calculated the transfer function associated with this model and Aime et al. [61] and Chelli et al. [60] have made experimental measurements which are in excellent agreement with it. Roddier [55] suggests that transfer functions based on log normal statistics could be used to restore information provided that an accurate determination of r_o could be made simultaneously with the observation.

It was decided that since a modelling method was to be used only as a temporary solution, very simple models should be investigated first. The autocorrelation window, as described section 3-6, contains vectors whose magnitudes are typically less than about 0.8 arcseconds. Thus most of the azimuthally averaged profile of a reference star autocorrelation will be occupied by the seeing component alone. It can be shown that the autocorrelation of a Gaussian distribution is also Gaussian. Thus an investigation was made of the fit between the profiles of reference star autocorrelations and a Gaussian distribution.

The autocorrelation of the non-analytic expression for the long exposure profile given by the Fourier transform of equation 5.1 is also a non-analytic expression. However, the near-Gaussian expression itself was tried as a possible model for the seeing component. Experiments have shown that both Gaussian and near-Gaussian curves fit very well over the central half-arcsecond of seeing component profiles obtained from reference star autocorrelations. Figure 5.2 shows the two curves superimposed on an azimuthally averaged autocorrelation profile obtained from the observation of a point source. The photon spike (not all shown) and speckle component occupy the inner ten or so pixels. The

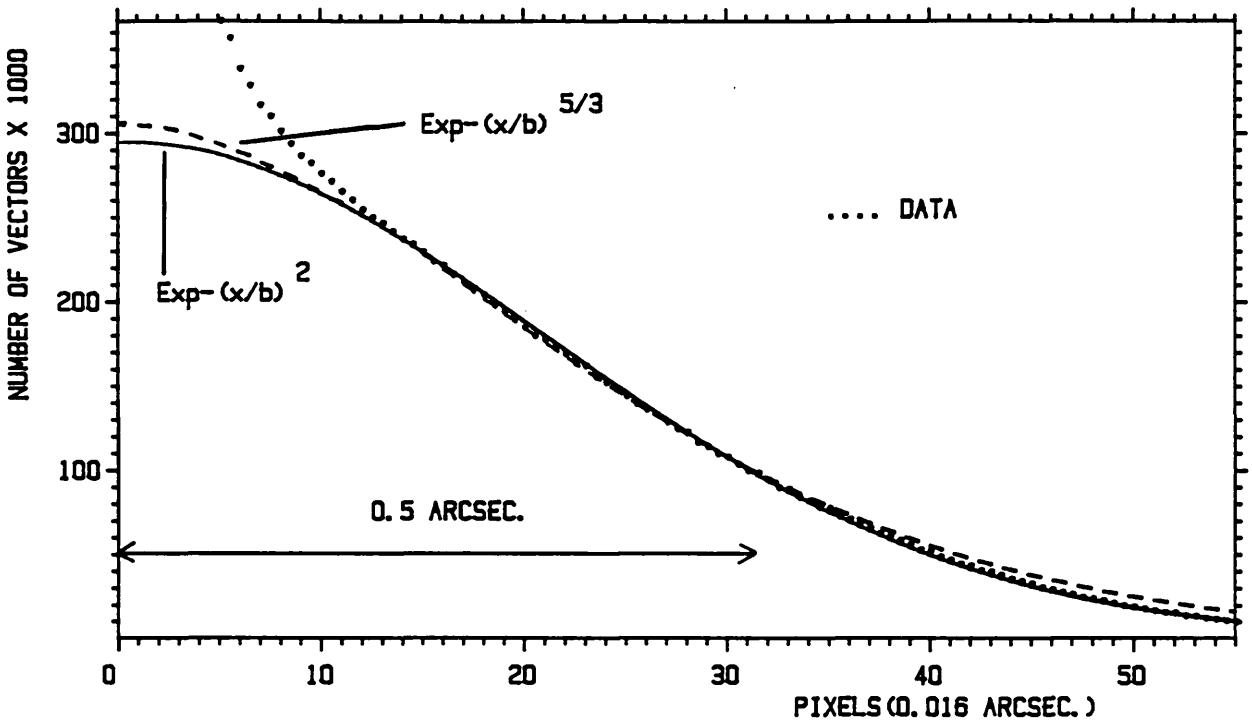

Figure 5.2 : Seeing component modelling

near-Gaussian fits slightly better at intermediate vector magnitudes while the Gaussian fits better at magnitudes greater than about 0.5 arcseconds. In practice curves are fitted by normalising to two arbitrary points on a profile which are both situated at sufficiently large vector magnitudes to be outside the region occupied by the speckle component. In figure 5.2 both curves are normalised to the data at pixel 15 and pixel 30. If the distribution of the object and reference star seeing vectors are assumed to be similar, a curve that fits the seeing component of the former will be expected to have a similar shape as a curve fitting the seeing component of the latter. This crude form of seeing component subtraction thus relies very strongly on the comparison of object and reference star data.

The match between data and a given model varies little between consecutive observations but data obtained from observations separated by a few hours, say, often do not match a given model to the same degree. Experiments show that the general shape of a best fit curve is little effected by changes in apparent brightness of the object (i.e. using neutral density filters) throughout constant seeing conditions.

Subtraction from the object profile of the reference star seeing component multiplied by a constant factor is very susceptible to shot noise in the reference star data and to slight changes in seeing conditions between observations. However, the crude modelling method assumes, correctly, a smooth distribution and accounts for slight changes in seeing conditions between observations by small adjustment of the exponent multiplying factor. Results obtained using this method are presented in chapter six.

5-4 The photon spike

Photon events occurring on the output phosphor of the image intensifier are imaged on to the Plumbicon tube of the TV camera so that they have a typical diameter equal to a spacing of about four TV field lines. The detected area of a given event will depend on the autocorrelator detection threshold but generally events are sampled over a diameter of between one and four pixels. As mentioned in section 2-5 this produces a central dominant component in the autocorrelation known as the photon spike. It is comprised of vectors between pixels situated within single photon events. The speckle centering device described in section 3-8 may be used to eliminate the photon spike but since it simply eliminates all vectors whose lengths are smaller than the dimensions of the photon events, information is lost. When photon counting, the autocorrelator's 512 pixel per frame limit (see section 3-6) is not normally approached so the centering device is not required to enable greater sampling rates either.

Figure 5.3 shows part of a typical azimuthally averaged autocorrelation profile obtained for a point source reference star. It indicates that a very large component dominates the central four pixels. Since, as is shown in section 5-5, the speckle component typically extends over the central ten pixels (the vertical scale of figure 5.3 is too large to indicate this) the photon spike covers only a part of the region containing diffraction limited information.

Because of the overwhelming dependence of the size and shape of the single event component on the video level (unlike the speckle and seeing components), reliable subtraction of it is extremely difficult. It is

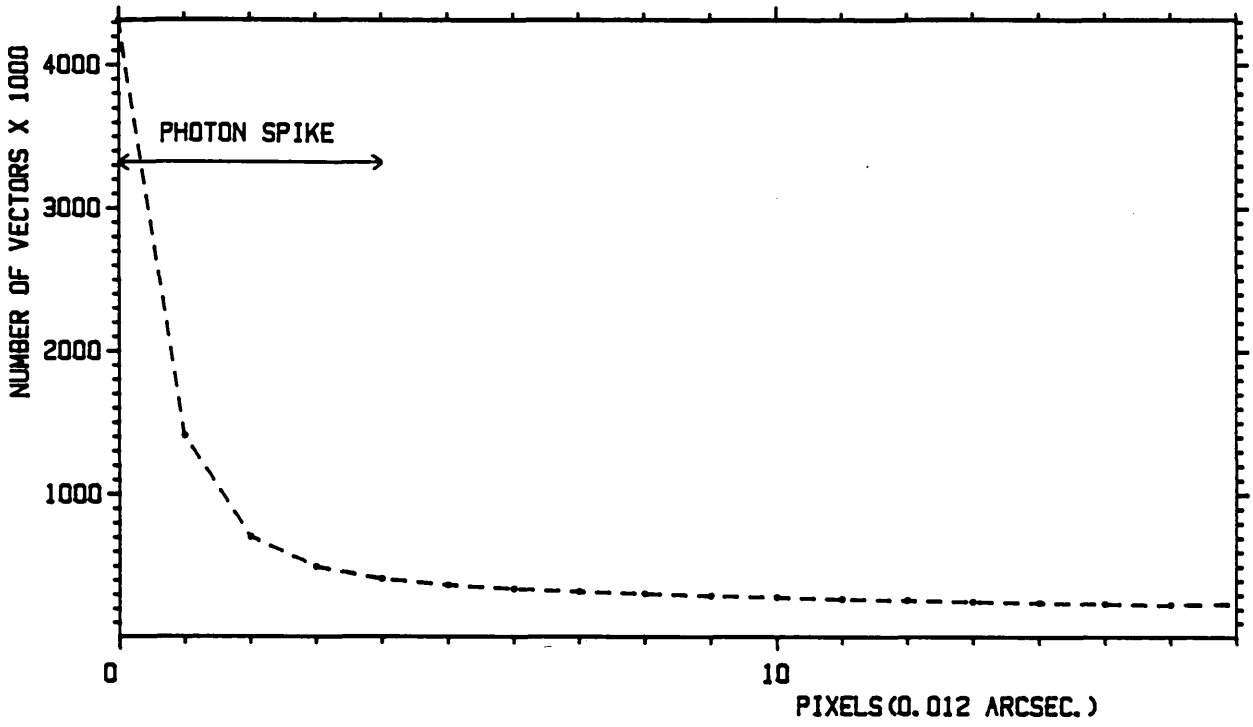

Figure 5.3 : A photon spike

considered that the best policy is to ignore the contents of the central four pixels and use the remaining uncontaminated region of the speckle component to derive available information. The success of this policy depends on choosing the image scale to ensure that sufficient speckle component data is outside the region of the photon spike (which is independent of image scale).

The effective diameter of photon events could be reduced by, say, halving the magnification between the image intensifier output and TV camera (which is currently one-to-one) while restoring the image scale to its former value by doubling the magnification produced by the objective lens. However, this would reduce the zenith angle over which atmospheric dispersion could be corrected with the existing prisms (486nm) from $\tan^{-1}2$ to $\tan^{-1}1$.

5-5 Speckle component modelling

Light from a stellar source which suffers identical atmospheric refractive index variations over the whole telescope aperture interferes

coherently to produce a single diffraction limited image, or speckle. Vectors between photon events occurring within the same speckle of a given quasi-instantaneous image will contribute towards a component within the data which may be considered as the two-dimensional autocorrelation of the photometric profile of the diffraction limited image. In order to determine the object intensity distribution, computer models of speckle components have been generated so that comparisons with the data can be made.

The intensity distribution of a single speckle is given by the quasi-monochromatic incoherent imaging equation (equation 2.2). Thus the autocorrelated speckle can be calculated from the expression given by equation 2.4 which is restated below.

$$C(x,y)=<[O(x,y) * P(x,y)] \bigstar [O(x,y) * P(x,y)]> \qquad (5.2)$$

where $O(x,y)$ = object intensity distribution,
$P(x,y)$ = point spread function of the telescope,
and * and $\bigstar$ denote convolution and spatial autocorrelation respectively.

In section 2-4 the process of spatial autocorrelation was represented in two ways. The first visualised the function as a distribution of vectors, representing the operation of the hardwired digital autocorrelator. The second equivalent approach considered an autocorrelation as the product of the overlapping regions between a distribution and a displaced version of that distribution as a function of their relative displacement. This second process represents the method employed to calculate model speckle components, as now described.

A speckle component modelling program is required to calculate a two dimensional intensity distribution of a speckle (assuming a non-aberrated telescope) and then autocorrelate that distribution digitally using the same sampling pixel area as the hardwired autocorrelator. The model speckle intensity distribution should be as close as possible to the analog photometric profile before the autocorrelation is performed. Since there are no simple analytic expressions for telescope point spread functions convolved with arbitrary object intensity distributions ,the computer is required to represent each function, and perform the

convolution, digitally. Both distributions are represented using a sample size equal to a quarter of the autocorrelator pixel width. Experiments have shown that this sampling cell is sufficient to ensure that the speckle profiles are smooth (i.e. similar to analog profiles) and that very little high frequency information is lost.

The modelling program was written in FORTRAN and is employed on a PDP-11 minicomputer. In a non-aberrated system the point spread function may be considered as equivalent to the Airy irradiance function or Airy pattern ([11] p352). Therefore the first task of the program is to calculate the Airy pattern of a given telescope. The intensity in the image plane of a telescope due to a point source is given by ([62] p424):

$$h(w) = h_o/(1-e^2)^2 .[\ 2J_1(z)/z - 2eJ_1(ez)/z\ ] \qquad (5.3)$$

where h_o = peak intensity,

$z = \pi Dw/\lambda$

D = aperture of telescope,

w = sine of angle subtended by point in image plane,

λ = wavelength,

e = obscuration ratio of the telescope (circular aperture),

and $J_1(z)$ represents the first order Bessel function of z.

On being provided with the aperture and obscuration ratio of the telescope and the wavelength and pixel size corresponding to the observation, the modelling program calculates a two dimensional Airy pattern which is digitised into quarter-pixels and stored in an array. A standard Bessel function subroutine is implemented.

Two versions of the modelling program exist, each providing a selection of possible object intensity distributions. The program known as MODELS calculates uniform (top hat) or limb darkened (cosine) intensity distributions of an object of any given angular diameter in an interval equivalent to a range between zero (a delta function) and fifty (typically equal to about 0.6 arcseconds) autocorrelation pixels. The second program, known as MODDIE, provides a fairly crude method of obtaining the autocorrelation speckle component profile from any centro-

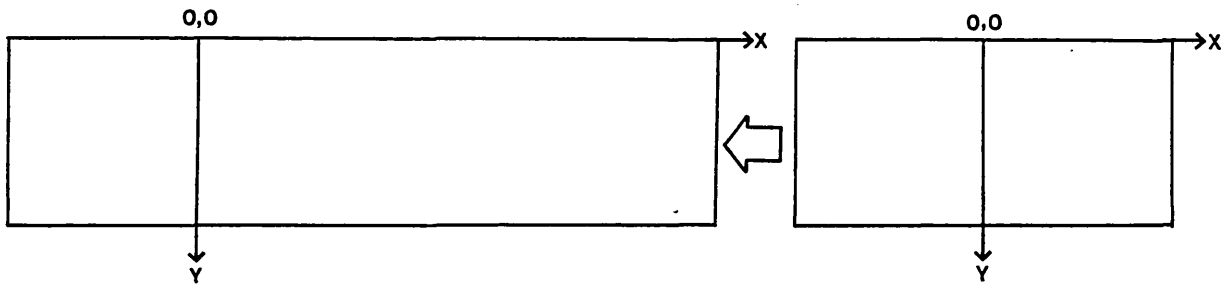

Figure 5.4 : Convolution between arrays

symmetric object intensity distribution. A one-dimensional object profile is entered in steps of quarter pixels and then expanded into a two dimensional array assuming linearity between any two adjacent points in the original profile. This method of expanding into a centro-symmetric distribution is reasonably accurate provided the profile is smooth.

The spatial intensity distribution of a speckle is equivalent to the convolution of the point spread function, or Airy pattern, with the object intensity distribution. Convolution between two functions may be performed in a similar manner to autocorrelation by overlap as illustrated in section 2-4. After reversing the sign of the coordinates of one of the functions (this is often called "flipping", see Hecht and Zajac [11] p405) convolution may be considered as the product of the overlapping areas of the two distributions as a function of their displacement. Because the distributions concerned here are both centro-symmetric, "flipping" produces no effect and is therefore not required. The convolution of two centro-symmetric functions is also centro-symmetric and therefore a great deal of computation can be

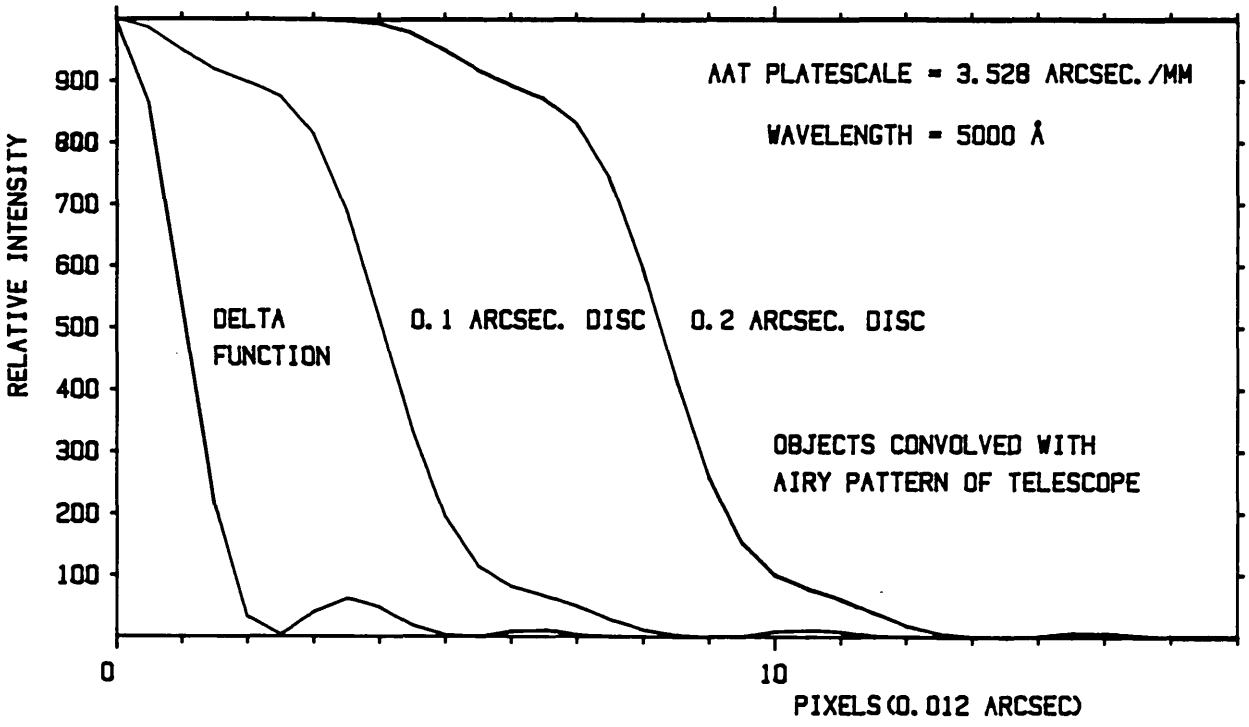

Figure 5.5 : Model image profiles

avoided by performing the process in one dimension and then expanding afterwards. Also, because of the symmetry, only one half of each distribution is required for computation and since no object and Airy pattern will overlap during displacement in one dimension by more than the extent of the Airy pattern, the object intensity distribution need only be determined over a narrow window as indicated in figure 5.4. The convolution of the two arrays as shown in figure 5.4 is computed by "superimposing" the X-axes of both and then calculating the sum of products of each overlapping pair of quarter pixels as a function of the displacement between the centres of the two distributions. All products between pairs not situated on the X-axes themselves are multiplied by two in order to account for the products effectively produced by the other half of each symmetric distribution.

The resultant one dimensional convolution profile represents the diffraction limited image of the object using a telescope with the given parameters. Figure 5.5 shows a series of image profiles calculated using the observational and telescope parameters as indicated.

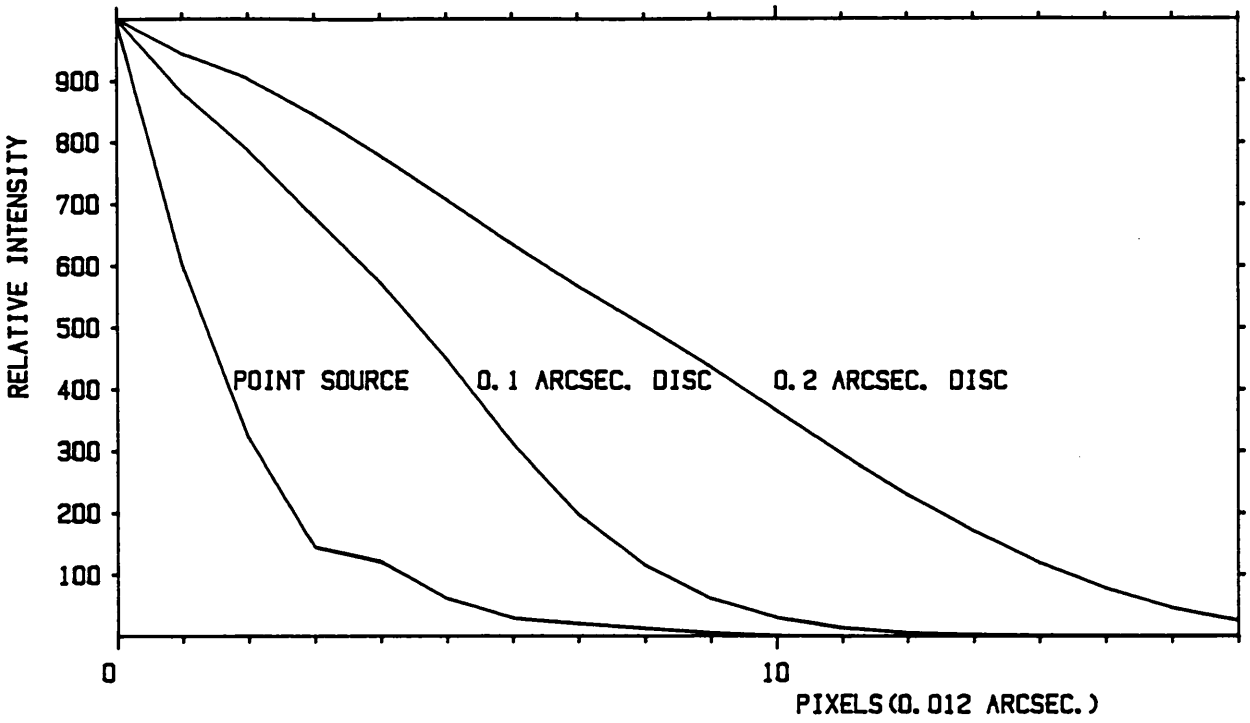

Figure 5.6 : Autocorrelated model speckles

In order to determine the digital autocorrelation of the speckle image, the convolution profile is expanded into two identical two-dimensional arrays using the method described earlier. Autocorrelation is then performed by finding the overlap products between the two arrays in an identical manner to the convolution (see section 2-4). The products are calculated for all overlapping pairs as the two arrays are displaced in steps equal to one whole autocorrelator-sized pixel. This process produces a one-dimensional profile representing the digital autocorrelation of a diffraction limited image using the same pixel size as the hardwired autocorrelator. Hence the profile should be a good approximation to the azimuthally averaged speckle component produced from the observation of an object with the given centro-symmetric intensity distribution.

Figure 5.6 shows model autocorrelated image profiles obtained for a point source and uniformly illuminated discs for AAT observations using a wavelength of 5000Å and a pixel size of 0.012 arcseconds. The profile for an unresolved source has a significant intensity extending to a radius of about ten pixels.

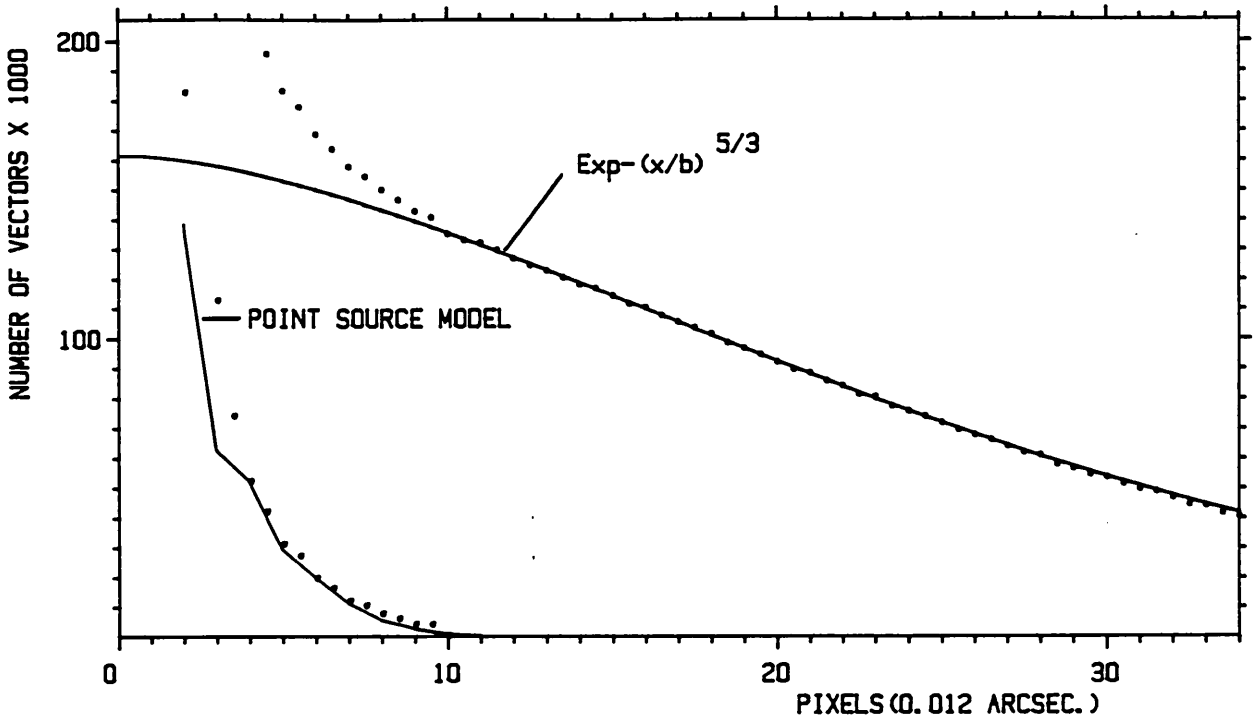

Figure 5.7 : Data analysis performed on the autocorrelation of an unresolved star

5-6 Angular diameter measurement of centro-symmetric objects

If the observed object can be considered as having a centro-symmetric intensity distribution, the first step in measuring its diameter is to obtain azimuthally averaged autocorrelation profiles of the object and its reference star. For a given number of events situated within a single speckle, the larger the speckle the greater the spread of vectors. Objects of small angular diameter, particularly point sources, therefore produce a greater number of speckle component vectors per given autocorrelation pixel than objects of larger angular diameter. Hence the speckle component produced by small speckles is usually exhibited more dramatically. When mean profiles have been obtained for both object and reference star a suitable seeing component model is fitted to the reference star profile at points well away from the region known to be occupied by the speckle component. Thus the seeing component is subtracted. A point source speckle component model, calculated using the known observing parameters and pixel size, is then fitted to the resultant curve at points outside the region contaminated by the photon spike.

Figure 5.7 shows the result of performing the above process on an azimuthally averaged autocorrelation profile of an unresolved source. It indicates that the computed model is in very good agreement with the speckle component. For unresolved or marginally resolved objects the choice of best-fit Gaussian or near-Gaussian seeing component model has negligible effect on the form of the estimated speckle component outside of the region contaminated by the photon spike.

If the process has worked sufficiently well using the reference star data, analysis of the object data can be undertaken with reasonable confidence. If it has not, and in the past this has only occurred when a reference star was proven to be binary, the error observed in the reference star measurement must be considered as a minimum margin of error associated with a measurement of the object. For reasons that were explained earlier, the point on an extended object autocorrelation profile at which the speckle component joins the seeing component is not always immediately obvious. However there will exist a point corresponding to a very definite, though small, anomalous change in gradient which is often best identified by viewing the profile edgeways on, along the line of the profile.

When this "kink" has been identified a model seeing component may be fitted at radii larger than that at which the kink occured. It is then subtracted from the profile. As explained in section 5-3, a near-Gaussian model fits seeing component data profiles better than a Gaussian at intermediate vector magnitudes. Thus a near-Gaussian model is generally used when the object is estimated as being no larger than about 0.3 arcseconds in diameter. At large vector magnitudes a Gaussian is a better approximation. However, if a fit is necessary at radii much greater than about 0.5 arcseconds, such simple models are often not accurate enough for the resulting curve to yield a reliable object intensity distribution. However, by assuming, say, a uniform illuminated disc model, a very accurate value for the mean diameter of the object may be obtained. Figure 5.8 (see section 5-8) shows the result of such analysis on the data obtained from an observation of Europa, a moon of Jupiter, which had a comparatively large angular diameter of 0.945 arcseconds. For extended objects of diameters less than 0.5 arcseconds this form of seeing component subtraction is usually

sufficient for the resulting speckle component to be compared with models of varying intensity distributions and for a reasonable estimate of the visual appearance of the object to be made.

5-7 Investigation of non-symmetric objects

Unfortunately complex non-centro-symmetric object intensity distributions can not necessarily be uniquely reconstructed from two dimensional spatial autocorrelations alone. Methods which have been proposed to solve the problem of image reconstruction are discussed in section 2-7. The only useful information that can be immediately derived from the autocorrelation obtained from the observation of an irregularly shaped object is that it is indeed irregular. Some of the asteroids observed recently (see chapter six) were known to be highly irregular in shape. Occultation observations have shown that nearly all major asteroids can not in fact be regarded as having centro-symmetric intensity distributions. However, given some assumptions about the object, such as that it has an elliptical shape and is uniformly illuminated, other information, such as the maximum and minimum diameters of the ellipse, can be determined.

5-8 Calibration observations

It was mentioned in section 4-8 that a small amount of time is spent observing objects having very well known parameters in order to determine the reliability of the instrumentation and the data reduction technique. An example of such an observation is that of the bright binary star ADS 1123. This was one of the first observations made when the hardwired autocorrelator began operation. The star and its autocorrelation are briefly described in section 4-5. Obtaining the striking result shown in figure 4.3 enabled further observations to be performed with increased confidence in the effectiveness of the system.

Many difficulties have been encountered by observers who have tried to determine the magnitude difference of binary stars from speckle data (see section 5-2). Beddoes [14] describes how the creation of artificial binary stars can be implemented in order to evaluate magnitude differences. A doubly-refracting prism is placed in the

optical path of the interferometer so that it produces two parallel beams of light of opposite polarization. By placing a rotatable polarizer in the optical train the relative intensities of the beams can be controlled while the total intensity remains constant. When inserted during the observation of a point source the device produces images with a double speckle appearance, similar to those of a binary star. Two calcite prisms have been made, enabling a choice of effective angular separation of the artifical binary star. From the known orientation of the polarizer with respect to the prism the effective magnitude difference of the binary star can be calculated. In principle, at least, the autocorrelation of records obtained in this way can provide a good indication of magnitude difference as a function of the relative size of the secondary peak. In practice, however, variables such as image brightness and video level complicate the effectiveness of this form of calibration.

In order to test the data reduction technique on a suitable extended object, Europa, a moon of Jupiter, was observed using the 1.9m Kottamia telescope in Egypt (shown in figure 5.9). Fly-by observations by the Voyager spacecraft in 1979 have enabled the diameter and albedo of the lunar-sized object to be determined very accurately [64]. Europa may be considered as having a uniform centro-symmetric intensity distribution with an angular diameter of 0.945 at the time of observation. Figure 5.8 shows three diagrams which illustrate the data analysis process for extended objects (as described in section 5-6) as performed on the azimuthally averaged autocorrelation profile of Europa. A kink indicating the edge of the speckle component was identified at about pixel 28. A Gaussian curve was then fitted to the data at larger radii as shown in the top illustration of figure 5.8. The diagram in the centre indicates the same Gaussian extrapolated over the remaining data. The kink can clearly be seen at a position approximately corresponding to the point where the Gaussian appears to diverge from the data. Finally, the bottom diagram shows the whole profile after subtraction of the Gaussian. A speckle component model was computed using the known angular diameter of Europa, assuming a uniform illuminated disc, and is superimposed on the data in the bottom illustration. The Gaussian fit was not ideal since it required fitting at radii where such simple models are known to be less accurate. A measurement of the angular

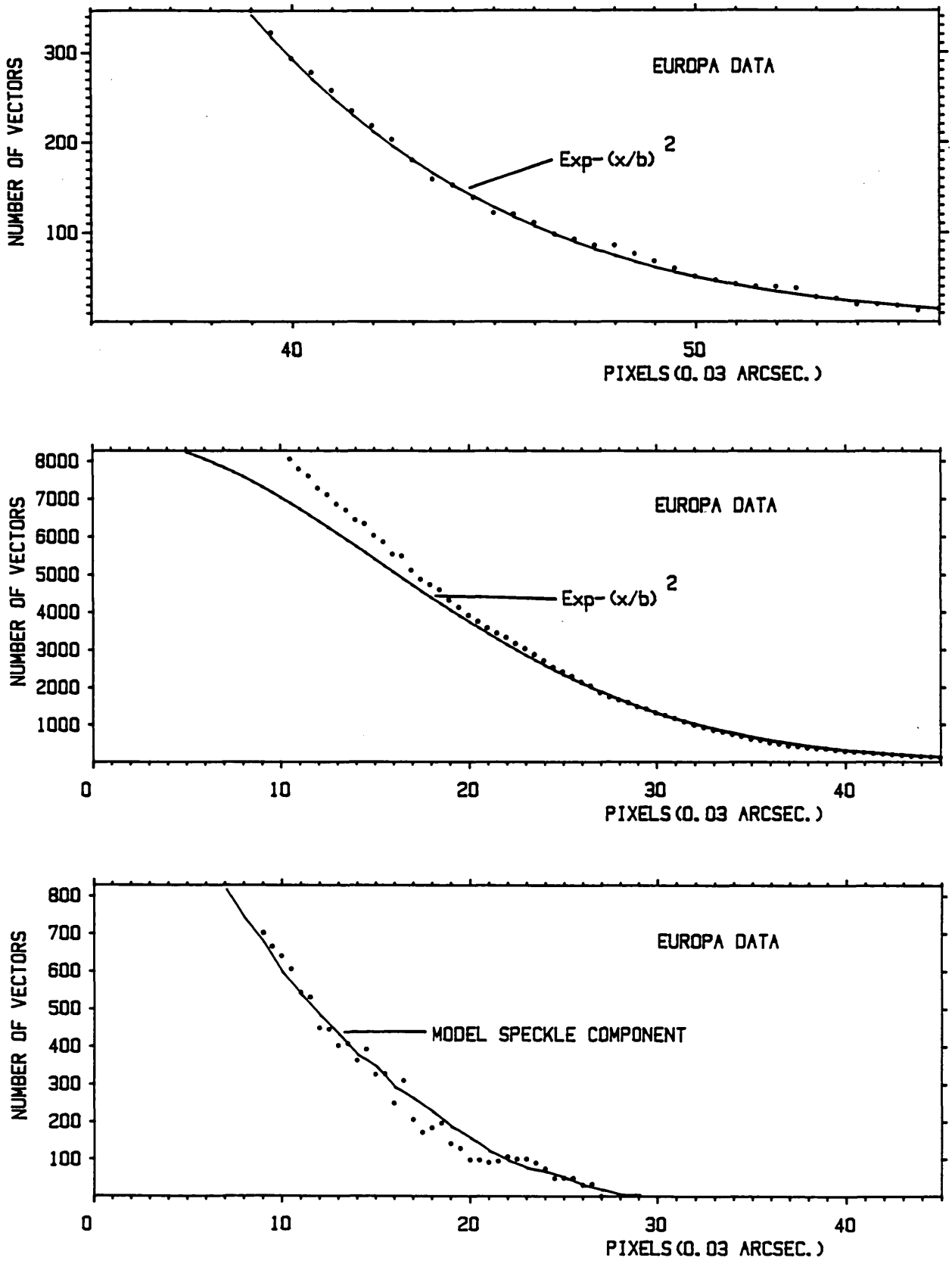

Figure 5.8 : The data reduction technique applied to the autocorrelation of Europa

Figure 5.9 : The 1.9m Kottamia telescope in Egypt

diameter of Europa by comparison with models corresponding to various angular diameters demonstrates an accuracy of about 15 percent. Nevertheless the result obtained appears to confirm that the reduction technique is very effective.

5-9 Sources of error

Speckle interferometry enables separations and position angles of binary stars to be measured very accurately. In practice the error in such measurements is usually no greater than the width of a single pixel. If the signal-to-noise ratio for the observation is exceptionally good, however, the position of the exact centre of a secondary peak can be estimated to within a fraction of a pixel.

It has been stressed throughout this chapter that the data reduction technique for extended objects is still at an experimental stage and has involved some simple, perhaps over-simplistic, interim measures. Crude forms of seeing component subtraction must obviously involve a degree of error (since the atmosphere is known not to conform to such models), though maybe not appreciably more than the crosscorrelation method which is currently being investigated.

As explained in section 3-3, photon events occur on the output phosphor of the image intensifier with a range of intensities such that, at a given detection threshold, they generally have a detected diameter of between one and four pixels. Figure 5.3 shows the effect this has on the central four pixels of a typical autocorrelation profile. If every single photon event had a detected diameter of, say, four pixels, speckles (i.e. the speckle component) would appear correspondingly broadened. However, the shape of a typical photon spike suggests that the majority of events are, in fact, detected as single pixels and relatively few occur with a detected diameter of three and four pixels. Experiments with reference stars have shown that for reasonably high signal-to-noise data the sampling level has negligible effect on the form of the speckle component. Therefore the overall shapes of speckle components are not appreciably affected by the apparent size of detected photon events. Nevertheless, if such broadening is observed on the reference star profile, an equivalent broadening error must be

associated with a measurement of the object.

Naturally, it is expected that the smallest object diameter which may be determined using the methods described in this chapter will not be less than the diffraction limit of the telescope. Figure 5.6 shows that there is significant intensity variation between the expected speckle component profiles produced by objects of 0.2, 0.1 and zero (point source) arcsecond diameter. In practice, however, the "lower resolution limit" depends on the signal-to-noise ratio of a given set of data. In most cases this limit is estimated as being between 0.03 and 0.1 arcseconds when the diffraction limited resolution is about 0.03 arcseconds. If a speckle component of a large extended object is clearly indicated then its diameter may usually be estimated to within the dimensions of a single pixel, typically about 0.012 arcseconds.

All forms of seeing component modelling assume negligible change in seeing conditions (constant r_o) over the duration of the observation. In practice this is not always so, particularly when the sky contains thin cloud. The autocorrelation of a point source observation which experiences, say, a period of one arcsecond seeing followed by a period of 0.8 arcsecond seeing will contain two distict seeing components. This would produce an anomaly in the gradient of the autocorrelation profile which could, perhaps, be confused with the presence of a large extended component in the object. A crosscorrelation indicates the same effect, of course, but prior to the operation of the hardwired crosscorrelator the only way of eliminating such a possibility was to autocorrelate separate parts of the video record.

It will be shown in chapter six that the data reduction technique has enabled a number of very valuable astronomical discoveries and measurements to be made. Progress towards greater accuracy has hopefully begun with the introduction of the hardwired crosscorrelator and may continue with the possible utilisation of one or more image reconstruction techniques in the future. This would overcome the awkward restriction which limits observations to objects having, or at least which are assumed as having, centro-symmetric intensity distributions.

Chapter Six

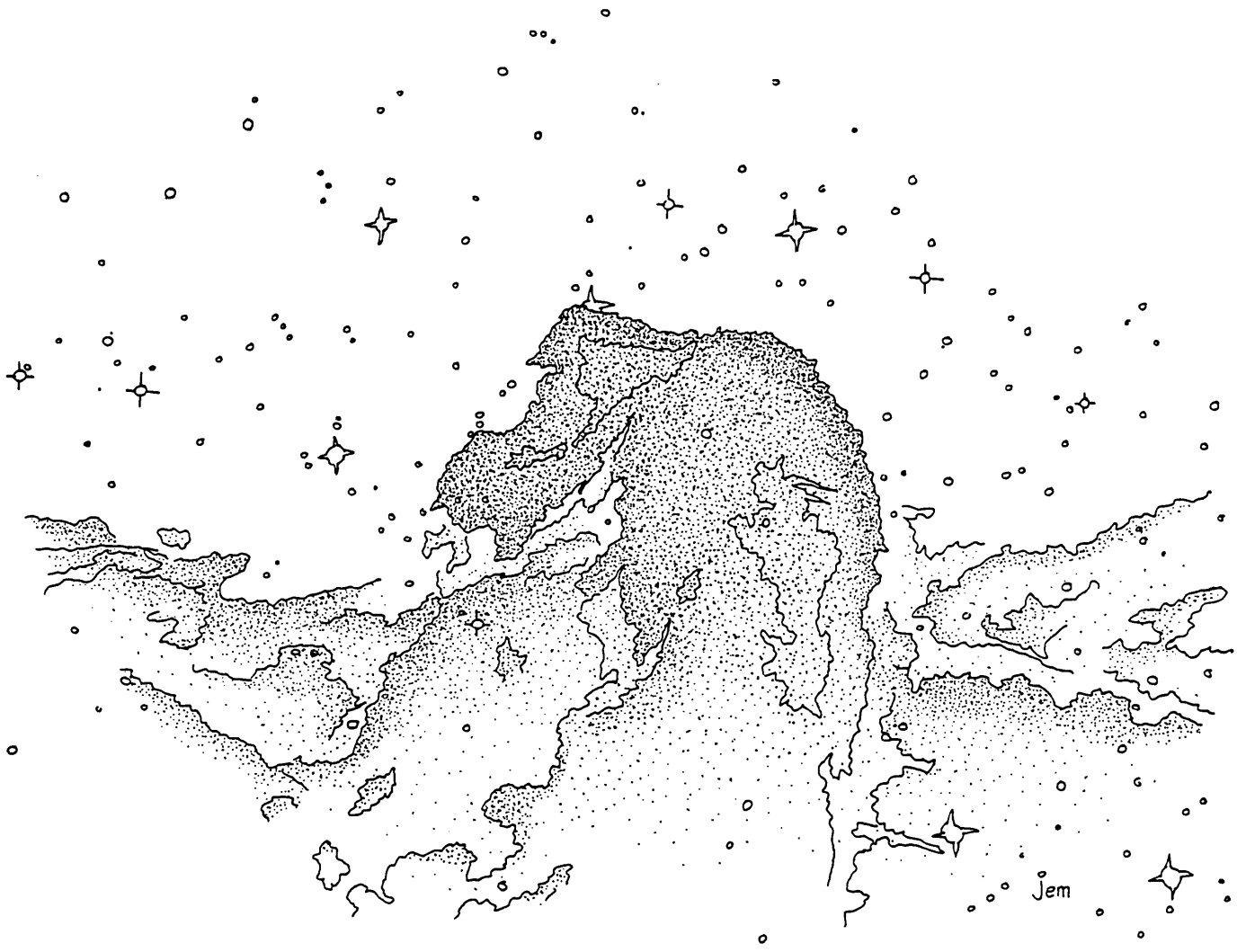

Chapter Six : Astronomical Results

6-1 Introduction

Throughout the development of the system described in earlier chapters, several collaborative observing programmes have been undertaken and many significant astrophysical results have been obtained. The results presented here have all been achieved using the hardwired autocorrelator prior to the introduction of the cross-correlator. Each result represents the product of detailed analysis of video records in the laboratory.

A programme of observations requiring the detection of binary stars is currently being undertaken and the results obtained so far are presented in section 6-2. Recent attempts to determine the form of some of the larger asteroids are described in section 6-3 and a preliminary measurement of the mean diameter of Herculina is given. Sections 6-4 to 6-8 describe in detail the investigations made in collaboration with Dr John Meaburn of the University of Manchester.

6-2 Hipparcos stars

In chapter one it was mentioned that the Space Telescope, which will have a 2.4m aperture, is due to be placed in orbit around the Earth in 1986. For the first time it will be possible to directly obtain stellar images which are unaffected by atmospheric turbulence. Naturally observations of faint extragalactic objects will be of particular interest. Within about two years of the introduction of the Space Telescope, the European Space Agency (ESA) plans to launch the Hipparcos Astrometry Satellite [82]. This will scan the celestial sphere making accurate measurements of the positions of about one hundred thousand stars in order that a large stellar reference frame can be established. It is required, however, to relate this reference frame with a number of extragalactic objects and 75 radio sources have been selected for this purpose [83]. Since few of the sources are sufficiently bright at optical wavelengths for measurement by the Hipparcos satellite, indirect methods are being applied. It is intended to link the Hipparcos reference frame to the extragalactic frame

observed by the Space Telescope. In order to achieve this a number of stars which may be observed by both instruments are required. The fine guidance sensor of the Space Telescope has a maximum field of view of approximately 18 arcminutes. Thus a Hipparcos link star must be situated within 18 arcminutes of the radio object. In order to protect the sensitive Space Telescope detector system from exposure to excess intensity, observation without filters is restricted to objects no brighter than ninth magnitude. The smaller aperture Hipparcos satellite telescope is limited to the observation of stars no fainter than thirteenth magnitude.

It is hoped that the accuracy of the measurement of the angular separation between an extragalactic object and a Hipparcos star will be within ± 2 milli-arcseconds [81], which is of the same order of accuracy as that of a positional measurement by the Hipparcos satellite [85]. To achieve this accuracy it is necessary that neither of the objects shall display structure above the optical resolution limit of the Space Telescope, which is about 0.05 arcseconds. Additionally, there must be no companion star of comparable brightness within 15 arcseconds of the the Hipparcos link star. A star located in this region would be included in the instantaneous field of view of the Hipparcos satellite and would thus perturb the measurement unless that companion was at least 3.5 magnitudes fainter. ESO and SRC sky survey prints were examined for stars which were suitable for linking the two reference frames. The stars that were selected had no visible companion between the resolution limit of the prints, which is about 2 arcseconds, and 15 arcseconds. Most of the selected stars are the SAO or AGK3 star nearest to the radio object concerned.

Speckle interferometric observations enable structure below the 2 arcsecond limit to be detected. Thus it was arranged for stars in the northern hemisphere to be tested by Hemenway, Franz and McAlister at the Lowell Observatory while the southern stars are examined using the Imperial College speckle interferometer and hardwired autocorrelator in collaboration with Dr Noel Argue of the University of Cambridge [104]. Incidentally, the candidate stars situated in the declination range +5° to -5° are being observed by both parties in order to demonstrate the reliability of the respective systems.

Most of the 37 southern stars tested so far have been observed using the AAT which has a diffraction limited resolution in the visible of 0.03 arcseconds. During a recent visit to Lowell Observatory (see section 6-3) a small number of the southern candidate stars were observed using the Perkins 1.8m telescope which has an optical resolution limit of about 0.06 arcseconds.

The autocorrelator's facilty to provide real-time on-site results proved to be extremely useful. Each autocorrelation was briefly examined using the storage monitor as described in section 3-10. If there was any evidence of structure, another link star associated with the same source was selected to be observed next. If the star showed no structure, a candidate star associated with a different source was chosen. Most of the AAT observations used a 20ms exposure time (increased to 40ms during a short period of moderate cloud cover), a 50mm focal length objective and a 5000Å filter with a 220Å bandwidth.

All the video records of the stars were later examined in detail in the laboratory. Of 37 of these, three showed definite evidence of binary nature and seven others exhibited marginal evidence of structure. The upper limit for detection of structure imposed by the autocorrelation window corresponds to a binary separation of about 0.7 arcseconds for the AAT observations and about one arcsecond for the few observations made with the Perkins telescope. The three confirmed binary stars and their observed separations and position angles (± 180°) are listed below.

Star	Date	U.T.	Separation (arcsec.)	Position Angle
SAO 230558	28-Oct 82	10:20	0.179	142°
SAO 126934	28-Oct 82	11:11	0.256	235°
SAO 165283	28-Oct 82	12:05	0.262	245°

Table 6.1 : Confirmed binary stars

A complete list of all the 37 stars observed, including those of suspected multiple nature, is given by Argue et al. [104]. Figure 6.1 shows the secondary peaks exhibited in each of the autocorrelations

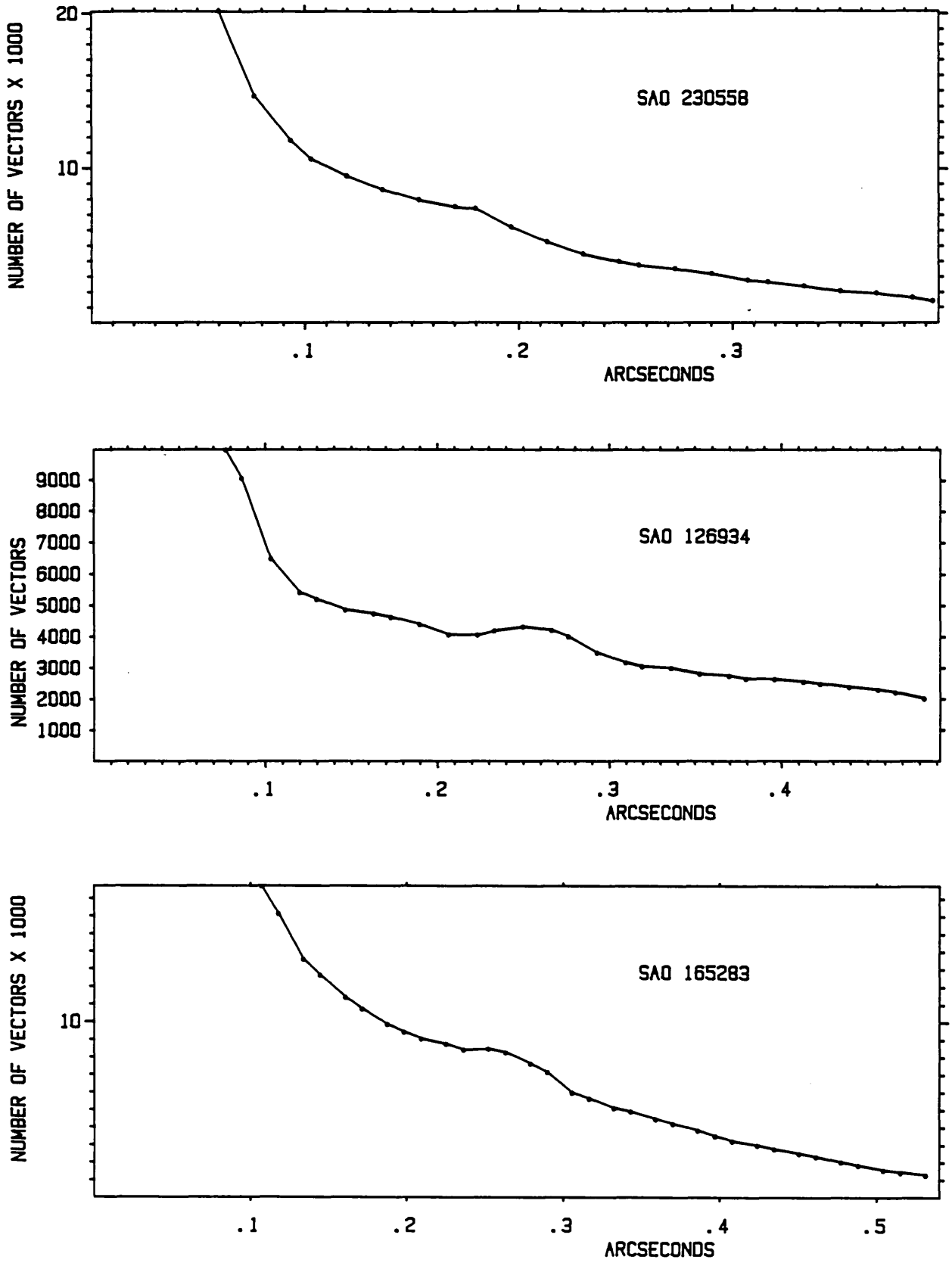

Figure 6.1 : Secondary peaks in three Hipparcos star autocorrelation profiles

produced from the observations of the three confirmed binary stars.

These candidate stars may still have separations between 0.7 arcseconds and the two arcsecond limiting resolution of the sky survey prints. This range of separations is the subject of a special investigation by de Vegt at Hamburg. Further Hipparcos link stars are due to be observed using the AAT and the 1.9m telescope at Mount Stromlo Observatory during the summer of 1984. Initial observations using the smaller telescope will enable stars with structure above a resolution limit of about 0.06 arcseconds to be eliminated. The remaining stars will then be observed using the 3.9m AAT.

6-3 Asteroids

A number of speckle observations of asteroids have been made in collaboration with Dr Edward Bowell of Lowell Observatory, Flagstaff. In February 1981 Ceres, Vesta, Hebe and Victoria were observed with the 3.8m UK Infrared Telescope (UKIRT) at Mauna Kea, Hawaii [86]. The estimated angular diameters of these asteroids were between 0.1 and 0.8 arcseconds (calculated from previous occultation measurements). Further speckle observations of these and other asteroids were made in December 1981 using the 1.8m Perkins Telescope, as shown in figure 6.2, at Lowell Observatory. The observed asteroids have magnitudes in the range from about $m_v=6.5$ to $m_v=11$ but the brighter objects required attenuation with neutral density filters to ensure that the system was detecting individual photon events.

Although most asteroids are considered as having irregular (i.e. not centro-symmetric) intensity distributions, a preliminary attempt has been made to estimate the mean diameter of the asteroid Herculina. Figure 6.3 shows the azimuthally averaged autocorrelation profiles of an unresolved reference star and Herculina. A simple seeing component model has been fitted to both profiles. Figure 6.4 shows the resultant data from each profile after the model seeing components have been subtracted. A model representing the expected speckle component for an unresolved source was then calculated as is shown superimposed on the reference star data. A number of speckle component models were also calculated for uniformly illuminated discs of various angular diameters.

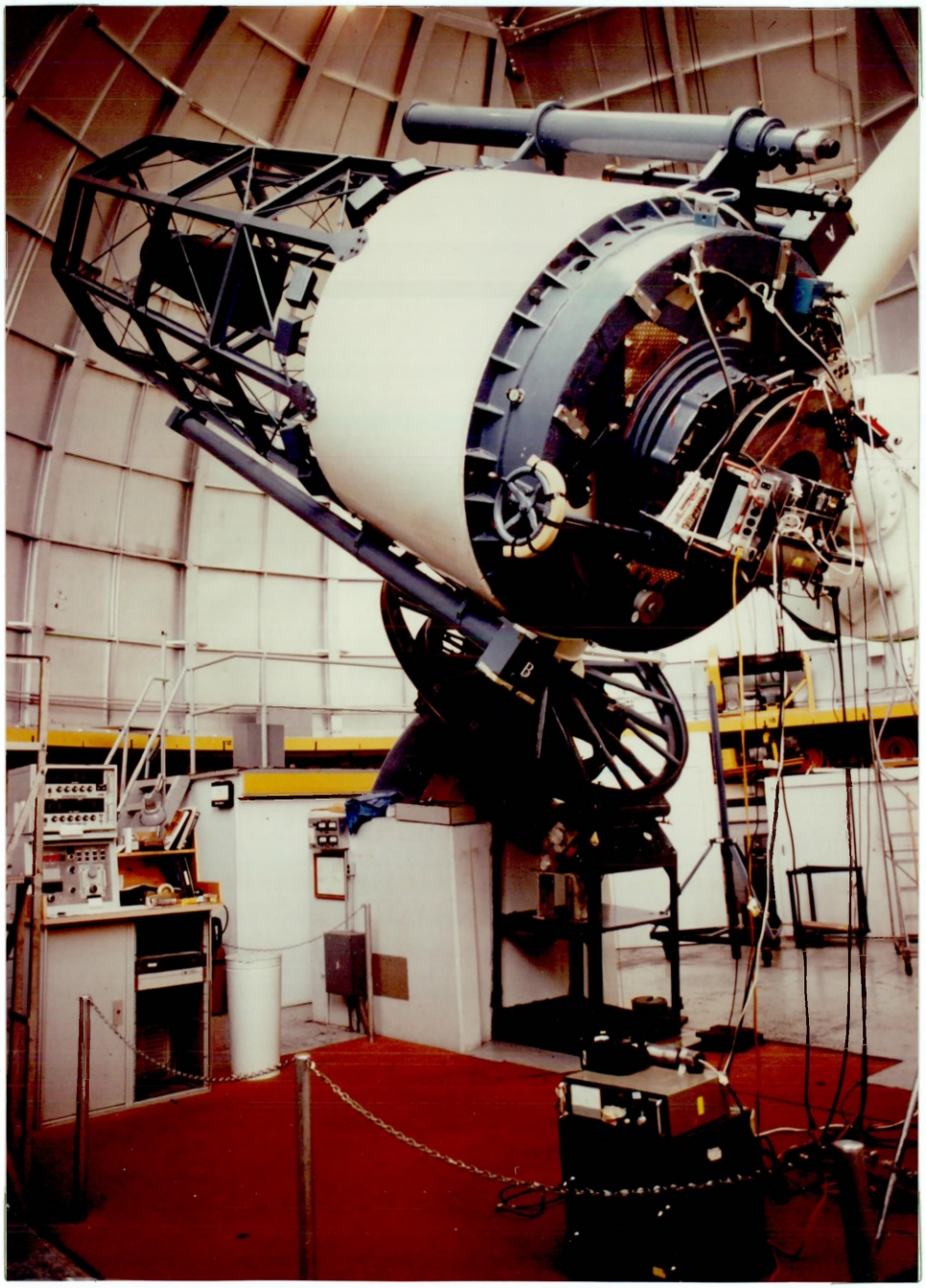

Figure 6.2 : The 1.8m Perkins telescope, Lowell Observatory, Arizona

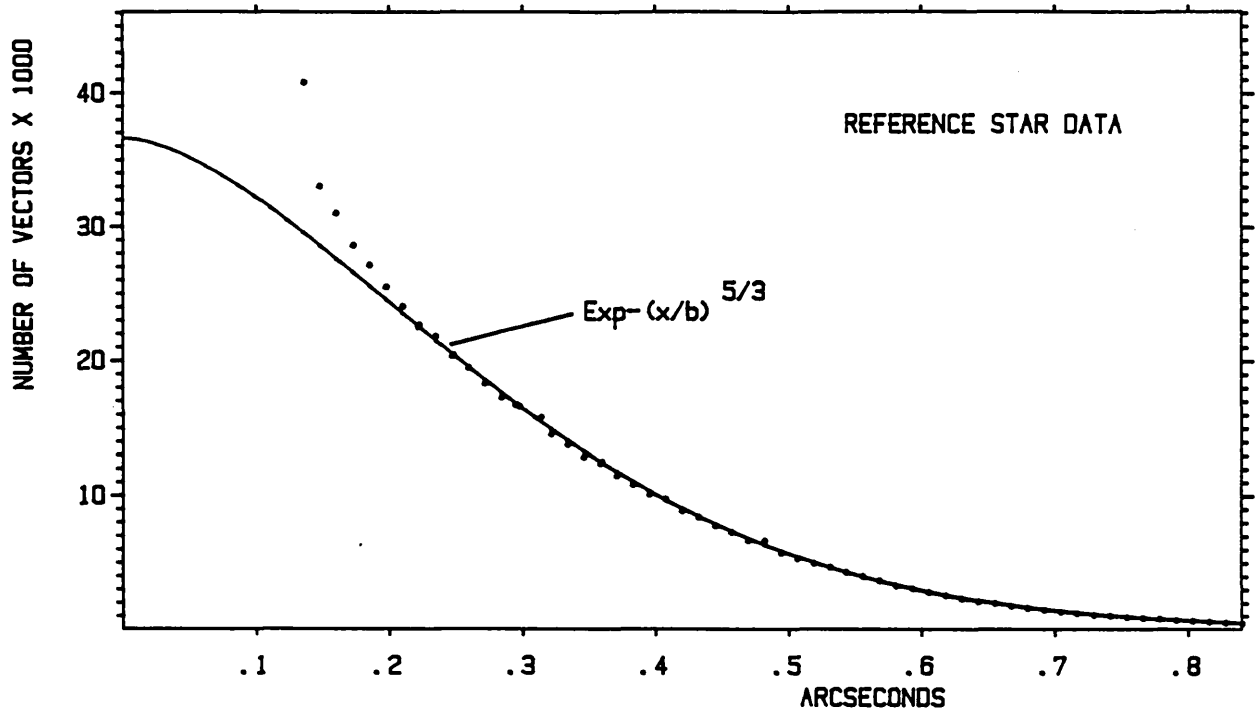

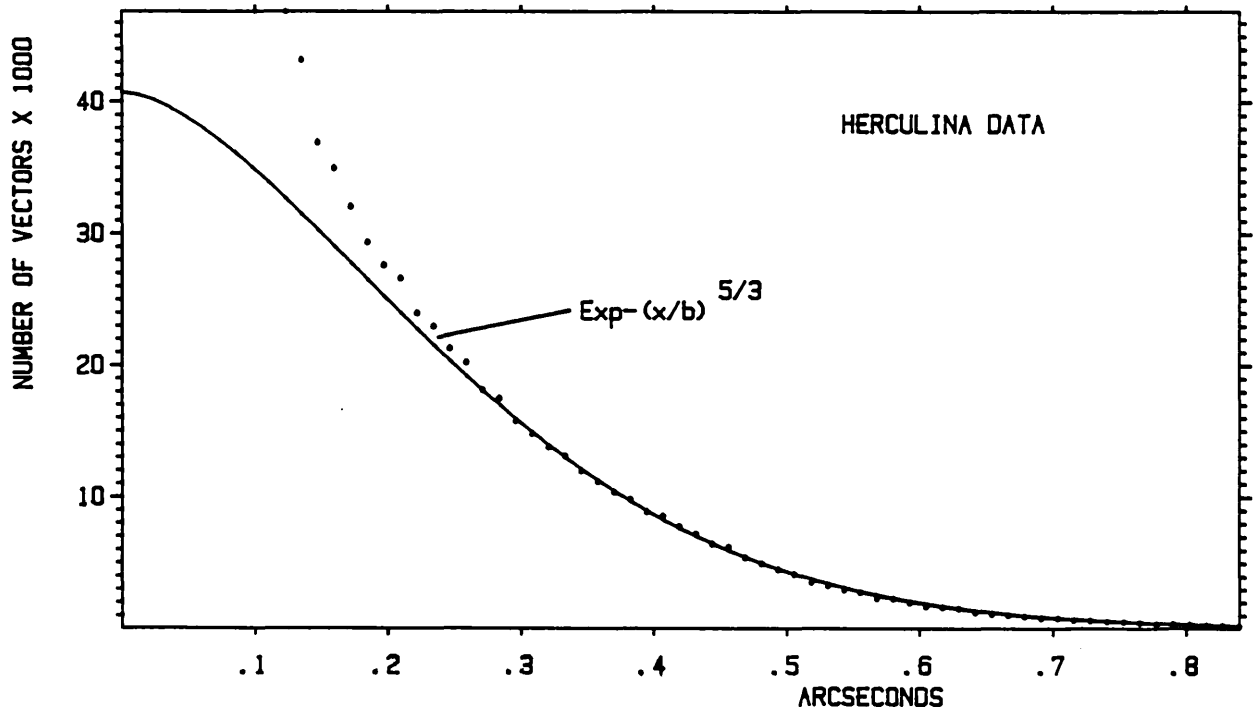

Figure 6.3 : Azimuthally averaged autocorrelation profiles of a point source and Herculina

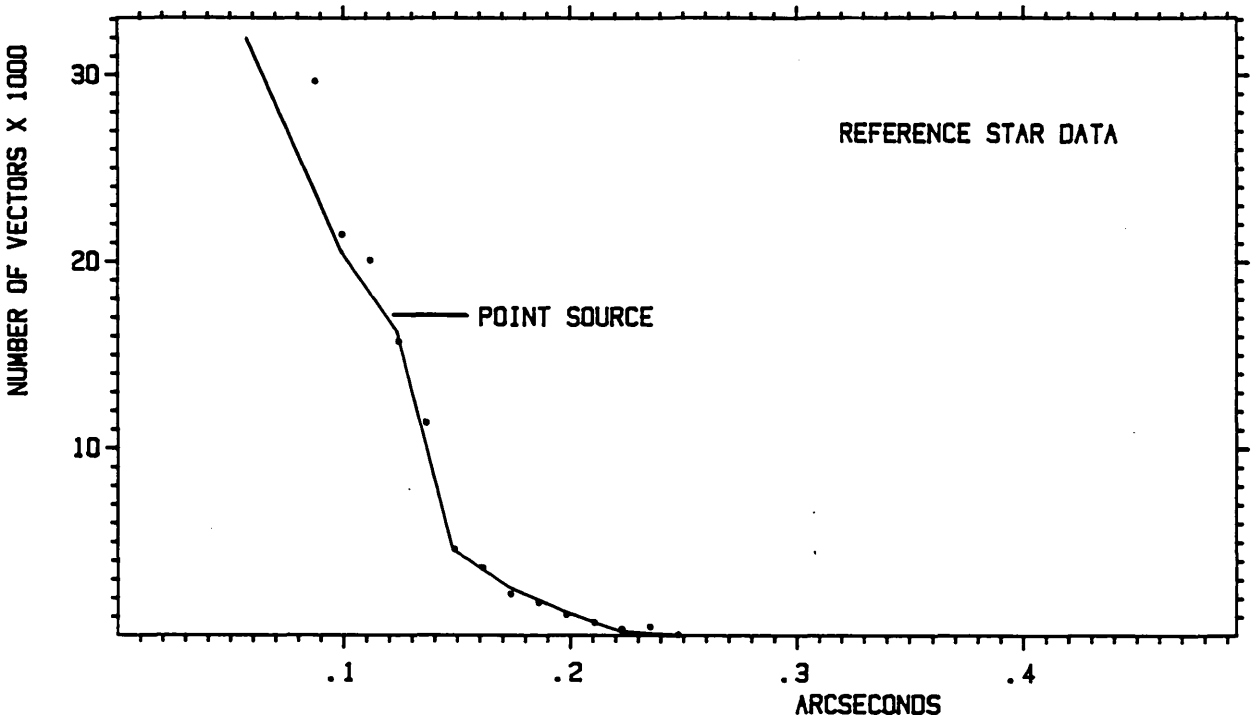

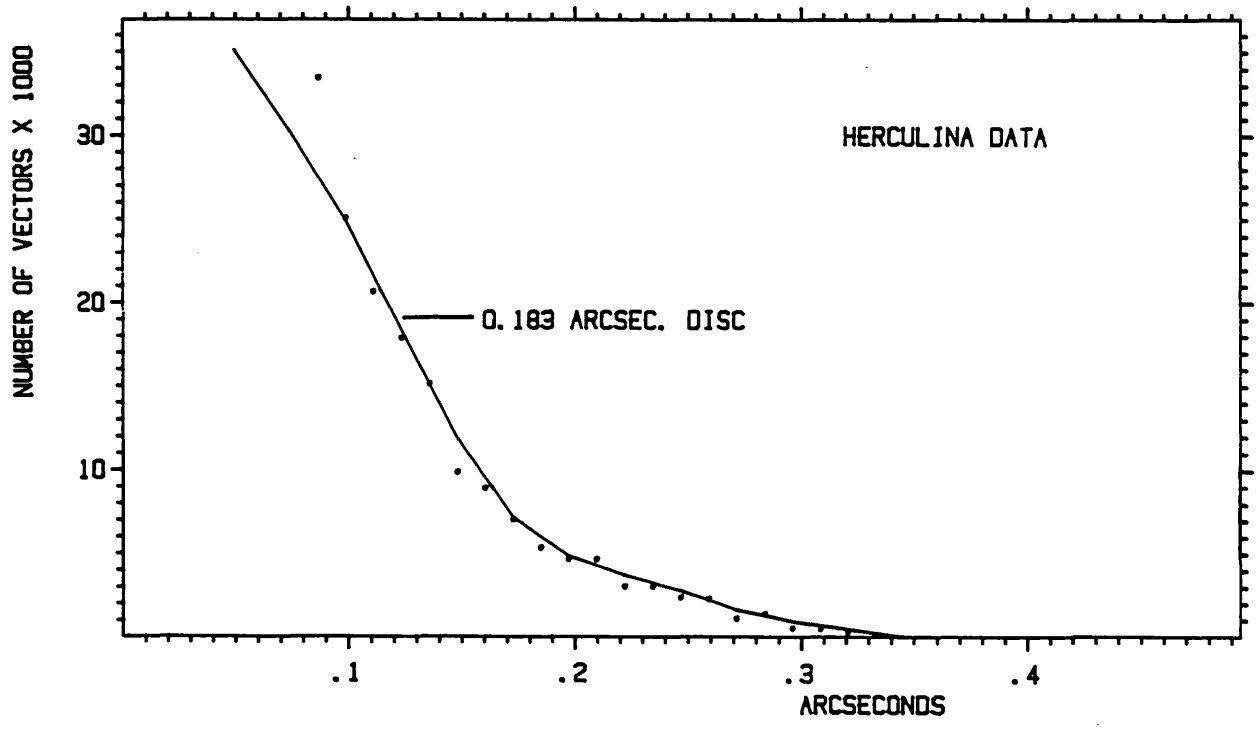

Figure 6.4 : Isolated speckle components of a point source and Herculina

The best-fit model for the Herculina data, as shown in figure 6.4, was found to have an angular diameter of 0.183 arcseconds. There was little variation from the best-fit curve over the range ± 0.025 arcseconds. At the time of observation Herculina was situated at a distance of about 1.88 AU which yields a mean diameter of 250 ± 35 km. The rather large error involved is mainly due to the relatively large pixel size used (0.0247 arcseconds per pixel) in relation to the angular size of the object. Note that the result does not strictly represent a value for the mean diameter but, more precisely, is the measurement obtained from the analysis of the mean autocorrelation profile. Nevertheless, this result corresponds quite well with the value of 217 ± 15 km obtained from an occultation measurement in June 1978 [121]. If data reduction priorities allow, similar measurements will be performed for other observed asteroids in the near future. The introduction of the hardwired crosscorrelator will hopefully enable greater accuracy.

Also of particular interest is the possible identification of asteroid satellites [87] and the observation of their motion relative to the parent asteroid. Hege et al. [124] have previously found evidence of such a satellite associated with Victoria. Our observations of Victoria have shown marginal evidence of the existence of a faint companion to Victoria with a separation of about 0.33 arcseconds.

6-4 The Seyfert nucleus of NGC 1068

In 1943 Seyfert noted that a number of galaxies contained exceptionally bright nuclei [88]. The nuclei of these Seyfert galaxies, as they are now known, often exhibit very intense radio emission and evidence of very turbulent (high velocity) motion. The Sb spiral galaxy NGC 1068, otherwise known as M77, has such a nucleus. Assuming a value of Hubble's parameter of 75 km $s^{-1}Mpc^{-1}$ implies that NGC 1068 is situated at a distance of 16 Mpc.

Observations of NGC 1068 by Bertola [89] have revealed a twelfth magnitude stellar-like inner nucleus with a diameter no greater than 160 pc (two arcseconds) which emits 9 percent of the total visible continuum of the galaxy. Radio observations with a resolution of about one arcsecond show that there is a very intense unresolved source of non-

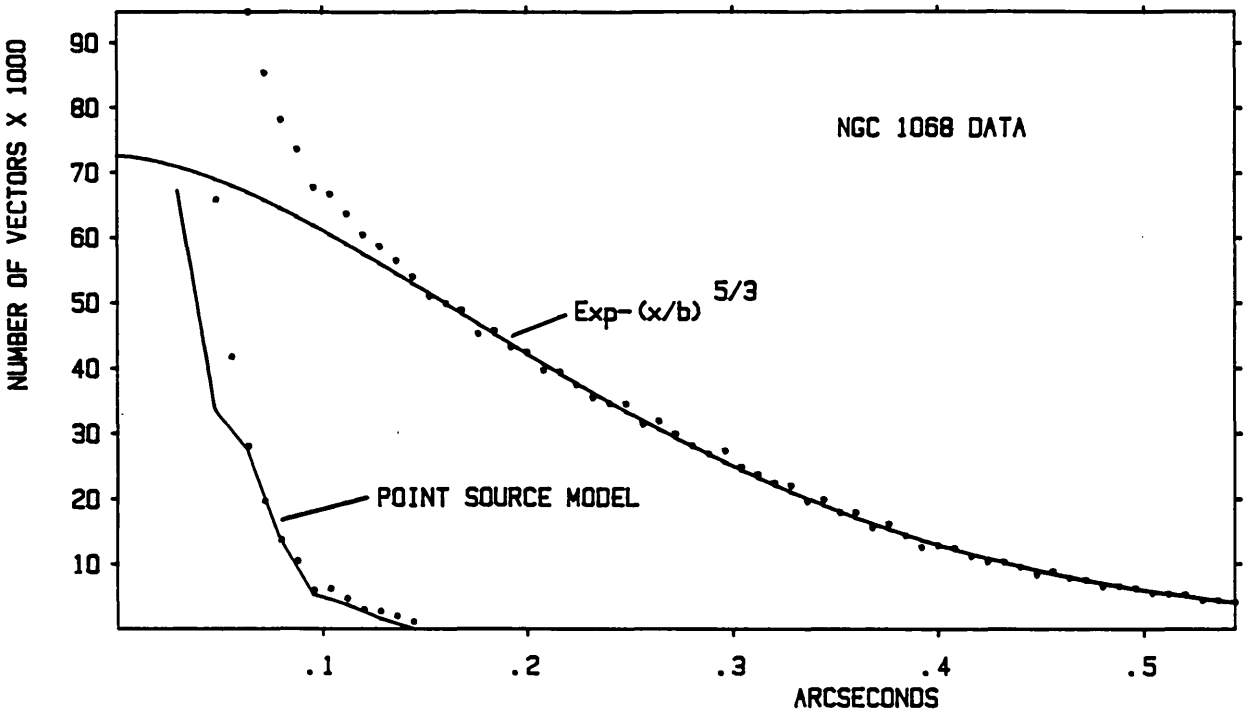

Figure 6.5 : An azimuthally averaged autocorrelation profile of the nucleus of NGC 1068

thermal radiation [91]. However, very-long-baseline interferometry (VLBI) radio observations have so far failed to detect a central source of emission [93].

Speckle observations of the inner nucleus of NGC 1068 were made using the AAT in November 1981 [71]. The field of view examined by the hardwired autocorrelator was equivalent to a 3 x 3 arcsecond square and the existence of any angular structure between 0.03 (optical resolution limit of the telescope) and 0.9 (upper limit imposed by autocorrelation window) arcseconds was investigated. NGC 1068 and a reference star were observed for about 20 minutes each. A 5000Å filter of 550Å bandwidth was employed. Non-overlapping photon events were observed for both objects (i.e. photon counting) without requiring attenuation with a neutral density filter. Several autocorrelations were obtained in the laboratory using suitable detection thresholds.

Figure 6.5 shows a typical azimuthally averaged autocorrelation profile obtained from the observation of the nucleus of NGC 1068. A seeing component model has been fitted and the profile resulting from

its subtraction is indicated. A computer-generated speckle component for an unresolved source is also shown. The excellent fit between this model and the data indicates that NGC 1068 is dominated by a stellar-like source which is most likely unresolved at the diffraction limit of the telescope. An identical result was achieved with the reference star data. Experiments with other models suggest an upper limit of about 0.03 arcseconds for the diameter of the object. If unresolved, the nuclear emission must originate within a region of diameter no greater than 2.3 pc (0.03 arcseconds) with a luminosity of about $5 \times 10^9 L_\odot$. Initial examination of the data exhibited marginal evidence for the existence of multiple sources surrounding the central object but these have since been found to be spuriae.

A number of possibilities for the nature of the central source of NGC 1068 have been considered [71]. If the optical emission is due to intense synchrotron radiation then the failure of radio VLBI observations to detect this object suggests synchrotron self-absorption is occurring. This requires a turnover frequency of about 10^{10} Hz and therefore implies an angular size no greater than 0.0001 arcseconds (0.025 light-years). However, the existence of optical circular polarization [94] is not consistent with this argument since synchrotron produces linear polarization only.

If a simplistic mass-luminosity relationship is applied, the central source could be explained as a very compact cluster of many stars with a total mass of about 5×10^9 $M_\odot$ and a density in excess of 8×10^8 $M_\odot$ pc^{-3}. However, if this cluster is gravitationally bound, the stars must possess orbital velocities of at least 5000 km/s, which is much larger than the velocities of up to 1450 km/s deduced from the observed broadening of the OIII emission lines [90].

A more likely possibility is that the nucleus of NGC 1068 contains a single supermassive compact object similar to that believed to be located in the core of M87 [95]. Recent very-large-array (VLA) radio observations by Van der Hulst et al. [96] have shed further light on the nature of the nucleus. The VLA, operating at a wavelength of 2 cm, produced a map of the central region, two arcseconds (250 light-years) in diameter, with a resolution of 0.2 arcseconds. The map indicates a

very compact central source surrounded by jet-like extensions.

NGC 1068 emits more than 90 percent of its luminosity at wavelengths longer than 2.2 μm [92] and thus it is a very interesting object to observers operating in the near-infrared. Its infrared structure was first investigated by Neugebauer et al. [97] in 1971 who found an unresolved core with a diameter no greater than 2.5 arcseconds. Recent infrared (2.26 μm) speckle interferometric observations by McCarthy et al. [72] show an unresolved inner core whose size has an upper limit of 0.2 arcseconds.

One interpretation of these observations involves the accretion of matter onto a single supermassive central object, possibly followed by ejection of jets of matter. Associated with this, perhaps, are beams of radio-wave radiation emitted along the rotation axis of the object. Incidentally, reviews in Sky and Telescope (July 1983) and The Times (29th March 1982) both interpret the observations as being consistent with the discovery of a black hole.

6-5 R136a

Radcliffe 136 (R136; HD 38268) is the central bright object located in the 30 Doradus, or Tarantula, nebula (NGC 2070). The nebula, as shown in figure 6.6, is a giant region of ionized hydrogen situated in the Large Magellanic Cloud (LMC). Optical studies of R136 by Feitzinger et al. [98] reveal the presence of three components situated within four arcseconds of each other. The brightest ($m_v \simeq 9$) and bluest of these is known as R136a. Far-ultraviolet observations with the International Ultraviolet Explorer (IUE) satellite by Cassinelli et al. [99] indicate that R136a has a surface temperature of about 60000 K and that it emits an extremely powerful stellar wind of $10^{-3.5}$solar masses per year at a speed of about 3500 km/s. Meaburn [105] suggests that the observed large scale disturbance of the surrounding interstellar medium could be evidence of the interaction of this wind. Combining the above temperature with estimates of the absolute visual magnitude implies a luminosity of about one hundred million times that of the sun. Observations also suggest that R136a dominates the ionisation structure of the 30 Doradus nebula and that the total mass of this peculiar object

Figure 6.6 : The 30 Doradus nebula

is possibly as large as 2500 solar masses.

Three possibilities concerning the nature of R136a have been considered [98],[99]. The luminosity and temperature are consistent with a very dense cluster of hot stars; for example about thirty O3 and WN3 stars could be confined within a volume of less than 0.1 pc in diameter. At the distance of the LMC (55 Kpc) this implies a maximum diameter of about 0.5 arcseconds. However, the variability of the visible emission [98] could not originate within a large group of stars. Near-infrared spectroscopic observations of R136a by Vreux et al. [106] indicate an absence of Wolf Rayet characteristics but strong similarities with some bright O stars.

Another alternative interpretation of the observations is that the radiation from R136a is due to a single superluminous object with a radius of about one hundred times that of the sun and of mass equal to about 2500 solar masses. This would render R136a the most massive star known and it would probably be a very short-lived phenomenon with a life no longer than about 100000 years. The angular diameter of such an object would only be about 0.02 milli-arcseconds.

The third possibility is that R136a could be an amorphous region of matter with a much larger diameter, which is undergoing proto-stellar collapse into a single object.

Speckle observations of R136a were made using the AAT in November 1981 [101]. Three different bandpass filters were used: 3800Å (bandwidth 200Å), 5000Å (550Å) and 5672Å (70Å). Detailed examination of autocorrelations produced from these observations failed to detect any structure with an angular separation in the range from about 0.03 to 0.9 arcseconds. Figure 6.7 shows the mean autocorrelation profile of the R136a observation obtained with the 5000Å filter. A model seeing component has been fitted and subtracted from the data. The excellent fit between the resultant speckle component and the model for a point source as shown indicates that the object is probably unresolved. The observations made using the other filters yielded identical results as did that of the reference star. In November 1983 a further observation of R136a was made using a blue (4050Å) filter which confirmed that the

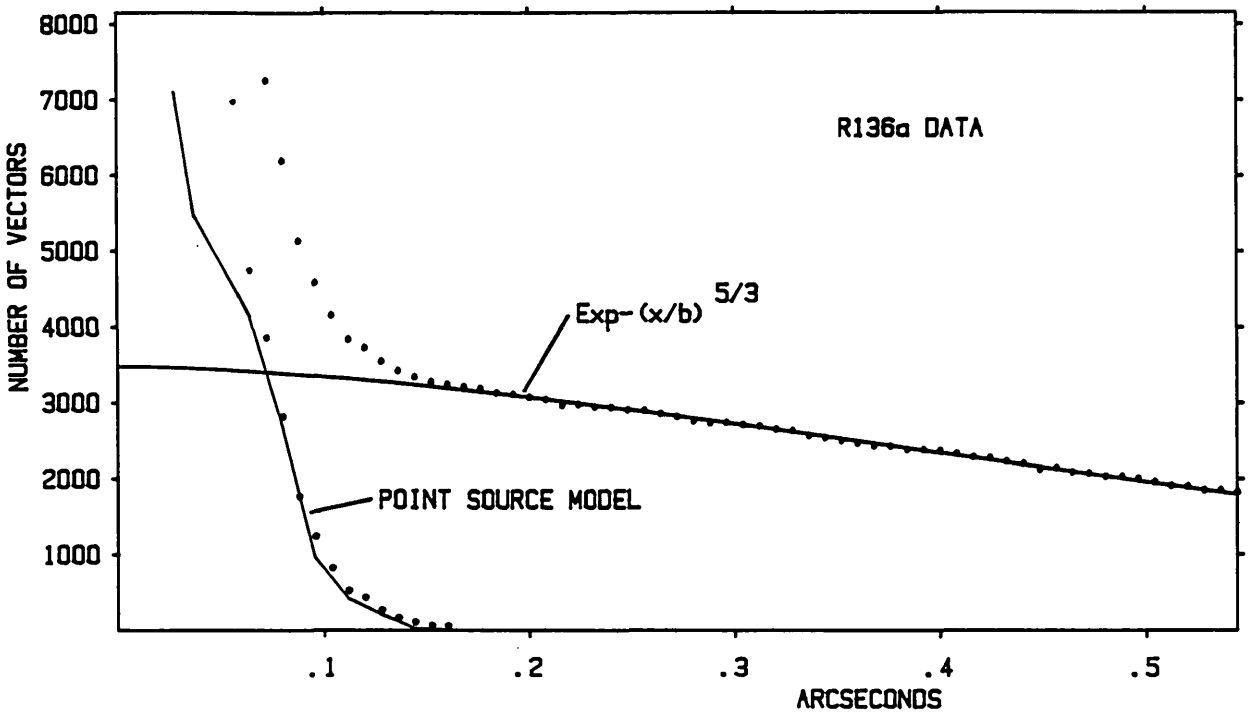

Figure 6.7 : An azimuthally averaged autocorrelation profile of R136a

object still appears unresolved at a diffraction limit of 0.02 arcseconds. The data was compared with several model speckle components corresponding to resolved discs with diameters between 0.01 and 0.1 arcseconds. The upper limit to the angular diamater of R136a was thus found to be about 0.02 arcseconds.

If R136a is comprised of thirty O3 or WN3 stars, the mean density is at least 3×10^{10} $M_\odot pc^{-3}$ and their mean separation is only about 0.007 light-years, which seems remarkably small [101]. R136a could still be a large object with a maximum diameter of about 0.02 arcseconds. The mean density would therefore be of the order of 10^{10} $M_\odot pc^{-3}$ though it need not necessarily have a homogeneous distribution. The most likely possibility, however, is that R136a is a single star with a mass of about 2500 solar masses.

Recent infrared photometric observations by Panagia et al. [107] suggest that R136a is a very massive star (>2000 $M_\odot$) with a strong mass loss of about 5.2×10^{-4} stellar masses per year. By combining mass loss and luminosity values for R136a with those of known galactic

supergiants, Panagia et al. [107] derive a mass-luminosity relationship which is coincident with that determined for galactic main-sequence stars. Further IUE observations recently reported by Savage et al. [139] suggest that R136a is either a single supermassive hydrogen-burning star or a compact multiple system of supermassive stars.

6-6 Eta Carinae

In 1845 Eta Carinae, a star located in the centre of the nebula NGC 3372 (shown in figure 6.8), temporarily became the second brightest star in the night sky after Sirius [108]. Its brightness increased rapidly from fourth magnitude to a magnitude of about -1. By 1880 the magnitude of Eta Carinae had declined to about 7, though a brief 1.5 magnitude outburst was observed in 1889 [108]. Since 1940 there has been a gradual rise of about 1.5 magnitudes such that it is now about a sixth magnitude object. This peculiar behaviour of Eta Carinae over the last 140 years is described in more detail by Feinstein and Marraco [109].

Observations have shown that the spectrum is complex [110],[111] and the strong optical continuum is characterized by a temperature of about 30000 K [112]. The bolometric absolute magnitude of Eta Carinae is -12.5 for a distance of 2800 pc, which is equivalent to a luminosity of about 10^7 $L_\odot$ [113].

In the infrared 10-20 μm region Eta Carinae is the brightest object outside the solar system [114]. Infrared mapping indicates a compact hot (425 K) core surrounded by a diffuse halo of cooler (250 K) dust with a diameter of about 8 arcseconds [115],[116]. Hyland et al. [117] have observed two peaks in the infrared emission whose separation increases from 1.1 arcseconds at 3.6 μm to 2.2 arcseconds at 11.2 μm. They suggest that this may arise from the thermal emission of a dust ring surrounding the central source viewed almost edge on. Recent one-dimensional infrared (4.6 μm) speckle observations by Chelli et al. [118] have revealed a bright unresolved core of diameter no larger than 0.3 arcseconds, surrounded by two secondary peaks in intensity situated about one arcsecond from either side of the central source. This result was obtained by implementing a form of the Knox-Thompson phase retrieval algorithm (see section 2-7).

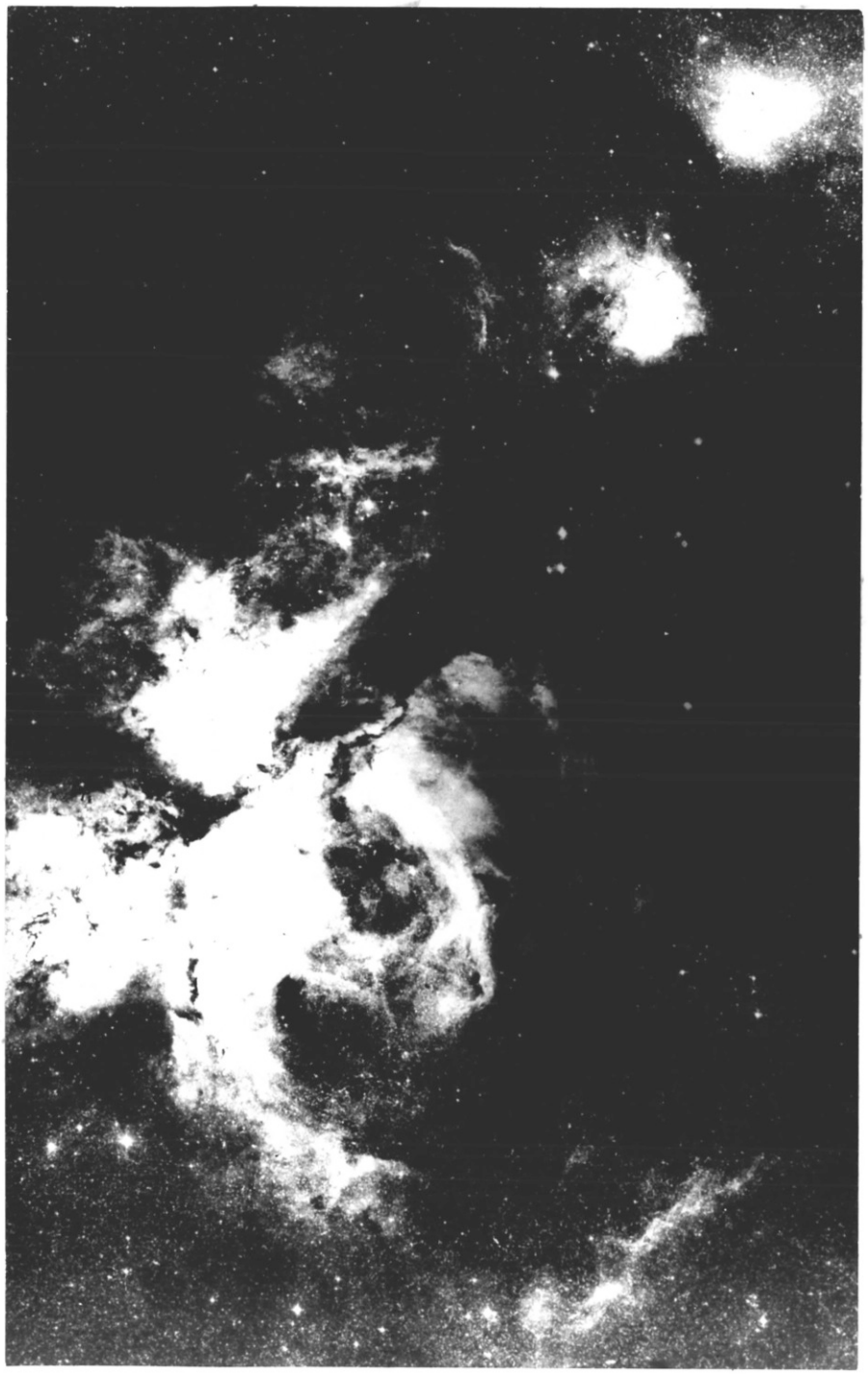

Figure 6.8 : The nebula NGC 3372

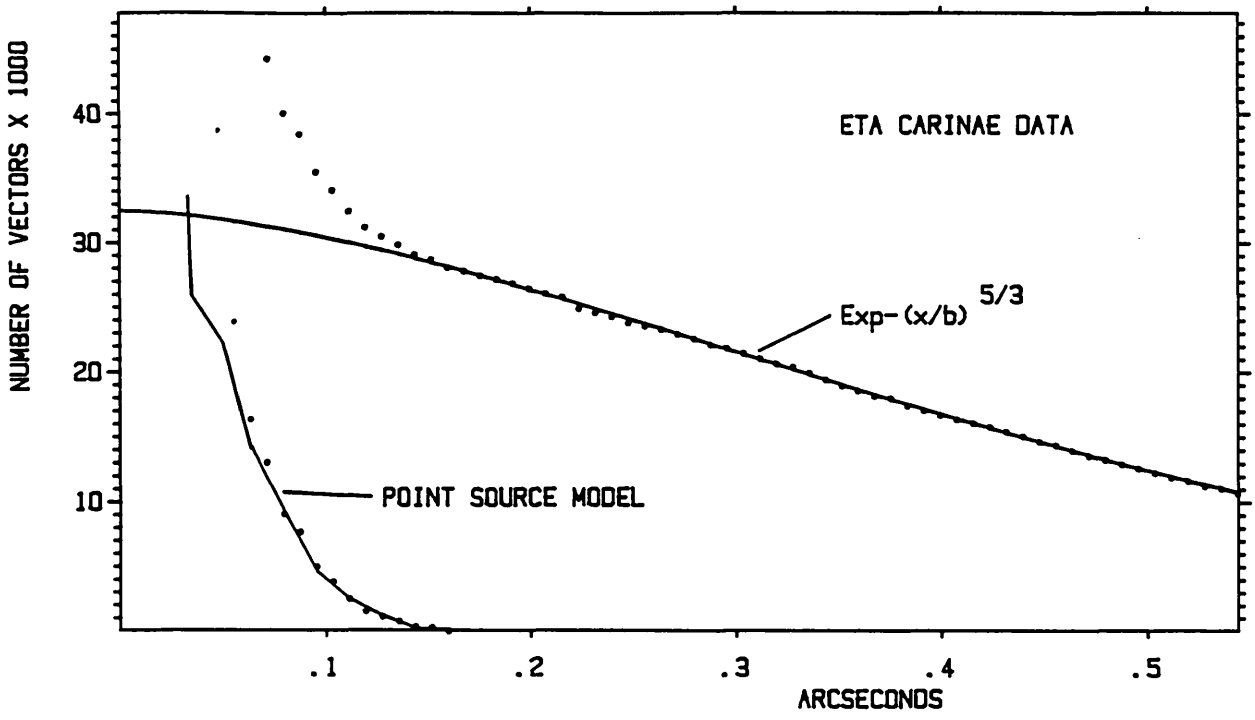

Figure 6.9 : An azimuthally averaged autocorrelation profile of Eta Carinae

Optical observations of Eta Carinae during good seeing conditions have indicated a diffuse dusty halo of about 2 arcseconds in diameter which is surrounded by an irregular condensation shell (the "Homunculus") of about 10 arcseconds in diameter. Walborn et al. [119] have detected the presence of velocities of up to 1400 km/s within the condensation shell which are directed away from the central object. Polarization maps made by Warren-Smith et al. [120] show that the Homunculus is dominated by reflected light from Eta Carinae and evidence was obtained which suggests that there might exist a luminous optically thick ring of about 2.5 arcseconds in diameter.

It has been suggested that Eta Carinae is a 100 $M_{\odot}$ star which is losing mass at a rate of about 0.02 solar masses per year [117]. Alternatively the object has been considered as a binary system which is undergoing large-scale mass transfer between the component stars [120]. A third possibility is that Eta Carinae is made up of a compact group of hot O and B stars confined within an angular diameter of about one arcsecond.

Speckle observations of the central object in Eta Carinae were made using the AAT in November 1981 which enabled structure between 0.03 and 0.9 arcseconds to be determined [102]. A 5672Å filter having a 70Å bandwidth was employed. A thorough examination of the full two-dimensional autocorrelation of the Eta Carinae observation contained no indication of any binary component within this range but instead exhibited the characteristics of a single unresolved source. No evidence for any extended halo having a diameter less than 0.9 arcseconds was found. Figure 6.9 shows the azimuthally averaged autocorrelation profile of Eta Carinae with a best-fit model seeing component added. The data, after subtraction of this model, coincides extremely closely with the computer-generated model for the speckle component of an unresolved source.

Comparison with various speckle component models indicates that the upper limit to the extent of Eta Carinae is about 0.03 arcseconds which is equivalent to a diameter of 84 AU for a distance of 2800 pc. Therefore the most likely solution is that Eta Carinae is a single massive (100 $M_\odot$) star with a luminosity of $10^7 L_\odot$ and a radius no greater than 42 AU, which is undergoing huge and variable mass loss.

If Eta Carinae is an unresolved binary star, the separation of such a system must be within < 84 AU. The following mass-luminosity relationship for bright (bolometric magnitude < 7) stars [122]:

$$m(bol) = 4.7 - 9.5 \log M \qquad (6.1)$$

where M = total mass of the system expressed in solar masses,

suggests that the mass of Eta Carinae is about 65 $M_\odot$. It can be shown using Kepler's third law that a binary of this mass and with an orbital radius of < 42 AU has a period of less than 34 years [102]. UBV photometry observations by Feinstein and Marraco [109] show weak evidence for a 3 year cycle. This would imply an orbital radius of about 8.4 AU (0.003 arcseconds) for a 65 $M_\odot$ binary system.

Stars as massive as Eta Carinae have relatively short lifetimes and, because of their huge mass, end their lives in the form of a supernova

explosion. Since Eta Carinae is already quite mature and has demonstrated recent unstable behaviour, it has been suggested [123] that this event may not be very far off. Should this happen Eta Carinae will temporarily become an object of about magnitude -5, brighter than every stellar object except the sun and moon.

6-7 The binary star in the Red Rectangle

The Red Rectangle is the remarkable bipolar nebula associated with the ninth magnitude B8-AIII star HD 44179. The optical appearance of the nebula depends on the wavelength at which it is observed. In the blue the nebula is amorphous, centred on HD 44179. In the red the nebula appears rectangular with spikes extending from the corners. The object has been studied in great detail and at a variety of wavelengths by Cohen et al. [125]. The spectrum contains a unique broad (800Å) continuous component centred on 6400Å [128] on which is superimposed both broad and narrow emission lines which are possibly molecular in origin [127],[130]. Infrared (7.7 μm) observations by Russell et al. [129] have indicated the presence of unidentified emission features which do not arise from simple molecular emission.

Polarization maps of the Red Rectangle made by Perkins et al. [126] show that the object is consistent with the reflection of light from a central source by a biconical distribution of dust. The broad red emission, however, was found to originate from the nebular medium itself.

The star HD 44179 was first identified as a visual double by Aitken in 1915 (ADS 4954). Cohen et al. [125] list many of the subsequent observations of this binary and these are summarized in figure 6.10. The position angle, separation and magnitude difference obtained for each observation is illustrated. Since the magnitude difference in each case is zero or nearly zero, each measurement of the position angle may differ by 180°. However, observations of HD 44179 made in 1948 and 1975 failed to resolve the binary system. Two possibilities for this have been suggested. The first and most obvious explanation is that the separation was so small (< 0.1 arcseconds) at the time of observation that the visual technique was not sufficient to resolve the star. The

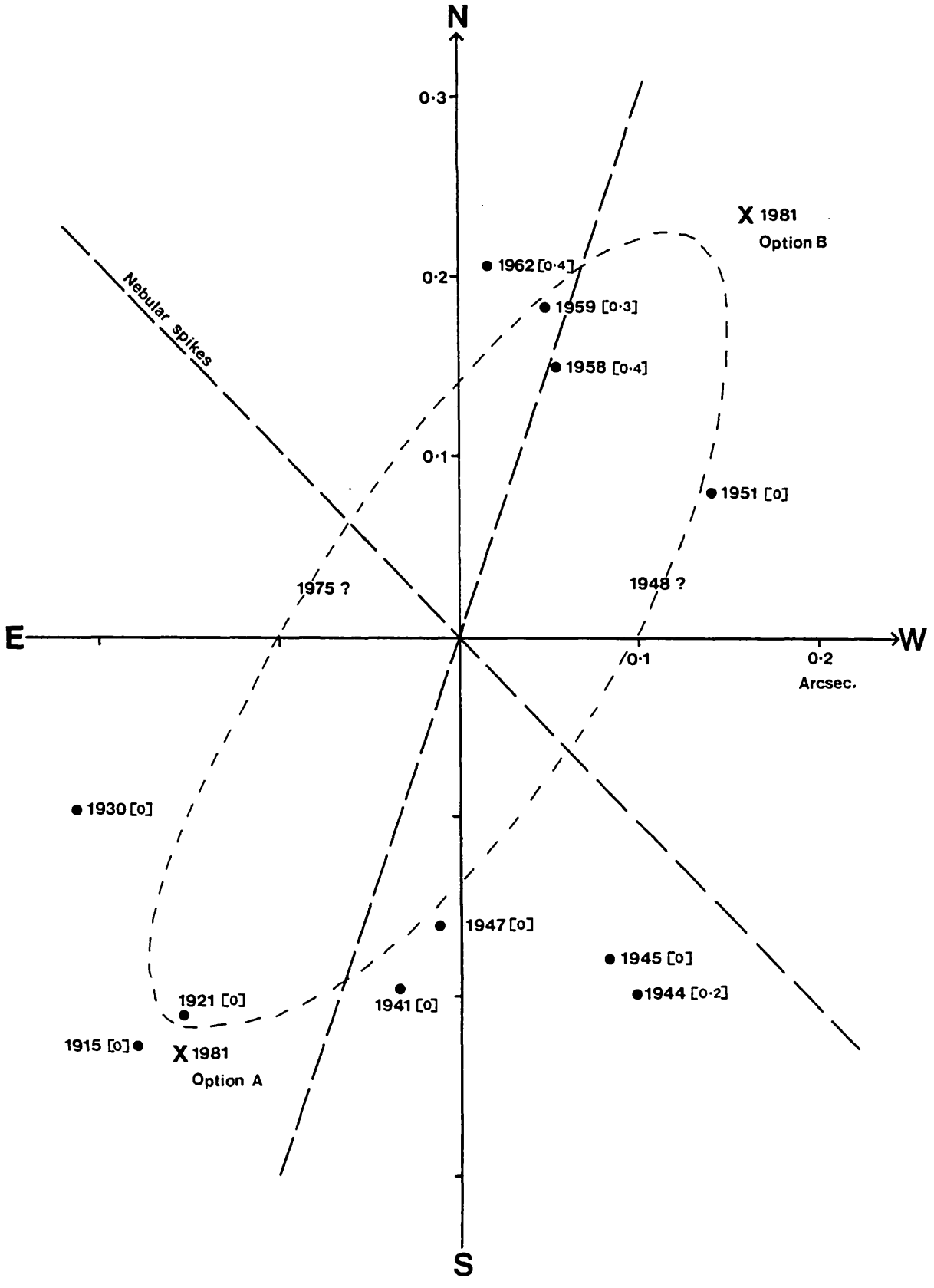

Figure 6.10 : Position angle and separation measurements of the binary star in the Red Rectangle nebula

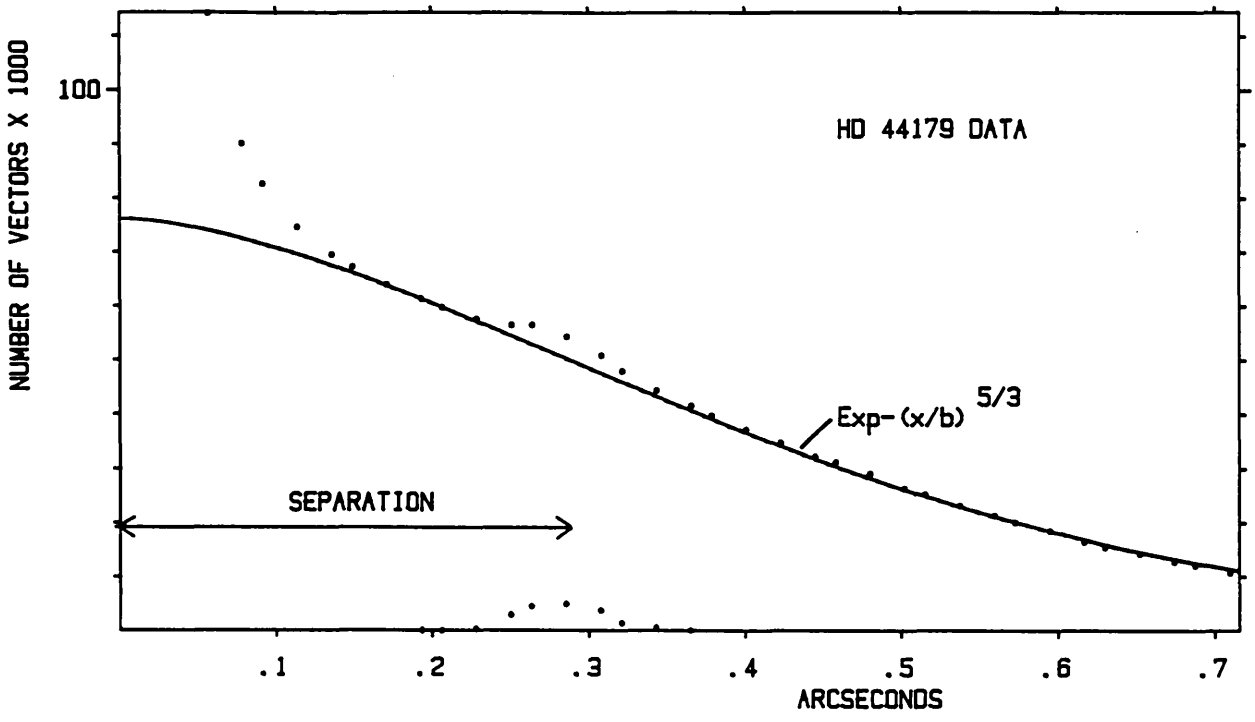

Figure 6.11 : The secondary peak contained in the autocorrelation of HD 44179

second possibility is that one component may have become heavily obscured by dust. Small changes in the estimated magnitude differences could, perhaps, be explained by variable obscuration by dust.

Speckle observations of HD 44179 and a suitable reference star were made on November 11th 1981 using the AAT [103]. A 5000Å filter (220Å bandwidth) was employed. Several autocorrelations were obtained from the video records of each object. Preliminary investigations of the data identified a secondary peak located within the autocorrelation of the HD 44179 record. The autocorrelation profile which approximately bisects the secondary peak, as shown in figure 6.11, corresponds to a position angle of $146^\circ \pm 3^\circ$ ($\pm 180^\circ$). Figure 6.11 also shows a model seeing component which, when subtracted from the data, yields a separation of 0.29 ± 0.02 arcseconds. Experience of binary systems of known magnitude difference suggests that the magnitude difference is no greater than one magnitude.

Figure 6.10 shows two possible positions (options A and B) corresponding to this result. Despite the large spread of values for

both 1915-1930 and 1941-1947 observations, which may be due to the inaccuracy of the visual technique for small (< 0.3 arcseconds) separations, the results appear to be consistent with an orbital period of 60 ± 5 years in an anticlockwise direction [103]. The maximum angular diameter of the orbit is about 0.3 arcseconds. Option A is therefore the most likely. In this case the major axis of the projected ellipse (eccentricity = 0.33) of a circular orbit for two equal masses could be at about 150°± 10° [103]. This configuration would imply that the failure to resolve the binary in 1948 and 1975 may be due to a small (< 0.1 arcsecond) separation at the time of observation. Hence obscuration by dust need not be invoked. The possible 1948 and 1975 positions are indicated in figure 6.10 and the approximate form of the proposed orbit is shown.

A clockwise orbit with a 15 year period could fit many of the observations (or the 180° counterparts) though mass-luminosity considerations make this less plausible. Spectroscopic and photometric observations by Cohen et al. [125] suggest that the Red Rectangle is located at a distance of 330 pc. For two equal stars separated by 4.6 x 10^{-4} pc (equivalent to 0.29 arcseconds or 96 AU) the total mass of the system for 60 and 15 year orbits is approximately 31 and 492 solar masses respectively [103]. The bolometric luminosity of HD 44179 is found to be about 1050 $L_\odot$ [125] which, from the mass-luminosity approximation given below (see Allen [146] p208) implies a mass of about 7.5 solar masses.

$$\log L = 3.45 \log M \qquad (6.2)$$

where L = total luminosity ($L_\odot$),
and M = total mass ($M_\odot$) of the system.

Though this value does assume main-sequence rather than type III characteristics, the 60 year period appears to be more likely than the 15 year period.

Some astronomers predict that planetary or proto-planetary nebulae are created by mass ejection from a binary star and that the ejection occurs either perpendicular or parallel to the plane of the orbit [131].

However, there does not appear to be any definite correlation between the plane of the orbit, as indicted in figure 6.10, and the spikes of the nebula.

It is hoped that more speckle observations of this object can be made over the next few years so that the orbital parameters can be determined more precisely. If these results are combined with high dispersion spectroscopic measurements of the orbital velocities of each component, the distance of the object and the mass of each star can be calculated.

6-8 Preliminary results concerning NGC 2346

The central star in the bipolar planetary nebula NGC 2346 is known to be a single-lined spectroscopic binary with a period of about 16 days [132]. The red-shift velocity of the system coincides with that of the nebula to within 5 km/s so it is very likely that the two are associated. It has been suggested that the central object consists of an 11th magnitude A-type star and a less massive, less luminous hot star [132]. Photometric observations by Kohoutek [135] in 1982 revealed unexpectedly large light variations. Eclipsing behaviour was observed which contained a deep and very broad minimum and which had a period coincident with that of the binary. How, observers have asked, can a drop of 2.2 magnitudes of the A-type star be accomplished by a hot and presumably small companion? Possible explanations include : a) the companion star is very extended, b) the stars follow an extremely elliptical orbit viewed edgeways on, and c) obscuration is caused by a third body [135]. Further optical observations by Mendez et al. [133] have confirmed this extraordinary behaviour and they interpret their results as consistent with an eclipse by a dust cloud. Recent analysis of IUE low dispersion spectrograms of NGC 2346 by Feibelman and Aller [138] showed features typical of a high-excitation planetary nebula but the observations were unable to resolve the important questions raised by this perplexing object.

A detailed description of the photometric variation over an extended period is given by Kohoutek [134] who estimates that the present eclipsing behaviour began on the 29th of November 1981 ± 5 days.

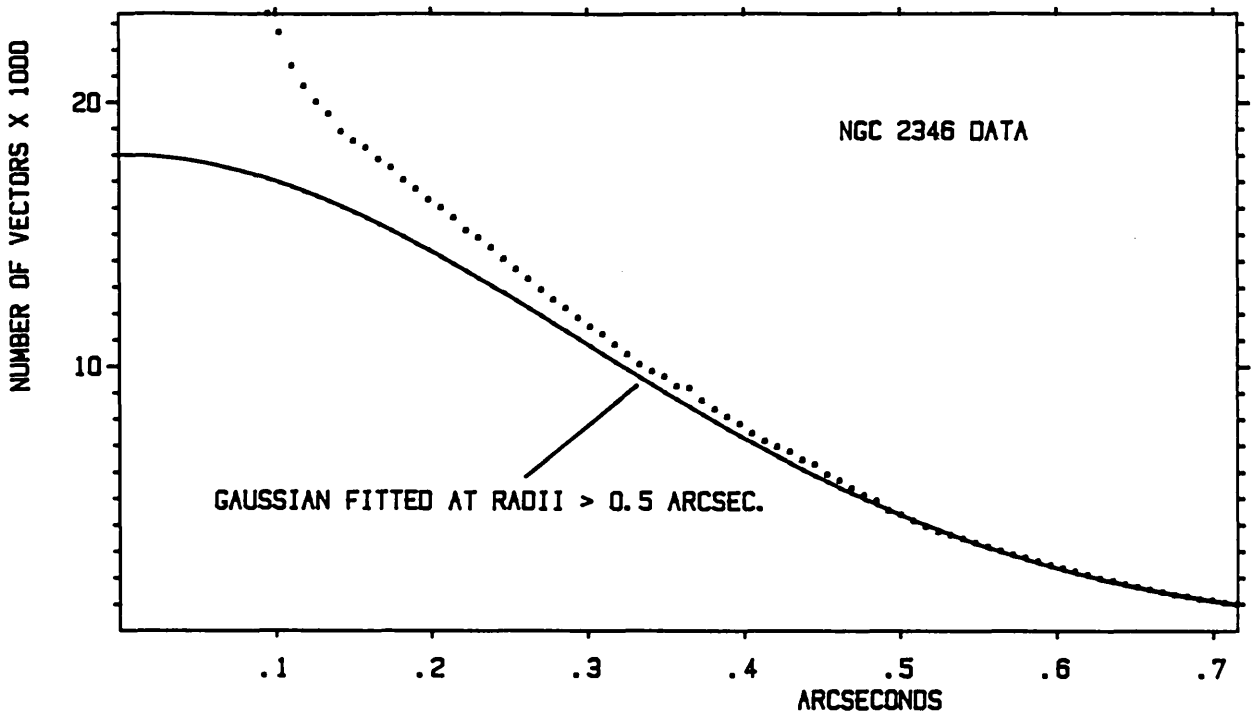

Figure 6.12 : An azimuthally averaged autocorrelation profile of the central star in the nebula NGC 2346

Speckle interferometric observations of this object were made on the 11th of November 1981 using the AAT, a few days before the estimated start of the peculiar behaviour. A 5000Å (550Å bandwidth) filter was employed. Examination of the 30 minute observation has so far failed to detect a secondary peak in the range 0.03 to 0.9 arcseconds. However, preliminary investigations have revealed the presence of a very extended speckle component. Figure 6.12 shows a typical azimuthally averaged autocorrelation profile obtained from the observation of the central star in NGC 2346. A very noticable "kink", which indicates the point at which the speckle component joins the seeing component profile, is observed at a radius corresponding to an angular separation of about 0.5 arcseconds. Another prominent "kink" is located at about 0.15 arcseconds. This suggests that the object probably consists of a large uniformly illuminated disc which contains a smaller and brighter component which may be unresolved.

Because the speckle component extends out to at least 0.5 arcseconds, seeing component subtraction by simple model comparison is unreliable (see section 5-6). Prior to the introduction of the

hardwired crosscorrelator, which should enable a reasonable subtraction to be made, only a preliminary estimate of the form of the mean speckle component profile has so far been achieved. This estimate is shown in figure 6.13. Comparisons were made between this profile and a number of model speckle components. The model which was found to correspond most closely to the data is also shown in figure 6.13. The estimated centro-symmetric intensity distribution which was used to generate this model consists of a central bright region, with a diameter of about 0.1 arcseconds, surrounded by a broad uniformly illuminated disc of about 0.54 arcseconds in diameter. Comparison with a number of models of this form has indicated that the central region is between fifty and two hundred times brighter. The model speckle component and object intensity distribution illustrated in figure 6.13 both correspond to a brightness ratio of one hundred. Alternatively there might exist a slightly more gradual rise in brightness at small radii (as indicated by the dotted line in figure 6.13) which could be consistent with the illumination of dust by a central source. Unfortunately the estimated speckle component of the nucleus of NGC 2346 is not known sufficiently accurately in order to distinguish these models. There is no evidence of any limb brightened shell surrounding the central source.

The bright central component may represent either a single resolved object or a close binary star with a separation of the order of 0.05 arcseconds. The broad uniform component may be due to an illuminated concentration of dust surrounding the central object. This would agree with the theories presented by Koppen [136] and Aitken and Roche [137] who suggest that the role of dust in planetary nebulae may be greater than expected. It is therefore possible that this cloud (or shell) of dust is moving from the the nucleus of NGC 2346. If the dust has an inhomogeneous distribution, the recent observed light variations may be caused by the eclipsing of the A-type star behind denser optically thick regions of dust during its orbit around a fainter companion. A more detailed investigation is required before further conclusions can be made.

6-9 Other observations

Preliminary analysis of the observation of HD 65750, the central

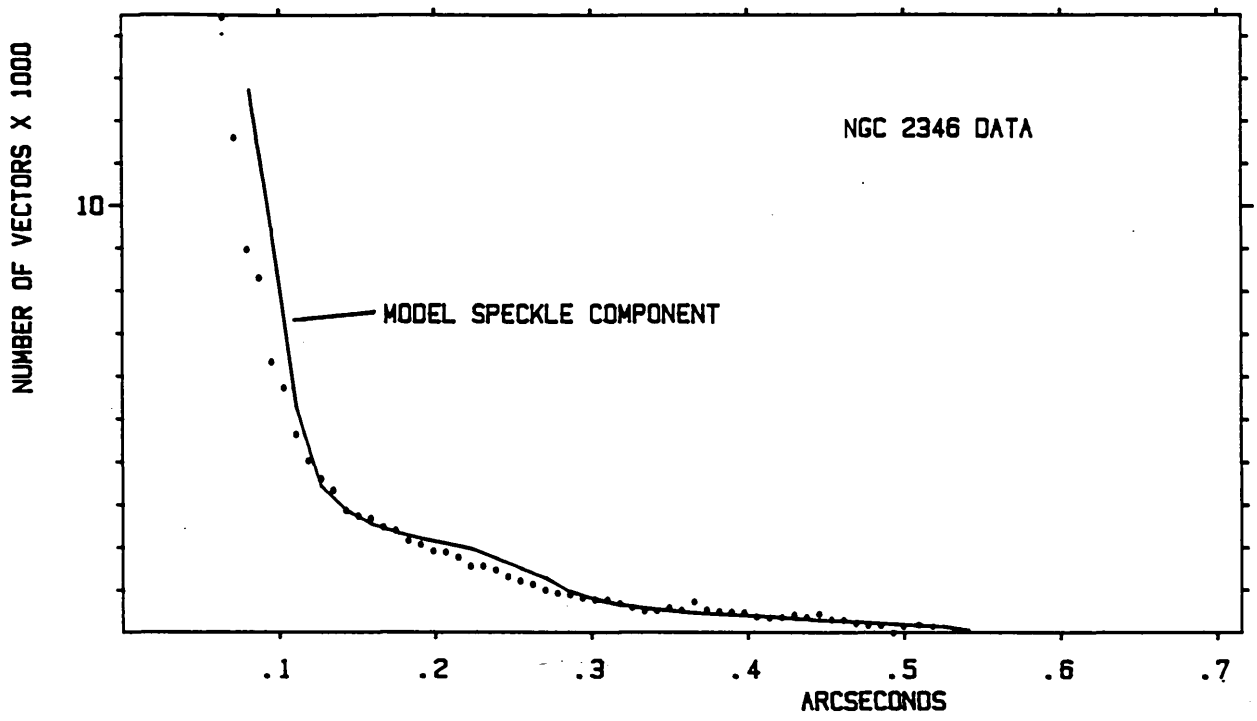

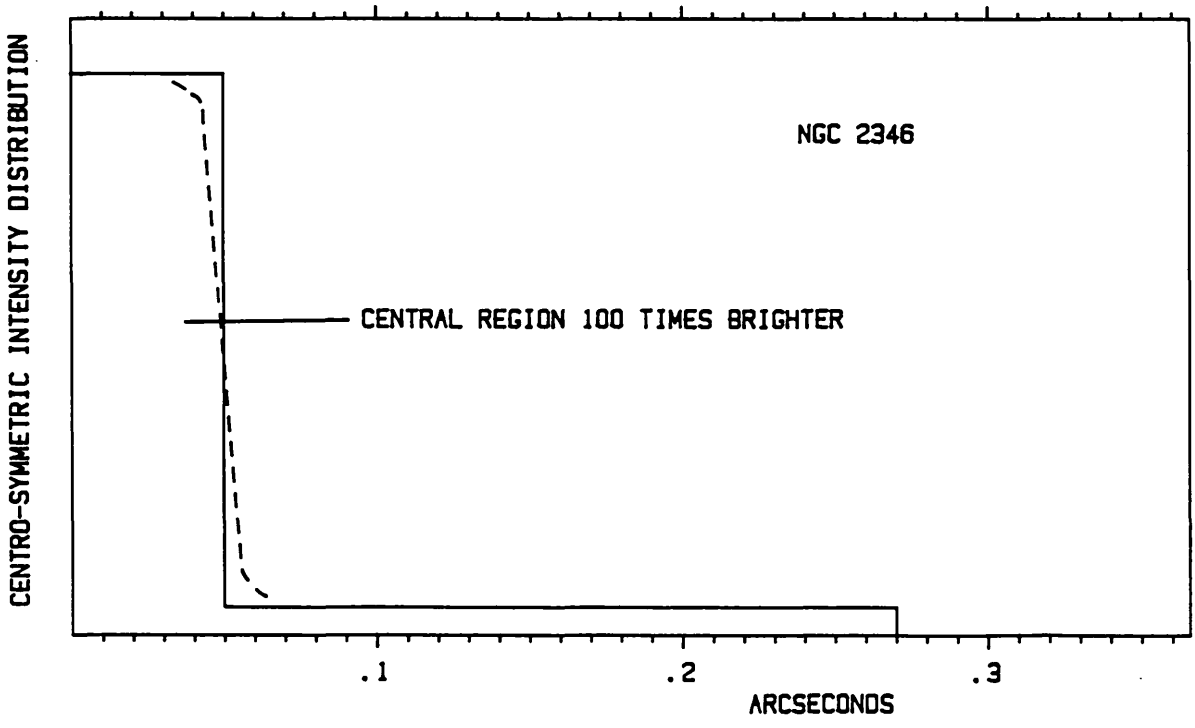

Figure 6.13 : a) The estimated speckle component of the central star in the nebula NGC 2346

b) The estimated object intensity distribution

star in the bipolar Toby Jug nebula (IC 2220), has revealed that it is an unresolved source with an angular diameter no greater than about 0.05 arcseconds. Initial examination of the autocorrelations obtained from the observation of the central region of the nebula NGC 6572 has revealed evidence of asymmetry. This may be due to a single elongated object or may be produced by a binary object having one, or possibly two, extended components. Unfortunately NGC 6572 was observed during a period of variable seeing conditions caused by moderate cloud cover. Because of the the subsequent loss of light, reliable determination of the form of this object from the existing record is not possible.

Analysis of a few recent observations has failed to achieve reliable results due either to cloudy observing conditions or excessive noise (e.g. ion-events, electrical interference) on the video record. Observations that have been affected in this way include those of the Seyfert nuclei of NGC 4151 (cloud), 3C120 (cloud) and 1Zw1 (bright hum bars on the video record). Nevertheless, it is hoped that further observations of these objects can be made in the near future. A summary of likely future observing programmes is given in section 7-3.

Chapter Seven

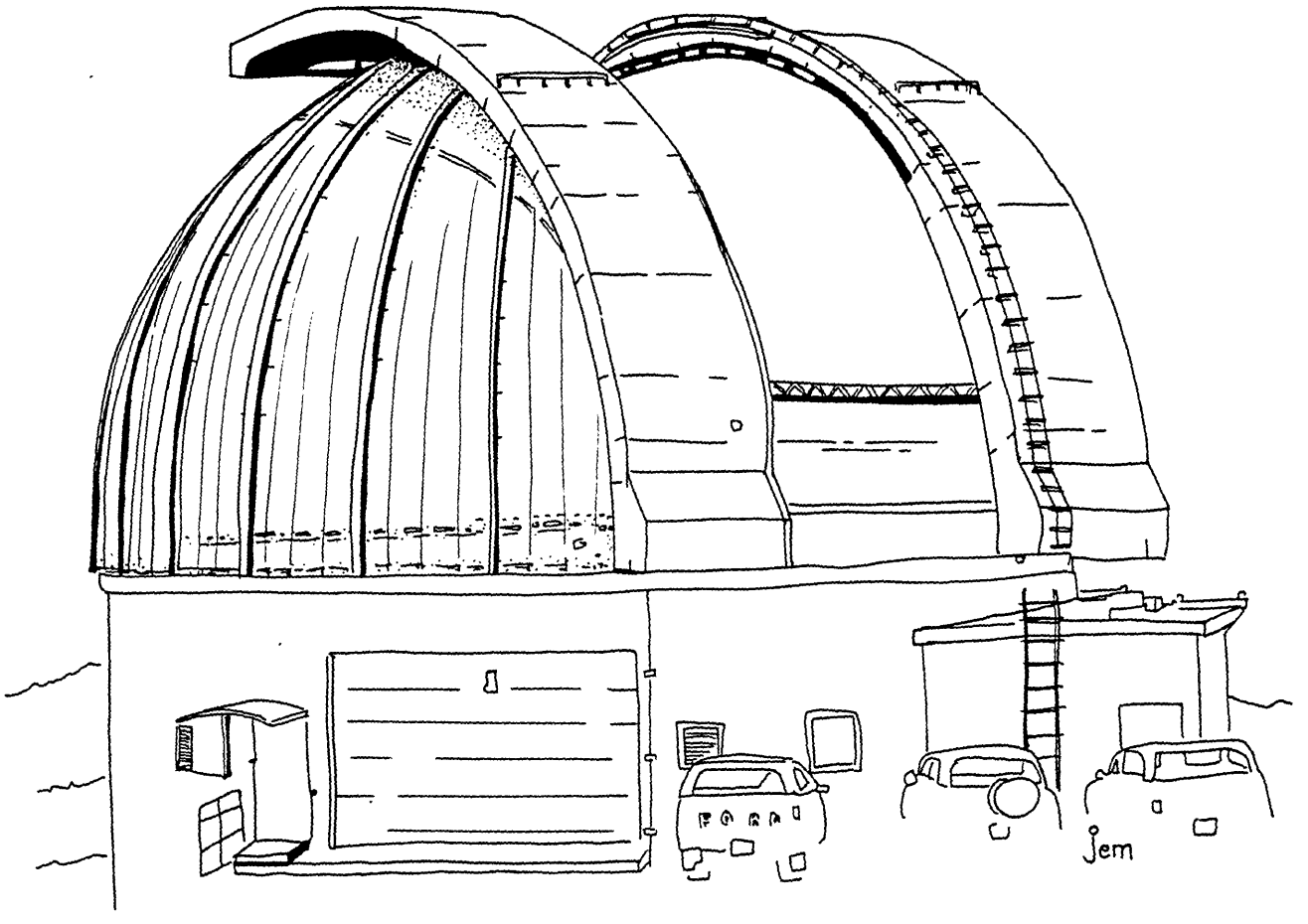

Chapter Seven : Conclusions And Future Work

7-1 Technique

Since the technique of speckle interferometry was first proposed by Labeyrie [1] many physicists have sought to find better ways of implementing the basic principles involved. Recently a great deal of emphasis has been placed on the requirement to retain phase information from speckle data in order to reconstruct images. Though valuable information can be obtained without using phase retrieval techniques, such methods are not being exploited to the degree one might expect. This suggests that there is, perhaps, a general dissatisfaction with results based on intensity information alone. Alternatively it may be that observers who have traditionally dealt with images are unhappy with less familiar concepts such as Fourier transforms and autocorrelations. However, so far very few results of outstanding astronomical significance have been achieved in the process of testing new ideas for obtaining images.

The research presented in the earlier chapters is concerned primarily with the requirement to obtain useful astronomical information from autocorrelations of speckle data and to devise, as when necessary, ways of improving the means to that end. The results reported in chapter six illustrate that this aim has been achieved very successfully. The implementation of alternative data processing methods which might improve the present system will be considered if and when they arise. At present there is no single method of phase retrieval which has been shown to be practicable for all classes of object currently being investigated using speckle interferometry. However, Dainty [2] suggests that such a method may be devised in the near future or may result from the amalgamation of two or more existing techniques.

The exponential filter method, as proposed by Walker [38] (see section 2-7), has proved to be very successful in computer simulations [22] though it has yet to be thoroughly tested using real astronomical data. Dr John Walker is currently using some of the video records obtained with the Imperial College system for this purpose. If these tests prove to be successful it is possible that ways to adapt the

present system in order to implement the technique may be discussed. The possibility of building a hardwired device which could perform the Knox-Thompson algorithm [27] has also been suggested but the method is known to be highly susceptible to noise [2],[30] and observations would probably be restricted to bright objects only.

The Welter and Worden [19] data reduction technique is known to be based on unrealistic assumptions (see section 5-1) and the data analysis method described in chapter five involves a number of additional approximations. Nevertheless, some very valuable astrophysical measurements have been made with an accuracy far beyond that possible before the introduction of speckle interferometric techniques. These results are summarized in section 7-3.

The data reduction system is still subject to continuous development. Software is being developed which will automatically perform the subtraction of the seeing component of the autocorrelation by comparison to a crosscorrelation. Experiments are being performed to find out whether the crosscorrelation requires adjustment before the subtraction is performed in order to account for the possible effects of large scale image movement. Additionally, the technique is known to be less accurate when the average number of events per frame is small (see section 2-6) and the possible effects of this are also being investigated. The interim design of the crosscorrelator, as described in section 3-9, allows the correlation interval to be adjusted. A series of experiments are being performed in order to determine the effects produced by varying the correlation interval.

When the crosscorrelation subtraction process is fully operational it will be possible to obtain immediate on-site results for the form of the (photon spike contaminated) autocorrelation speckle component. Unfortunately the length of time required to obtain a result is still dictated by the comparatively long period of time it takes to produce computer-modelled speckle components and for comparisons with the data to be made. However, a far quicker method for obtaining approximate best-fit model speckle components may be possible. The hardwired autocorrelator can produce a near-instantaneous two dimensional autocorrelation of a given TV frame. If the Apple microcomputer were to

generate suitable model speckles on its TV monitor display, the autocorrelator could produce an almost immediate autocorrelation of that image. The autocorrelation produced may then be compared to the real data and, perhaps, the model adjusted accordingly. The best-fit model may then be obtained via a fast converging loop. However, since the autocorrelator can only sample images in two dimensions, the microcomputer would be required to generate a series of speckles consisting of individual "events". The distribution of model events within speckles generated over a number of successive frames would be equivalent to the analogue intensity distribution of the speckle. The feasabilty of this method, known as real-time modelling, requires further investigation. Implementation of this technique would not, however, overcome the restriction which limits observation to objects having centro-symmetric intensity distributions.

7-2 Apparatus

After the autocorrelator first became operational, experience of faint and extended object observation prompted several additions to the circuitry (see section 3-8). It is possible that the crosscorrelator, which has recently begun operation, will undergo similar development. For instance, it has been suggested that the crosscorrelation subtraction method is more reliable if the images are successively recentred before crosscorrelation [55].

It is probable that the speckle interferometer, as described in section 3-1, would be completely rebuilt should the two image intensifiers presently being employed require replacement. Future supply of these devices from EMI has been uncertain for some time. Alternative image intensifiers which may be employed in future might involve microchannel plates (MCPs). A proximity focus MCP image intensifier has been built by Airey et al. [100] at Imperial College. It is much smaller than the EMI magnetically focussed image tube and does not require a focussing solenoid. A speckle interferometer incorporating such a device would be very much smaller and lighter and, since no mirrors would be required to keep the system compact, would suffer less light loss.

If it is considered sufficiently worthwhile and desirable to do so, the interferometer could be made operable entirely by remote control. The atmospheric dispersion correction prisms, as described in section 3-2, require adjustment at least once every twenty minutes, otherwise the effects of dispersion become appreciable. The prism settings are dependent on the telescope observing coordinates and thus the prisms could be driven simultaneously with, and possible by, the telescope itself. This would subsequently reduce the number of manual adjustments to the interferometer and would thus benefit the "overworked" observer. A simple step motor controlled by the microcomputer would achieve this. Selection of filters using remote controlled filter wheels would also be of great benefit to the observer.

It is current practice to reduce the image intensity when considered necessary by placing neutral density filters in the optical path. An easier and more efficient way to do this would be to shorten the exposure time of the image. Shorter exposure times would also improve the coherence so that the speckles are better defined. Thus it is intended that a shutter (or series of shutters) will be installed which can provide a large selection of speeds.

The reliability and image quality of the present video recording system has been matched, if not superceded, by the smaller video cassette systems now being manufactured. Though the recorders employed at present still function correctly, it is unlikely that replacements will be obtainable and it is possible that the reel-to-reel tapes themselves may soon be unavailable. The acquisition of a new system is being considered.

It was mentioned in the previous section that possible future technical developments of the system might include the building of a hardwired device capable of producing reconstructed images. Processing of speckle images inevitably involves a very large quantity of data and thus speed is necessarily an important criterion. If real-time processing is required then building hardwired apparatus is, at the present, the only adequate solution. However, as mentioned in section 1-2, computers incorporating parallel processors may soon enable far greater processing speeds to be achieved using software.

7-3 Results

Until all astronomers who require diffraction limited information at optical wavelengths have sufficient access to large orbiting telescopes, or perhaps even to telescopes located on the moon, speckle interferometry will have a valuable role to play. Over the next decade it is likely that interest in high resolution optical astronomy will be stimulated by the Space Telescope. However, the Space Telescope will only have an optical resolution of about 0.05 arcseconds which is not as large as that obtainable using speckle interferometry on the 3.9m AAT. As mentioned in the opening section of the first chapter, if ground based diffraction limited imaging does become a reality even for faint objects, establishing expensive telescopes in space will be significantly less beneficial. Extremely high resolution, maybe one hundred times that attainable with the Space Telescope, is theoretically possible using VLBI techniques (see section 1-3). This idea has recently been taken one step further by Stachnik and Labeyrie [140] who describe the advantages of a long baseline (10km) space telescope.

Speckle interferometric observations have been made of almost every type of visible stellar object, from the solar features reconstructed by Stachnik et al. [26] to the triple quasar resolved by Hege et al. [50]. The results presented in chapter six further demonstrate the versatility of the technique. The whole observing programme has shown how a speckle system may be used in the way any common-user instrument may be used on a telescope. The Hipparcos star programme demonstrated how well established the data reduction process has become for the observation of binary stars.

The nature and origins of the asteroids have been the subject of much speculation ever since the first was discovered at the beginning of the nineteenth century. Some theories, such as that put forward by Ovenden [144], suggest that they are fragments of a recently exploded planet; the "missing" planet between Mars and Jupiter predicted by the Titus-Bode "law" of planetary distances. Alternatively, the asteroids have been regarded as the debris remaining after the formation of the planetary system. In 1944 Schmidt (see Safronov [145]) suggested that the asteroids originate as a result of an interruption of the

accumulation of a planet. This, Schmidt suggests, was due to perturbations by the massive Jupiter which had time to grow somewhat earlier. If questions about the nature of the asteroids can be answered with the use of speckle interferometry or otherwise, then perhaps the origins of the planets themselves can be determined more accurately.

The speckle observations of NGC 1068, both by ourselves [71] and by McCarthy et al. [72], have become two of the most widely quoted results obtained using the technique. Hopefully observations of other Seyfert galaxies with bright nuclei, such as NGC 4151, M87 and 1Zw1, will be made soon. The determination of the structure in the centre of these galaxies may enable astronomers to learn more about the core of our own galaxy which is entirely obscured by dust at visible wavelengths.

The discovery of supermassive objects in the cores of active nuclei requires the introduction of new concepts in order to explain their extraordinary behaviour. On the other hand, some objects which have been known to exhibit anomalous behaviour have become significantly less mysterious following speckle interferometric observations. Often such behaviour has originally been attributed to various complex mechanisms whereas, as in the case of the central star in the Red Rectangle nebula, it is sometimes best explained by the simplest and most obvious reasons, namely the ineffectiveness of previous techniques to resolve the star.

The nature of R136a continues to be the subject of great debate by observers operating at various wavelengths. The existence of faint companions to R136a with separations less than one arcsecond has recently been suggested by other observers though nothing supporting this has so far been published. However, re-examination of our data has failed to find any evidence consistent with this suggestion.

Recently a new observing programme has been undertaken which involves the observation of planetary nebulae in collaboration with Dr Mike Barlow of University College, London. A planetary nebula is an expanding and usually symmetrical cloud of gas that has been ejected from a dying star. The star may possibly be in the form of a red giant. The gas is thought to have formed all or part of the outer layer of the star. The nebulae are usually either ring-shaped or hourglass-shaped

and some are known to contain spectroscopic binary stars. NGC 2346, observed in collaboration with Dr John Meaburn (see section 6-8), is a planetary nebula containing such a binary star.

The aim of the new programme is to determine the angular diameters, and thereby the ionized nebula masses, of a number of planetary nebulae located in the Magellanic Clouds. These nebulae are unresolved in typical seeing conditions. Their expected angular diameters can be estimated by comparison to galactic planetary nebulae with similar physical properties and should fall in the range 0.2 to 0.8 arcseconds. A measurement of the radius of the nebula, combined with its distance and known spectral properties, enables the total mass of the ionized gas to be calculated.

Possible future observations include an investigation of the central intensity distribution of elliptical galaxies. Speckle observations would be able to determine the extent of the cores of these objects in order that a limit may be placed on the degree of the central condensation of stars. A variety of theoretical and empirical laws fit the observed intensity distribution with various degrees of satisfaction. However, unambiguous differentiation between these models can only be made at either very large radii, where the surface brightness is much less than the sky brightness, or at very small radii which fall within the seeing disc. Schweizer [141],[142] claims that nearly all elliptical galaxies in a sample provided by King [143] contain unresolved cores.

It has been shown how system development can be successfully combined with active observing programmes in order that a number of valuable astrophysical results can be obtained. Both equally important features of the research will hopefully continue to be productive in the future. There is no shortage of ideas for ways to improve the basic technique or data reduction methods, nor is there any lack of objects of which speckle observations could be made in order to significantly enhance our knowledge of the universe.

Publications

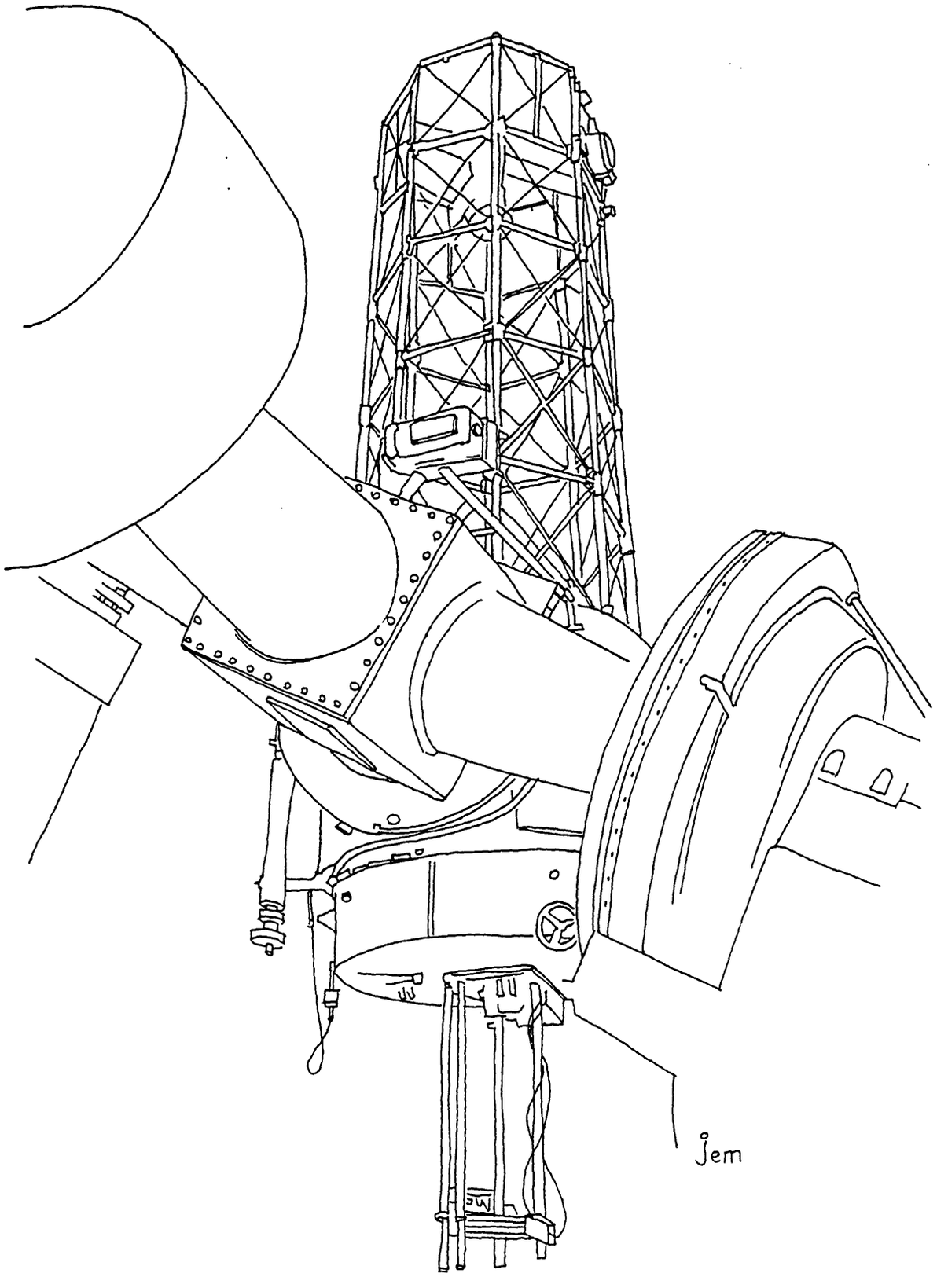

Publications

1. Speckle interferometry using a hardwired real-time autocorrelator.
   Hebden,J.C.,Morgan,B.L. and Vine,H.
   SPIE Proceedings of "Instrumentation in Astronomy V"
   Volume 445. September 1983

2. Speckle observations of R136a.
   Meaburn,J.,Hebden,J.C.,Morgan,B.L. and Vine,H.
   Monthly Notices of the Royal Astronomical Society
   Volume 200, page 1P. 1982

3. Speckle observations of Eta Carinae.
   Meaburn,J.,Walsh,J.R.,Hebden,J.C.,Morgan,B.L. and Vine,H.
   Monthly Notices of the Royal Astronomical Society
   Volume 204, page 41P. 1983

4. Speckle observations of the central binary star in the Red Rectangle.
   Meaburn,J.,Walsh,J.R.,Hebden,J.C.,Morgan,B.L. and Vine,H.
   Monthly Notices of the Royal Astronomical Society
   Volume 205, page 53P. 1983

5. Speckle interferometry of Hipparcos link stars.
   Argue,A.N.,Hebden,J.C.,Morgan,B.L. and Vine,H.
   Monthly Notices of the Royal Astronomical Society
   Volume 206, page 669. 1984

Speckle interferometry using a hardwired real-time autocorrelator

J.C. Hebden, B.L. Morgan and H. Vine

Blackett Laboratory, Imperial College of Science and Technology,
Prince Consort Road, London SW7 2BZ, England.

Abstract

The specification and performance of the Imperial College hardwired real-time autocorrelator are described in detail. The application of the autocorrelator to the technique of stellar speckle interferometry is illustrated and results obtained are discussed. Emphasis is given to developments of the system prompted by our experience in observing faint and extended objects.

Introduction

Stellar speckle interferometry, invented by Labeyrie[1], is a technique which allows diffraction limited information to be obtained from large telescopes despite the effects of the turbulent atmosphere which normally limit the resolution to one arcsecond or worse. Short exposure monochromatic images of unresolved stars are composed of a random pattern of speckles enclosed in the seeing disc. Speckles are formed by the coherent addition of light from all parts of the aperture, the relative phases and amplitudes of the wavefronts being random, and are of the same order of size as the Airy disc of the telescope. Labeyrie showed that diffraction limited information may be extracted by integrating the Fourier transforms or autocorrelation functions of short exposure images where the atmospheric turbulence is effectively frozen. Detailed reviews of this technique and it's extensions have been made by Dainty[2] and Worden[3].

The Imperial College speckle interferometer was initially designed to accommodate a cine camera system as described by Beddoes et al[4]. The introduction of a TV system and a hardwired real-time autocorrelator enables much fainter objects to be observed as well as facilitating the investigation of extended objects.

The interferometer is shown schematically in figure 1. Light from the telescope enters the system through a circular hole in the baseplate where it is either viewed through an eyepiece or is reflected down the optical axis of the interferometer. A rotating sector shutter enables the exposure time of the image to be controlled. Microscope objectives of various focal lengths determine the overall magnification of the system which is usually such that the field of view on the TV camera is about 4 arcseconds. Light which has been collimated by the microscope objective passes through a pair of prisms used to compensate for atmospheric dispersion. Two pairs of prisms are employed: one pair is designed for

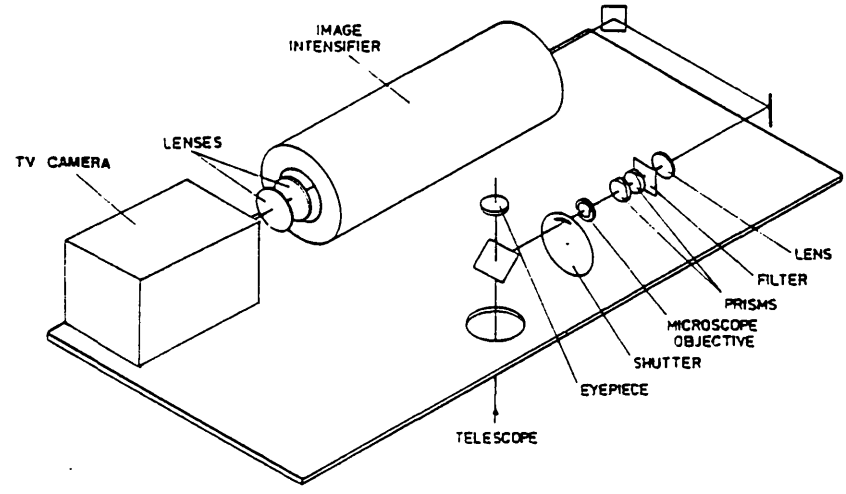

Figure 1. Schematic diagram of the interferometer.

operation at visible wavelengths, the other pair to permit observation in the near ultra-violet down to 340nm. The next element in the optical train is a bandwidth filter which ensures temporal coherence. A relay lens then focusses the light onto the photocathode of an EMI four stage cascade tube having a photon gain in excess of 10^6. The image on the output phosphor screen is then re-imaged onto the faceplate of a Plumbicon tube TV camera. Several LED's situated between the camera and the coupling lens provide a bias illumination which greatly improves the contrast of the TV images. The TV images are recorded onto magnetic video tapes as well as being processed in real time.

The hardwired real-time autocorrelator

Design requirements

The two dimensional spatial autocorrelation of an image comprising individual photon events is equivalent to the distribution of vectors between each event and every other event within the image. A hardwired digital autocorrelator has been built which is required to produce two dimensional autocorrelations of TV images in real time and to enable an immediate display of results.

The standard British TV system uses pictures consisting of two interlaced fields each of 293 lines of image information. Each field has an effective exposure time of 40ms. This can be reduced by placing in the system a shutter synchronised with the TV camera.

To reduce project costs only alternate fields are processed. This does reduce the effective resolution but in practice photon events appear significantly larger that the spacing between successive field lines. The autocorrelator examines the central 256 lines in a square of 256 by 256 pixels. Two identical memories within the autocorrelator enable one field to be scanned in order to record the locations of photon events while the

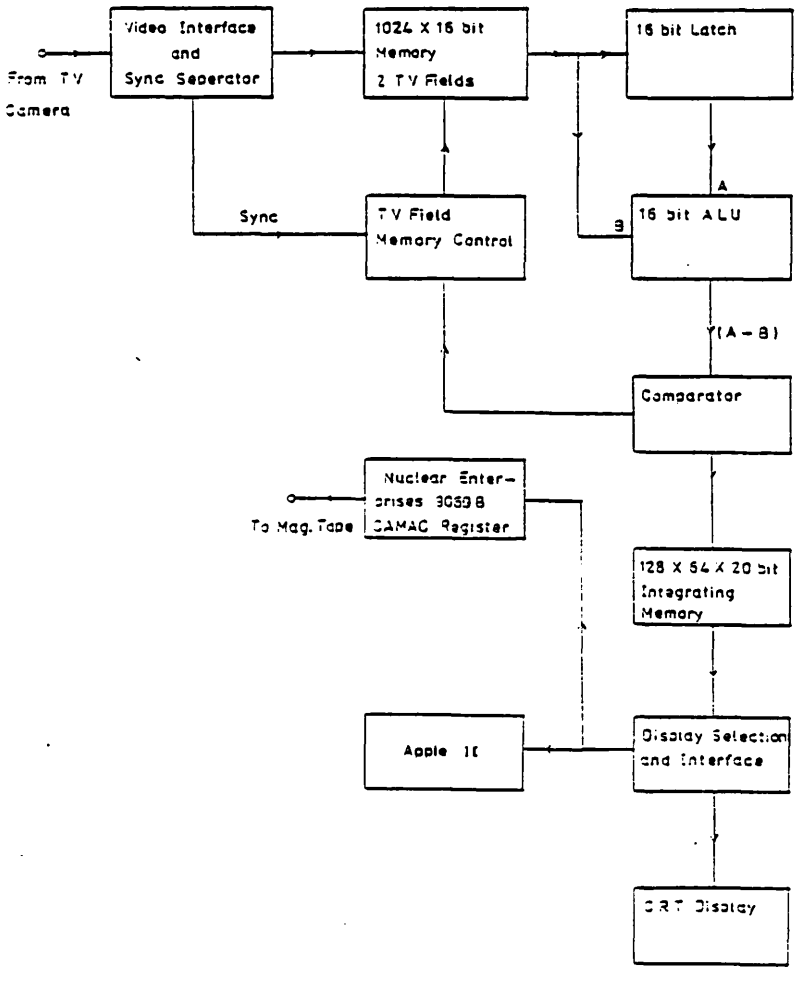

Figure 2. Schematic diagram of the hardwired real-time autocorrelator.

coordinates stored from the previous field are processed. Thus there are 40ms available to carry out the calculation. If the maximum number of occupied pixels per frame is M the number of vectors to be calculated will be $\frac{1}{2}(M^2 - M)$ or, for $M \gg 1$, $\frac{1}{2}M^2$ 'operations'. One operation, as will be expained shortly, consists of two eight bit subtractions and the increment of a 20 bit memory. If the operation time is t, we therefore require that

$$\frac{1}{2}M^2 \times t \leq 40 \text{ ms}$$

The technological limit within the available budget in 1977 limited t to a minimum of about 0.3 microseconds. The system was therefore designed to allow a maximum number of 512 occuped pixels per frame. Further increase in operation speed could only be achieved for a disproportionate increase in costs. Incidentally, present technology could improve it by at least a factor of four within the original financial limitations.

Most of the 293 field lines are examined and generally the optical magnification is chosen so that the seeing disc sits comfortably within this area. Only vectors within a 64 by 128 pixel window are recorded enabling a great saving in memory costs. The range of binary separations or object extensions detectable will depend on the magnification used.

Operation

The autocorrelator examines the signal at each pixel position and if the signal lies above the adjustable detection threshold (called the video level) the X and Y coordinates of that pixel are stored as 2 x 8 bits in one of the two 512 x 16 bit memories. If the signals in more that 512 pixels exceed the video level subsequent positions are ignored.

Meanwhile autocorrelation is performed on the coordinates previously stored in the other memory. The coordinates of the ith pixel are subtracted from those of the jth pixel where $j > = i$ and a memory location whose address is given by the result of the subtraction is incremented. If the result of the X subtraction is <-64 or >63 it is ingnored. If the Y subtraction is >63 it is ignored and since all subsequent Y differences will also exceed 63, the current j incrementation is terminated and the next value of i considered.

The number contained in an autocorrelation array pixel (x,y) represents the number of times that the difference between two image pixels was x in the X direction and y in the Y direction. The vectors (-x, -y) in the negative Y direction are identical in number, contain no new information and therefore are not recorded.

The autocorrelation array is a 128 x 64 x 20 bit integrating memory consisting of forty 4 K MOS static RAM chips arranged in twenty pairs.

Figure 2 shows a schematic diagram of the autocorrelator. It shows the video signal applied at the input where the TV synchronisation signal is used to drive the TV field memory control which acts as an address counter and a read/write mode selector. As mentioned above, whilst the pixel locations of a TV field are loaded into one of the 512 x 16 bit memories the data previously stored in the other memory are processed. The coordinates of the first occupied pixel are stored in the 16 bit latch memory and are subtracted from those of all the other occupied pixels in turn by the arithmetic logic unit. All the coordinates except those of the first are then re-written into the buffer memory and the coordinates of the second occupied pixel are stored in the latch memory and subtracted from the remaining coordinates and so on. The comparator unit distinguishes when X or Y limits are exceeded and increments the appropriate address counter. Otherwise the corresponding memory location of the integrating memory is incremented. The contents of this memory may be periodically displayed as described later.

System Developments

The autocorrelator was first used in late 1979 for a programme of binary star observations. Experience of faint and extended object observation has prompted several additions to the circuitry.

Photon events appear at the output of the image intensifier with a range of intensities. Sometimes it is desirable to sample every event possible, even the very faintest. Under these conditions high frequency background noise from the camera tends to be detected. To enable the autocorrelator to distinguish between the effect of camera noise spikes which persist for less than the pixel scan time and photon events, which are typically 3 or more pixels across, a high frequency discriminator has been built which discounts any signal persisting over less than about eighty percent of the pixel scan time.

Another addition is designed to prevent any bright hum-bars or lines due to tape damage or drop-out being sampled. This functions by rejecting any signal which persists over a scan time corresponding to about 22 consecutive pixels. The low frequency discriminator

rejects the entire TV line on which such a signal is registered. Both discriminators may be switched out if not considered desirable or necessary.

A video signal limiter may be used to establish an adjustable upper detection threshold above which a signal may be rejected. This unit reduces the effect of ion events on faint records and will also eliminate the saturated areas of very bright records which would otherwise produce a distortion in the autocorrelation.

Another modification enables the autocorrelator to distinguish 'odd' or 'even' fields so that two distinct records are available from the same video tape recording. This facilitates the identification of spuriae due to transients such as ion events in the image intensifier.

The Crosscorrelator

The cross-correlation of pairs of speckle images sufficiently well separated in time will have a mean intensity representing the seeing-limited long exposure image.

The Imperial College crosscorrelator has been designed to store the image positions of 25 fields, equivalent to one second's worth of information, in twenty five distinct 512 x 16 bit memories which are continuously replenished in a cyclic manner. The field stored most recently is crosscorrelated with the field which has been held the longest. Thus, for example, while the 25th field is being stored the 24this crosscorrelated with the first. Their temporal separation is therefore equal to twenty three field periods or 920ms which comfortably ensures that the images are uncorrelated. After the 25th is stored. the next is loaded into the memory which had contained the first field while the second is crosscorrelated with the freshly stored 25th and so on.

Apart from the use of 25 memories instead of just two, the logic and arithmetic arrangement is the same as that of the autocorrelator. The resulting crosscorrelation is stored in another 8K by 20 bit integrating memory.

Whilst this system is under development, an interim crosscorrelator has been built which utilises only two memories. In this arrangement the crosscorrelation interval is adjustable from ten fields to infinity.

Operational Procedure

The facility to obtain on-site autocorrelations is generally only used as an opportunity for a first look and a check on the suitability of the data. Back in the laboratory video taped data may be re-examined more thoroughly at varying detection thresholds with and without discriminators. It is useful to have a record of the background obtained on site with the TV camera capped in order to deduce the necessary threshold required to avoid sampling of background noise. A Camac interface enables autocorrelations to be stored on magnetic tape for display by on-site computers and by systems such as STARLINK. A Tektronix Storage Monitor allows autocorrelations to be displayed.

Data reduction is primarily carried out using an Apple II microcomputer. Autocorrelations are transfered to the computer memory and may be displayed as a whole in two or three dimensions. Sections through the autocorrelation may also be taken, and azimuthally averaged profiles may be calculated. Data is then stored on standard floppy discs enabling a sizable library of records to be built.

When extended objects are observed a record is obtained of a nearby unresolved reference star. This enables artefacts due to optical or electronic instrumentation to be recognised. It is important therefore to match as nearly as possible the brightness, seeing conditions and all other observing parameters for the reference star to those of the object. Video tape records are often autocorrelated in sections to eliminate localised effects due to specific tape defects or recorded noise such as bursts of ion events.

The autocorrelations generally consist of three components: the seeing component, the speckle component (vectors between pixels within same speckle) and the photon spike (vectors between pixels within isolated photon events). The photon spike can not yet be reliably subtracted though the seeing component can be approximated to a high degree by comparison to the crosscorrelation or to a Gaussian-like function. The speckle component is compared to computer models calculated for the specific observing conditions.

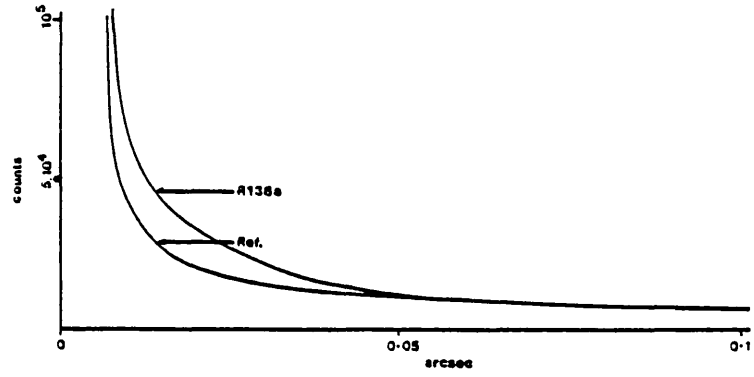

Figure 3. Sections through the Y axis of the autocorrelations of R136a and a reference star.

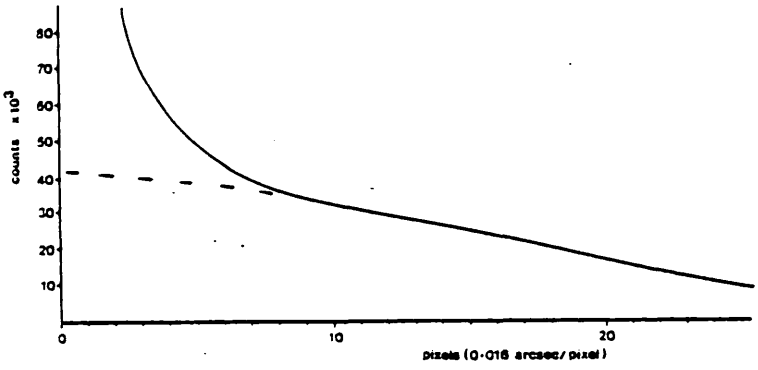

Figure 4. Section through the autocorrelation of eta Carinae. The best fit Gaussian-approximated seeing pedestal is indicated by the dotted line.

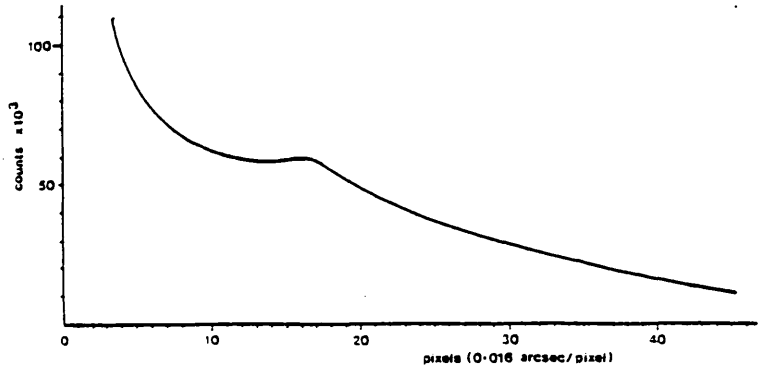

Figure 5. Autocorrelation of HD44179 indicates a secondary peak corresponding to a position angle of 146±3° and a separation of 0.29±0.02 arcsec.

Results

A great number of results have been obtained, the following examples give an idea of the scope of the technique.

Recent speckle observations of R136a, a blue supermassive star-like object in the 30 Doradus nebula, put an upper limit of 0.02 arcsec to it's diameter[5]. Figure 3 shows the sections through the Y axis of the autocorrelations of R136a and a reference star, indicating that it is most likely unresolved. These results are consistent with the possibility of R136a being a star cluster of 30 separate O3 or WN3 stars within a diamter of 5 x 10^{-3}pc or it could be a single supermassive star (2500 $M_\odot$) of the same extent.

Observations of the nucleus of the Seyfert galaxy NGC1068[6] reveal a very bright unresolved core with a diameter of $\leq$ 2.3pc. This emits an amount of visible light equivalent to that from 5 x 10^9 solar masses.

It has been found that eta Carinæ, a star-like object in the centre of the nebula NGC3372, is most probably a single unresolved star of about 100 $M_\odot$[7]. No evidence for any binary component with a separation of between 0.03 and 0.9 arcsec has been found. Figure 4 shows a section through the autocorrelation of eta Carinae. The data depart from the best fit Gaussian-approximated seeing pedestal consistent with calculated models for a single unresolved source.

Observations of the star HD44179 contained in the centre of the red rectangle nebula have confirmed its binary nature[8]. The secondary peak in the autocorrelation as shown in figure 5 indicates a position angle of 146±3° and a separation of 0.29±0.02 arcsec. This is the first confirmation of its binary nature for over twenty years and enables orbital period and total mass calculations to be suggested.

The original involvement of the Imperial College cine camera system with binary star work is echoed by the interest in the ESA Hipparcos Astrometry Satellite project[9]. It is required to relate the Hipparcos reference frame to the extra-Galactic frame observed by the Space Telescope. It is therefore necessary to select stars from the Hipparcos catalogue which will remain unresolved and show no multiplicity at the Space Telescope diffraction limit. Observations of many candidates have therefore been made in order to eliminate stars showing multiplicity[10,11].

Work has also been carried out on a programme of asteriod observations in collaboration with Ted Bowell of Lowell Observatory, Flagstaff, Arizona. Of particular interest is the possible identification of asteroid satellites and study of their orbital motions[12].

In addition to the above it is also essential to observe under varying conditions objects whose properties are well known. These calibration exercises have proved invaluable in assessing various aspects of the technique.

Future Work

The immediate priority is to have the crosscorrelator fully functional as soon as possible. Further improvements to the system being considered include making the interferometer operational by remote or microcomputer control. Improved techniques in modelling and comparison to data are currently being investigated. Ultimately, it is hoped that the equipment may be adapted to exploit recent theoretical advances in image reconstruction methods.

Acknowledgments

All this work has been generously supported by the SERC and in particular JCH is grateful for his SERC Research Studentship and HV for SERC support as Assistant Research Officer.

References

1. Labeyrie, A., Astron.Astrophys., 6, 85. 1970
2. Dainty, J.C., In "Laser speckle and related phenomena (Topics in Applied Physics vol.9)" ed. Dainty, J.C., Springer-Verlag. 1975
3. Worden, S.P., Vistas Astr., 20, 301. 1977
4. Beddoes, D.R., Dainty, J.C., Morgan, B.L.and Scaddan, R.L., J.Opt.Soc.Am., 66, 1247. 1976
5. Meaburn, J., Hebden, J.C., Morgan, B.L. and Vine, H., Mon.Not.R.Astron.Soc., 200, 1P. 1982
6. Meaburn, J., Morgan, B.L., Vine, H., Pedlar, A. and Spencer, R., Nature, 296, 331. 1982
7. Meaburn, J., Walsh, J.R., Hebden, J.C., Morgan, B.L. and Vine, H., Mon.Not.R.

Astron.Soc. (In press)
8. Meaburn, J., Walsh, J.R., Hebden, J.C., Morgan, B.L. and Vine H., Mon.Not.R.Astron. Soc. (In press)
9. Hipparcos Space Astrometry, Report of the Phase A Study. ESA,SCl (79) lO. 1979
lO. Argue, A.N., Baxter, R.D., Morgan, B.L. and Vine, H., Scientific Aspects of the Hipparcos Mission p53, eds. Perryman, M.A.C. and Guyenne, T.D. 1982
11. Argue, A.N., Hebden, J.C., Morgan, B.L. and Vine, H., Mon.Not.R.Astron.Soc. (In press)
12. Bowell, E., Morgan, B.L., Lumme, K., Dainty, J.C., Vine, H. and Poutanen, H., Bull. Am.Astron.Soc., 13, 3. 1981

Mon. Not. R. astr. Soc. (1982) 200, *Short Communication*, 1P–5P

Speckle observations of R136a

J. Meaburn *Department of Astronomy, University of Manchester, Oxford Road, Manchester M13 9PL*

J. C. Hebden, B. L. Morgan and H. Vine *Blackett Laboratory, Imperial College of Science and Technology, Prince Consort Road, London SW7 2BZ*

Received 1982 January 11

Summary. It has recently been suggested that R136a is a single, supermassive star ($2500 M_\odot$) with a surface temperature of 60 000 K. Speckle observations have now been made with the 3.9-m Anglo-Australian telescope which definitely puts an upper limit of $\simeq 0.02$ arcsec to its diameter and which *possibly* just resolve it as a disc of $\simeq 0.02$ arcsec ($\simeq 5 \times 10^{-3}$ pc).

Three possibilities are considered. The first is that R136a is a star cluster with 30 separate O3 or WN3 stars within a diameter of $\simeq 5 \times 10^{-3}$ pc or it could be an amorphous region of this same extent. Alternatively, this marginal evidence for its finite extent may be spurious and 0.02 arcsec could then be the upper limit for its diameter from these measurements. In this case R136a could be a single supermassive object $\simeq 5 \times 10^{-3}$ pc in diameter.

1 Introduction

The blue, stellar-like object R136a is the dominant source of ionizing photons, within the massive 30 Doradus nebula (Feitzinger *et al.* 1980; Cassinelli, Mathis & Savage 1981 and see Meaburn 1981a and b for recent summaries of the parameters of this giant interstellar complex). Its luminosity is equivalent to 10^8 times that of the Sun and the rate of emission ($\simeq 5 \times 10^{51}$ s^{-1}) of ionizing photons is equivalent to that expected from 30 O3 and WN3 stars.

Furthermore, recent ultraviolet observations (Cassinelli *et al.* 1981) have shown that its surface temperature is $\simeq 60\,000$ K (confirming the predictions of Feitzinger *et al.* 1980) and that it emits an extremely powerful stellar wind of $10^{-3.5} M_\odot$ yr^{-1} at 3500 km s^{-1} (Cassinelli *et al.* 1981). The large-scale disturbance of the surrounding interstellar medium (Meaburn 1981a) could be evidence of the interaction of this wind (and the intense radiation pressure).

Three possibilities (Feitzinger *et al.* 1980; Cassinelli *et al.* 1981) should be considered concerning the nature of R136a. The first is that it could be an unusually compact group of very hot stars. For instance, 30 O3 stars could be contained within a volume of $\lesssim 0.1$ pc diameter ($\lesssim 0.5$ arcsec at a distance of 55 000 pc). However, this is inconsistent with the optical spectrum (an associated population of cooler stars within such a cluster is absent)

and the variability (Feitzinger *et al.* 1980) of the visible emission could not originate within a group of stars.

Alternatively, R136a could be a single superluminous star with a mass of $2500 M_\odot$ and a radius of $100 R_\odot$ (Cassinelli *et al.* 1981) which is more massive than any known. In which case it is likely to be only a very short-lived phenomenon ($\lesssim 10^5$ yr) and its angular diameter would only be $\simeq 2 \times 10^{-5}$ arcsec ($\equiv 5.3 \times 10^{-6}$ pc at the distance of the LMC).

Finally, R136a could be at some state of its proto-stellar collapse into a single massive object. In which case its angular extent would certainly be much larger than that predicted for supermassive stars by Cassinelli *et al.* (1981) though the observable manifestation of this extended state are most uncertain at the present time.

Near ultraviolet and visible 'speckle' observations have therefore been made to determine the spatial extent of R136a.

2 Observations and results

R136a was observed with the Imperial College of Science and Technology (London) speckle interferometer combined with the *f*/15 focus of the 3.9-m Anglo-Australian telescope. (For the background to speckle interferometry see for instance Labeyrie 1970; Beddoes *et al.* 1976; Worden 1980; Weigert 1980; Fienup & Feldkamp 1980.)

This device has an EMI four stage image-tube (S20) combined with a Plumbicon TV camera and detects individual photon events over the image of a 3.07 arcsec square (256 x 256 pixels) field with the configuration of lenses used for R136a. An individual recording is obtained every 1/50 s of this atmospherically distorted image which is then auto-correlated on-line within 1/25 s. Over an extended observing period these separate two-dimensional autocorrelations are coadded and finally an autocorrelation is obtained for the 3.07 arcsec square area in which objects separated by $\lesssim 0.9$ and $\gtrsim 0.03$ arcsec (the limiting angular resolution of the telescope at 5000 Å for instance) are capable of being detected. This is stored on tape in an array from -64 to $+63$ pixels in the X dimension (right ascension) and from 0 to -63 pixels in the Y dimension (declination) where the 0 0 pixel is the zero of the two-dimensional autocorrelation and contains the 'photon spike'.

The integrated autocorrelation of the field, which contains the object under investigation, is then compared with that for a star known to be single. If this is very near in angular distance from the object, which is of nearly similar brightness and if the data is obtained for a similar integration-time, immediately afterwards through the same filter, then it can reasonably be assumed that the statistical properties of the turbulence in the atmosphere are similar in both cases and a significant comparison of the autocorrelations can be made.

A summary of the observations for R136a with this system is given in Table 1.

Similar exposures for a comparison star ($v = 8.7$) at $\alpha = 05^h\,38^m\,26^s.437$ $\delta = -69°\,59'\,12''.00$ (1950) were obtained as described above. This is 1° from the R136a ($v = 9$) $\alpha = 05^h\,39^m\,03^s.1$ $\delta = -69°\,07'\,37''$.

Table 1. Speckle observations of R136a.

Figures and Plate	Exposure time	Filter Å	Max resolution arcsec	Number of frames in autocorrelation
–	1200	3700–3900	0.02	3.6×10^4
–	860	5000–5600	0.03	2.6×10^4
Fig. 1 and Plate 1	660	5640–5710	0.03	1.65×10^4

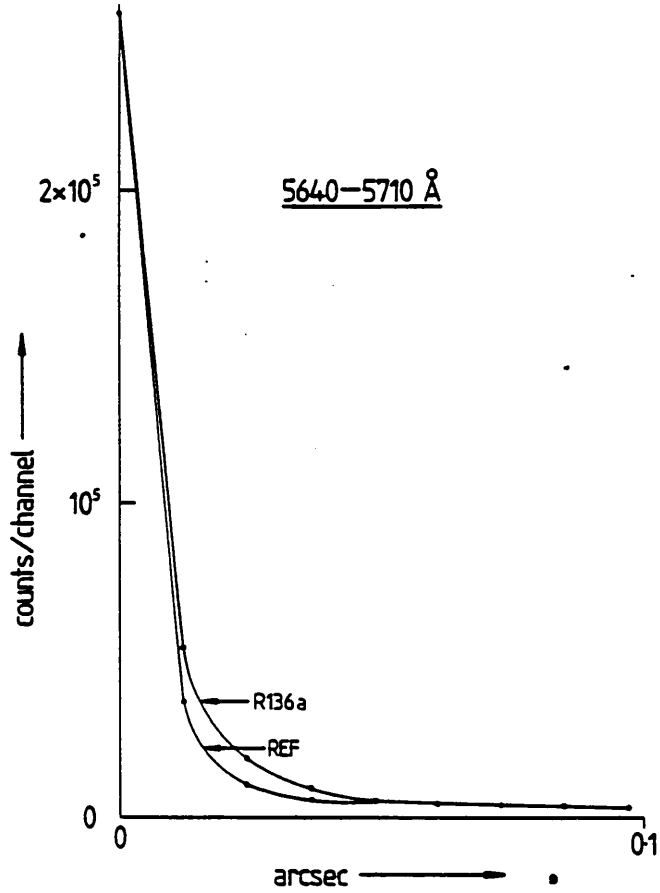

Figure 1. Sections are shown along the – Y axis (see Plate 1) of the two-dimensional autocorrelations for R136a and a reference star in the same 5640–5710 Å wavelength region. This is through the 0 0 pixel (containing the photon spike).

In Fig. 1 cuts through the 0 0 pixel in the – Y direction towards the 0, – 63 pixel) of the autocorrelations for R136a and the reference star, both for the 5640–5710 Å bandwidth (see Table 1) are compared.

In Plate 1 a greyscale representation of the whole of the autocorrelation is presented from which the cut in Fig. 1 for R136a was extracted. This was produced on the Manchester node of the STARLINK data processing network. Here only the very faint information in the outer regions of the data array is displayed. The bright centre around the 0 0 pixel (which contains the 'photon spike') is burnt out.

3 Discussion

The cuts in Fig. 1 and the whole autocorrelation shown in Plate 1 illustrate that the massively dominant component (A) of R136a is concentrated within a volume of $\lesssim 0.02$ arcsec diameter. Only a few maxima produced by secondary stars, which are $\gtrsim 81$ times fainter than the primary component, are present in Plate 1. The brightest of these (B in Plate 1) has $v \simeq 14$ and is 0.8 arcsec from the primary component A. (None of these appear on the comparable autocorrelation for the reference star.) Furthermore, the curves in Fig. 1 (and similar ones for the other two wavelength domains listed in Table 1) contain some

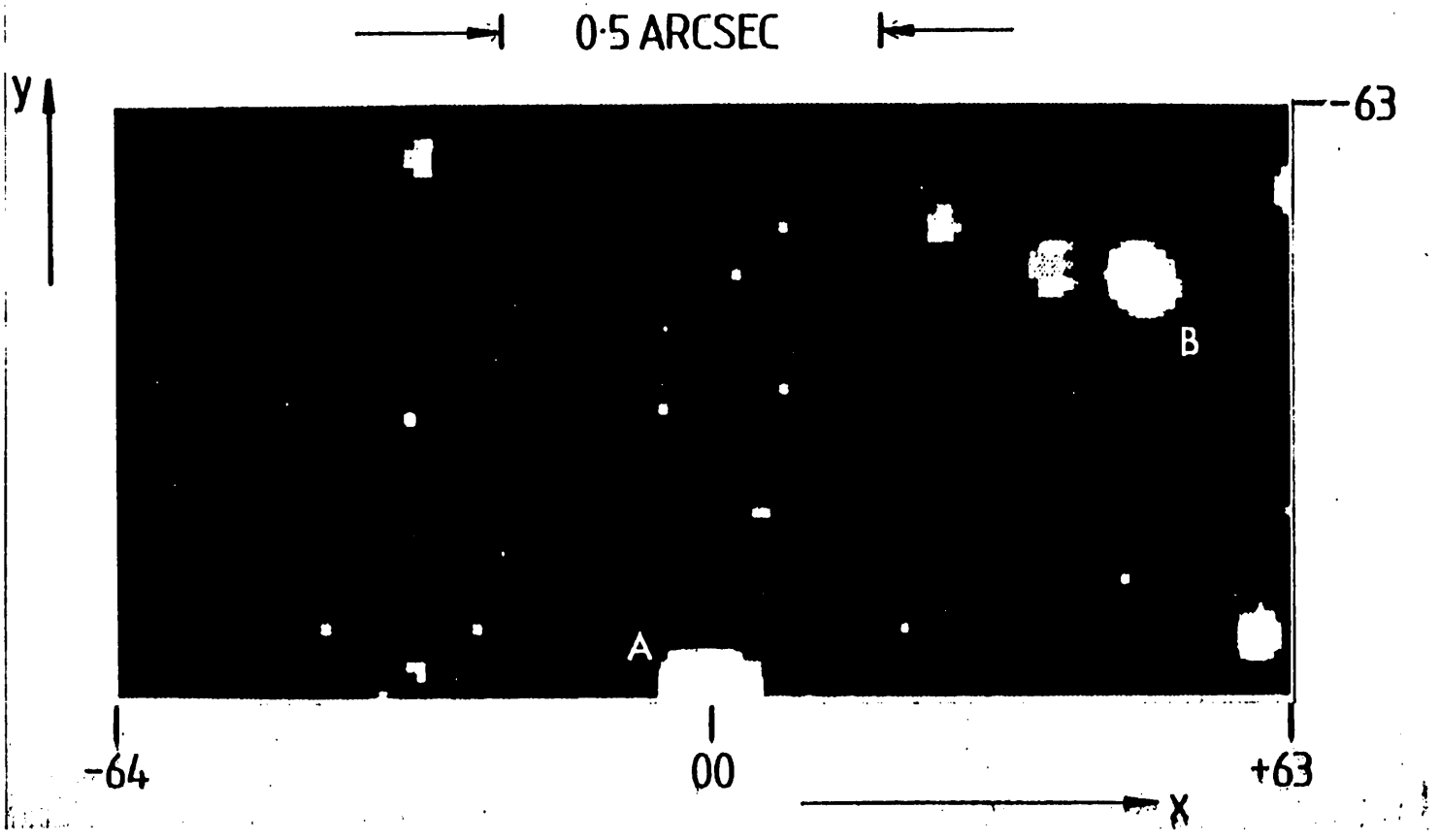

Plate 1. A greyscale representation is shown of the faint regions in the two-dimensional autocorrelation obtained in the 5640–5710 Å wavelength range (see Fig 1). The bright centre A which is primarily a consequence of a single dominant component in R136a is 'burnt out'. Several faint maxima are caused by autocorrelations of individual stars both with the primary object and each other. The brightest B shows that a faint second star is at 0.8 arcsec from the dominant component.

Facing page 31

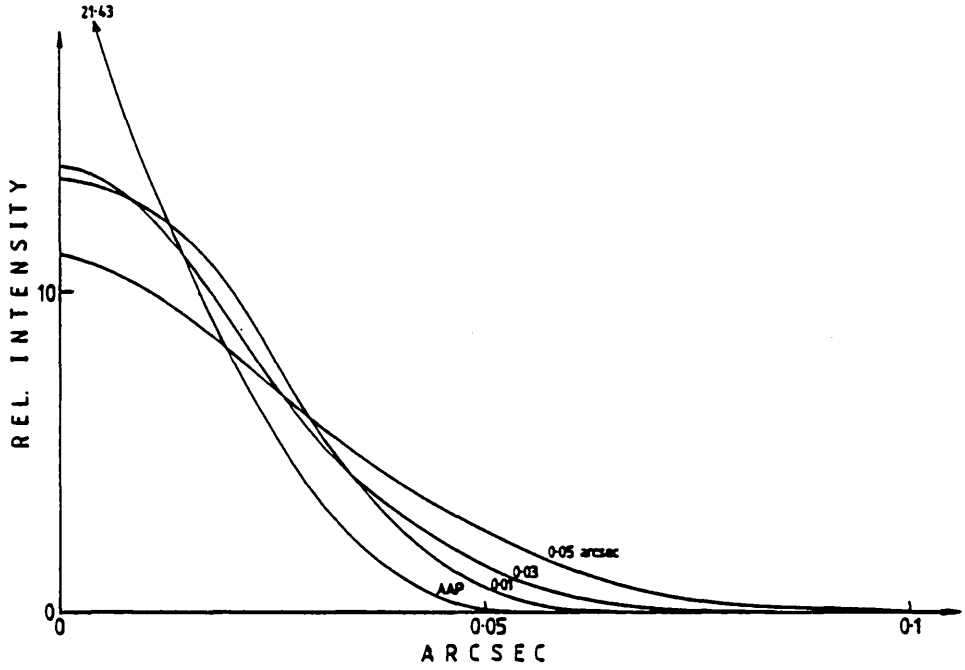

Figure 2. Autocorrelations of an Airy pattern (for the 3.9-m telescope at 5672 A) convolved with discs, of even surface brightness, of 0.01, 0.03 and 0.05 arcsec respectively. These are compared AAP to an autocorrelation of an Airy pattern alone (unresolved star).

evidence that R136a may be marginally resolved in these observations. All the curves for this object are somewhat more extended than those for the corresponding reference stars.

The implications of these broadenings, if real, can be appreciated by considering the curves in Fig. 2. Here an autocorrelated Airy pattern (AAP) (which represents an unresolved source observed at 5672 Å with the 3.9-m telescope) is compared with the autocorrelation of this Airy pattern convolved with discs of various angular diameters. The curves have been normalized to have the same area and thus represent the same brightness. In reality these curves would be superimposed on the very broad 'seeing pedestle' (see Fig. 1) and then the diameter of a resolved source can be approximately evaluated by noting the distance from the 0 0 pixel at which they merge with this pedestle. Comparison of the curves in Fig. 1 with those in Fig. 2 for R136a shows that this occurs with a resolved disc of 0.02 ± 0.01 arcsec diameter.

However, considerable caution should be applied before considering that this 0.02 arcsec extent for R136a is real for this is approaching the level of uncertainty of this technique. For instance, even minor 'seeing' changes between the reference star observations and those for R136a could produce the same marginal effect. It should be noted though that it is present in the three separate sets of measurements listed in Table 1.

However, if R136a does have this finite extent several possibilities for its nature should now be evaluated. For instance, this diameter ($\simeq 0.02$ arcsec is equivalent to $\simeq 5 \times 10^{-3}$ pc at the distance of the LMC) could be the outer envelope of a single, though not necessarily homogeneous object. For a spherical mass $M\,M_\odot$ in a diameter of d arcsec at a distance D pc then the average matter density $\bar{\rho}$ is given by

$$\bar{\rho} = 1.676 \times 10^{16} \frac{M}{d^3 D^3} M_\odot \text{ pc}^{-3}. \qquad (1)$$

Then for $M \simeq 2500\,M_\odot$, $d \simeq 0.02$ arcsec and $D = 55\,000$ pc in equation (1)

$\bar{\rho} \simeq 3 \times 10^{10}\,M_\odot\,\mathrm{pc}^{-3}$.

Alternatively, the 30 separate O3 or WN3 stars (see Section 1) could still be packed into this 0.02 arcsec diameter volume (though the optical variability makes this unlikely). In which case $\bar{\rho}$ is still $\simeq 3 \times 10^{10} M_\odot\,\mathrm{pc}^{-3}$. This should be compared with the central 0.2 pc diameter region of the Galaxy (Oort 1971) where $\bar{\rho} \simeq 2.6 \times 10^{7} M_\odot\,\mathrm{pc}^{-3}$ but $M \simeq 3 \times 10^{5} M_\odot$. It is interesting that if 30 separate O3 or WN3 stars within this very small volume of diameter d then where $\bar{s}$ is their mean separation $d/\bar{s} \simeq 30^{1/3}$ in which case, for $d \simeq 5 \times 10^{-3}$ pc ($\equiv 0.02$ arcsec), $\bar{s} \simeq 2 \times 10^{-3}$ pc is predicted which seems remarkably small.

However, if this $\simeq 0.02$ arcsec extent is spurious (and represents only an upper limit to these measurements) R136a could still be a single supergiant star of $\simeq 2500 M_\odot$ with an undetectable diameter of $\simeq 5 \times 10^{-6}$ pc.

Before speculating further as to the nature of this remarkable object we feel that more speckle observations to confirm its angular extent of 0.02 arcsec are essential. These would now be most desirable as near to the atmospheric cut-off ($\simeq 3200$ Å) as possible where the resolution of the 3.9-m telescope will be $\simeq 0.017$ arcsec and R136a, with a surface temperature of 60 000 K, will be very bright.

Acknowledgments

JM and HV are grateful to the staff of the Anglo-Australian telescope in 1981 November when these observations were made. All this work has been generously supported by the SERC and in particular JM is grateful for his SERC Senior Fellowship and JCH for an SERC Research Studentship.

References

Beddoes, D. R., Dainty, J. C., Morgan, B. L. & Scadden, R. L., 1976. *J. Opt. Soc. Am.*, **66**, 1247.
Cassinelli, J. P., Mathis, J. S. & Savage, B. D., 1981. *Science*, **212**, 1497.
Feitzinger, J. V., Schlosser, W., Schmidt-Kaler, Th. & Winkler, Ch., 1980. *Astr. Astrophys.*, **84**, 50.
Fienup, J. R. & Feldkamp, G. B., 1980. *Applications of Speckle Phenomena (SPIE)*, **243**, 95.
Labeyrie, A., 1970. *Astr. Astrophys.*, **6**, 85.
Meaburn, J., 1981a. *Mon. Not. R. astr. Soc.*, **196**, 19P.
Meaburn, J., 1981b. *Investigating the Universe*, p. 61, ed. Kahn, F. D., Reidel, Dordrecht, Holland.
Oort, J. H., 1971. *Nuclei of Galaxies*, p. 321, ed. O'Connell, D. J. K., North Holland Publishing Company.
Weigert, G. P., 1980. *Applications of Speckle Phenomena (SPIE)*, **243**, 103.
Worden, S. P., 1980. *Applications of Speckle Phenomena (SPIE)*, **243**, 66.

Note added in proof

A re-run of the raw data through the autocorrelator has suggested that the marginal broadening reported here is a consequence of a mismatch of the brightness of R136a and the reference star. Consequently, it is now thought most probable that R136a has an angular diameter of < 0.02 arcsec and is a single super-massive object.

Mon. Not. R. astr. Soc. (1983) 204, *Short Communication*, 41P–46P

Speckle observations of η Carinae

J. Meaburn and J. R. Walsh *Department of Astronomy, University of Manchester, Oxford Road, Manchester MI3 9PL*

J. C. Hebden, B. L. Morgan and H. Vine *Blackett Laboratory, Imperial College of Science and Technology, Prince Consort Road, London SW7*

Received 1983 April 6; in original form 1983 January 20

Summary. Speckle observations of the central star-like object in η Carinae with the AAT have shown that it is an unresolved (< 0.03 arcsec $\equiv 84$ AU) source which emits $10^7 L_\odot$. Most likely it is a single star of $\simeq 100 M_\odot$. No evidence of any binary component with a separation of between 0.03–0.9 arcsec has been found.

1 Introduction

η Carinae is the star-like object in the centre of the nebula NGC 3372 and is situated at the core of a complex which contains many early-type stars (Walborn 1973). Prior to the 1840s η Car was a fourth magnitude object, but in 1845 it brightened rapidly to magnitude -1, and remained brighter than +1 for ~ 10 yr (Innes 1903). It then declined to a visual magnitude ~ 7 by 1880, but underwent an outburst of ~ 1.5 mag in 1889 (Innes 1903). Since that date it has remained relatively quiescent, although there has been a gradual rise of ~ 1.5 mag since 1940 to its present value of ~ sixth magnitude (Feinstein & Marraco 1974). The spectrum at present displays many emission lines of Fe II, [Fe II] and Fe III together with the hydrogen recombination lines and forbidden lines of low ionization species (Aller & Dunham 1966; Thackeray 1967). There is also a strong optical continuum which may be stellar in origin (Rodgers & Searle 1967) and is characterized by a temperature of ~ 30 000 K (Davidson 1971). No reliable spectral type has been attributed to the object, although during the 1889 outburst it resembled an F-type supergiant (Walborn & Liller 1977).

In the 10–20 μm region, η Carinae is the brightest object outside the Solar System (Westphal & Neugebauer 1969) and its bolometric absolute magnitude is -12.5 for a distance of 2800 pc (Walborn 1973; Feinstein, Marraco & Muzzio 1973) ($L \sim 10^7 L_\odot$). This is equivalent to a visual magnitude of -1 which η Car attained in its 1845 outburst, and the thermal nature of the infrared excess is consistent with thermal emission from an optically thin dust shell which absorbs the radiation from the central star (Harvey, Hoffman & Campbell 1978). Infrared mapping of the source indicates a compact, hotter (~ 425 K) core with a more diffuse halo of cooler (~ 250 K) dust ~ 8 arcsec in diameter (Harvey *et al.* 1978; Aitken & Jones 1975). The core source consists of two peaks of infrared emission whose

separation increases with increasing wavelength from 1.1 arcsec at 3.6 μm to 2.2 arcsec at 11.2 μm (Hyland *et al.* 1979). It was suggested that these two peaks arise from thermal dust emission from a thin ring of dust viewed almost edge on and surrounding the central source (Hyland *et al.* 1979). Very recently Chelli, Perrier & Birand (1982) have obtained a speckle interferogram at 4.6 μm. An initial analysis of this indicates the presence of a bright unresolved central core of $\lesssim 0.3$ arcsec diameter surrounded by a halo with two secondary peaks $\simeq 1$ arcsec from either side of the centre.

The optical appearance in seeing conditions of $\simeq 1$ arcsec of the nebula surrounding η Car consists of a diffuse dusty halo ~ 2 arcsec in extent embedded within an irregular shell of condensations ~ 10 arcsec across ('the Homunculus'). The proper motions of the condensations indicate transverse velocities up to 1400 km s^{-1} and the velocity vectors point back to η Carinae (Walborn, Blanco & Thackeray 1978). The outermost condensations appear to move more slowly and may have been ejected at different epochs (Walborn *et al.* 1978). Spectra of one of these condensations show it to be nitrogen-rich (Davidson, Walborn & Gull 1982) which is an indication that η Car may be an evolved star which has undergone significant nuclear reprocessing to heavy elements. The overall structure of the Homunculus is dominated by reflected light from the central stellar-like object as revealed by polarization maps (Warren-Smith *et al.* 1979); the polarization of the central 3 arcsec region is ~ 35 per cent (Warren-Smith *et al.* 1979). The central illuminating source of the centrosymmetric polarization map is elongated in position angle 45° possibly suggesting a luminous optically thick inclined ring ~ 2.5 arcsec in extent illuminated from within (Warren-Smith *et al.* 1979).

Several possibilities have been suggested for the nature of the central source of this unique object:

(a) a single supermassive star ($\gtrsim 100\,M_\odot$) which is undergoing pulsational instability (Humphreys & Davidson 1979) and losing mass at a rate as great as $2 \times 10^{-2} M_\odot$/yr (Hyland *et al.* 1979).

(b) A binary system with either an accretion disc generated by Roche lobe outflow through the inner Lagrangian point or an excretion disc formed by outflow from the outer Lagrangian points (Warren-Smith *et al.* 1979).

(c) A compact group of O and B stars similar to the Trapezium in the core of M42 but with an angular extent of < 1 arcsec.

Speckle observations of η Carinae have now been made with the Anglo-Australian telescope to investigate the optical structure of the central source in the angular range of 0.03–0.9 arcsec.

2 Observations

The Imperial College of Science and Technology (London) speckle interferometer and hard-wired autocorrelator were combined with the *f*/15 focus of the 3.9-m Anglo-Australian telescope for the observations. This device has an EMI, four-stage, image intensifier (S20) combined with a Plumbicon TV camera and detects individual photon events. With the combination of lenses used for η Car, the image of a 4.06-arcsec square field ($\equiv 256 \times 256$ pixels) is detected. A television recording of this atmospherically distorted image is autocorrelated (Dainty 1978) for each 1/25 s exposure time. Over an extended observing period these independent two-dimensional autocorrelations are coadded and finally an integrated autocorrelation is obtained for the 4.06-arcsec square area of sky. In this area objects whose separations lie in the range 0.03 to 0.9 arcsec, may be detected. These limits are due to the

limiting angular resolution of the telescope at 5672 Å and the extent of the autocorrelation which comprises an array from −64 to +63 pixels in the X dimension (right ascension) and from 0 to −63 in the Y dimension (declination).

The object under investigation is observed first followed immediately by an observation of a reference star of similar magnitude made in similar 'seeing' conditions. The resultant two-dimensional autocorrelation of an unresolved single star has a central 'photon-spike' occupying a region ≃ 5 pixels radius around the 00 pixel. This contains the total number of counts recorded in the whole 4.06 x 4.06 arcsec^2 area as well as background counts. The autocorrelation of the telescope Airy pattern produces a component which extends to about 8 pixels. The combination of the two narrow distributions is superimposed on the very broad Gaussian 'seeing pedestal' produced by the autocorrelation of the events within individual speckles with those in all others spread over the 1–2 arcsec diameter seeing disc.

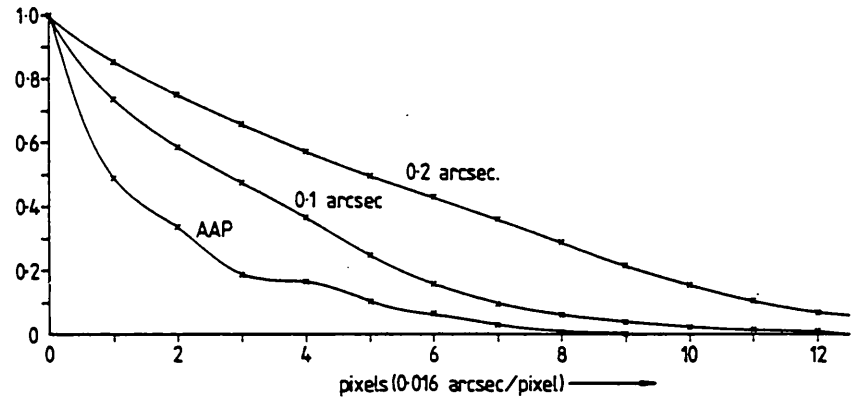

Figure 1. The autocorrelation functions of an unresolved star (AAP); and the autocorrelation functions of the Airy pattern convolved with uniformly illuminated discs of diameters 0.1 and 0.2 arcsec.

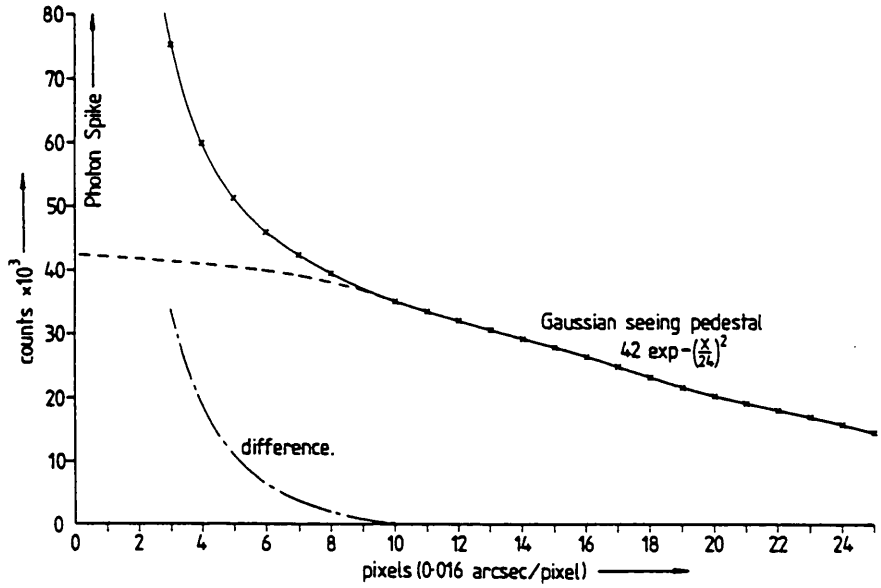

Figure 2. The observed autocorrelation in a north–south direciton for η Carinae. The photon spike and the Gaussian which fits the seeing pedestal are both indicated. The result of subtracting the Gaussian pedestal from the observed curve is also shown.

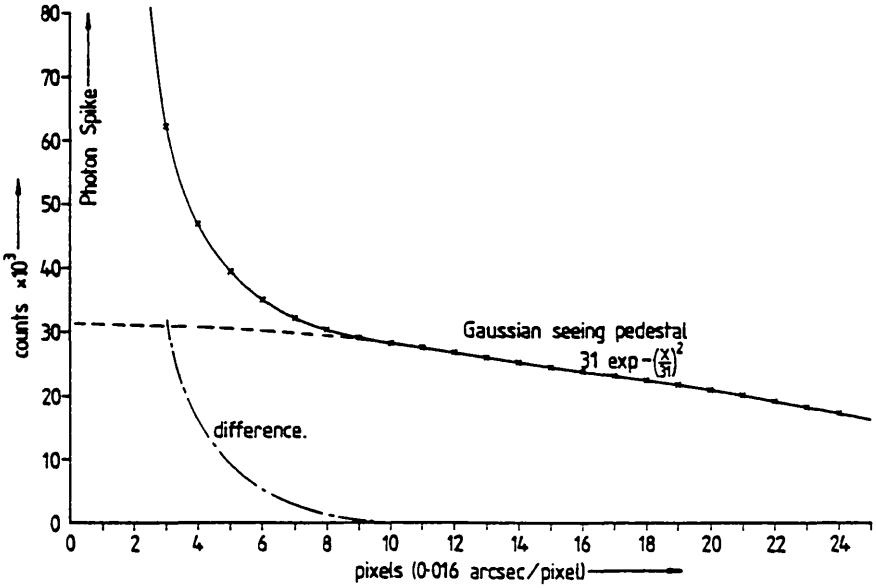

Figure 3. The observed autocorrelation of the reference star with the same parameters as for Fig. 2.

For the observations of η Car a filter of 70 Å bandwidth centred on 5672 Å was used. Altogether 2.4×10^4 separate frames were autocorrelated followed by a similar number for the reference star. Seeing was $\simeq 2$ arcsec during these exposures.

Fig. 1 shows the one-dimensional autocorrelation functions of an unresolved star (i.e. the autocorrelated Airy pattern, AAP) and the autocorrelation functions of the Airy pattern convolved with two uniformly illuminated discs of diameters 0.1 and 0.2 arcsec respectively. The calculations assume the instrumental parameters which were used in the actual observations of η Car. In practice the photon spike and the broad seeing pedestal would be superimposed on these curves.

North/south cuts through the two dimensional autocorrelations which were obtainable for η Car and for the reference star are shown in Figs 2 and 3 respectively. Gaussian profiles have been fitted to the 'seeing pedestals' well away from the photon spikes. The difference between these pedestals is mainly due to differential video sampling levels. Also shown are the results of subtracting the respective Gaussians from the observed curves.

3 Discussion

The full two-dimensional autocorrelation (not shown here) for η Car contains no indication of any binary component with a separation in the range 0.03–0.9 arcsec or any extended halo with structure within these limits.

Instead, the autocorrelation has the characteristics of a single dominant unresolved source, implying an upper limit to its extent of $\lesssim 0.03$ arcsec ($\equiv 84$ AU for a distance of 2800 pc). This is illustrated by the closely comparable shapes of the difference curves for η Car and the reference star in Figs 2 and 3 respectively. It is also noticeable that both of these intercept the Gaussian seeing pedestal at the ninth pixel as predicted in Fig. 1 for a source which is unresolved with this telescope (AAP).

It therefore seems most likely that η Car is a single star emitting $10^7 L_\odot$ in the infrared and visible, in which case it could be a star of mass $100 M_\odot$ with a radius of $\lesssim 42$ AU

($\lesssim 9030\,R_\odot$) which is undergoing huge and varying mass loss. Incidentally, the present observations would not reveal very clearly any component of the image which is reasonably uniform over an angular diameter of $\gtrsim 0.9$ arcsec.

If the unresolved continuum object actually refers to the high density envelope of a single stellar source, or possibly an accretion disc, then its radius is $\lesssim 42$ AU. This is strongly suggested by the presence of many Fe II lines indicating $N_e \sim 10^{10}\,\mathrm{cm}^{-3}$ and by the lack of a truly stellar continuum in η Car (Rodgers & Searle 1967), although the absence of a true stellar continuum does depend on the adopted reddening (see e.g. Leibowitz 1977).

On the other hand, if η Car is a binary star, as suggested by Warren-Smith *et al.* (1979) from the evidence for a bipolar souce with a circumstellar ring, then the ring does not appear as structure in the autocorrelation from 0.03–0.9 arcsec, thus perhaps implying that it is relatively uniform or optically faint over this range. The peaks of the infrared emission occur at a separation of 1.1 arcsec at 3.6 μm (Hyland *et al.* 1979) so the disc which could be scattering visible light is probably of $\gtrsim 1$ arcsec in extent.

No binary component having a separation of $\gtrsim 84$ AU is observed in these speckle observations. In which case, if the central dense core still contained a binary star, the radius of such a system is $\lesssim 42$ AU. Using a mass–luminosity relation appropriate to higher luminosity stars [mag (bol) < 7; Aller 1963]:

$$\mathrm{mag\,(bol)} = 4.7 - 9.5 \log M$$

where M is the total mass (in $M_\odot$) of any system gives

$$M = 65\,M_\odot.$$

However, the application of this empirical relation based on stars in the usual range of luminosities may not be appropriate to very high luminosity objects such as η Car. This value of the mass can be taken to be that of a single star, or of two stars in a binary system if the total luminosity is simply the sum of luminosities of both components. Then from Kepler's third law for a binary system, the period P is given by:

$$P = \left[\frac{1.0 \times a(\mathrm{AU})^3}{\mu(M_\odot)}\right]^{1/2} \mathrm{yr};$$

for $\mu = M_1 + M_2 = 65\,M_\odot$ and with an orbital radius $a \lesssim 42$ AU, then $P \lesssim 34$ yr. There is no conclusive photometric or spectroscopic evidence that such a binary exists although note that Feinstein & Marraco (1974) found weak evidence for a periodic 1110-day cycle of 0.2 mag amplitude. For a $65\,M_\odot$ binary system this implies a radius of the orbit of $\simeq 8.4$ AU ($\equiv 0.003$ arcsec at 2800 pc).

Acknowledgments

JM and HV are grateful to the staff at the Anglo-Australian telescope in 1981 November, when these observations were made. All this work has been generously supported by the SERC and in particular JM is grateful for his SERC Senior Fellowship, JRW for his SERC Fellowship and JCH for his SERC Research Studentship.

References

Aitken, D. K. & Jones, D., 1975. *Mon. Not. R. astr. Soc.*, 172, 141.

Aller, L. H., 1963. *Astrophysics. The Atmospheres of the Sun and the Stars*, p. 29, Ronald Press, New York.

Aller, L. H. & Dunham, T. Jr., 1966. *Astrophys. J.*, 146, 126.
Chelli, A., Perrier, C. & Birand, Y. G., 1982. In press.
Dainty, J. C., 1978. *Mon. Not. R. astr. Soc.*, 183, 223.
Davidson, K., 1971. *Mon. Not. R. astr. Soc.*, 154, 415.
Davidson, K., Walborn, N. R. & Gull, T. R., 1982. *Astrophys. J.*, 254, L47.
Feinstein, A. & Marraco, H. G., 1974. *Astr. Astrophys.*, 30, 271.
Feinstein, A., Marraco, H. G. & Muzzio, J. C., 1973. *Astr. Astrophys. Suppl. Ser.*, 12, 331.
Harvey, P. M., Hoffmann, W. F. & Campbell, M. F., 1978. *Astr. Astrophys.*, 70, 165.
Hyland, A. R., Robinson, G., Mitchell, R. M., Thomas, J. A. & Becklin, E. E., 1979. *Astrophys. J.*, 233, 145.
Humphreys, R. M. & Davidson, K., 1979. *Astrophys. J.*, 232, 409.
Innes, R. T. A., 1903. *Ann. Cape Obs.*, 9, 75B.
Leibowitz, E. M., 1977. *Mon. Not. R. astr. Soc.*, 178, 271.
Rodgers, A. W. & Searle, L., 1967. *Mon. Not. R. astr. Soc.*, 135, 99.
Thackeray, A. D., 1967. *Mon. Not. R. astr. Soc.*, 135, 517.
Walborn, N. R., 1973. *Astrophys. J.*, 179, 517.
Walborn, N. R. & Liller, M. H., 1977. *Astrophys. J.*, 211, 181.
Walborn, N. R., Blanco, B. M. & Thackeray, A. D., 1978. *Astrophys. J.*, 219, 498.
Warren-Smith, R. F., Scarrott, S. M., Murdin, P. & Bingham, R. G., 1979. *Mon. Not. R. astr. Soc.*, 187, 761.
Westphal, J. A. & Neugebauer, G., 1969. *Astrophys. J.*, 156, L45.

Mon. Not. R. astr. Soc. (1983) **205**, *Short Communication*, 53P–56P

Speckle observations of the central binary star in the Red Rectangle

J. Meaburn and J. R. Walsh *Department of Astronomy, University of Manchester, Manchester M13 9PL*

J. C. Hebden, B. L. Morgan and H. Vine *Blackett Laboratory, Imperial College of Science and Technology, Prince Consort Road, London SW7 2BZ*

Received 1983 August 15; in original form 1983 July 22

Summary. The binary nature of the central star in the Red Rectangle HD 44179 has been confirmed using the Imperial College speckle interferometer on the AAT. The position angle of $146 \pm 3°$ and separation 0.29 ± 0.02 arcsec are given for 1981 November 11.

An orbital period of 60 ± 5 yr and a total mass of the two components of the binary $\simeq 31 M_{\odot}$ are both predicted. No correlation between the inclination of the orbit and the striking geometry of the nebulosity is found.

1 Introduction

The Red Rectangle (see fig. 1c of Cohen *et al.* 1975) is a highly symmetrical bipolar (or biconical) nebula which is rectangular in appearance but with diagonal spikes most noticeable at red wavelengths (Cohen *et al.* 1975). The spectrum of the nebula is unique since it contains a continuous component which has a broad (800 Å) maximum centred on 6400 Å (Greenstein & Oke 1977). Superimposed on this are both broad and narrow emission features (Schmidt, Cohen & Margon 1980; Warren-Smith, Scarrott & Murdin 1981) which may be molecular in origin; Warren-Smith *et al.* (1981) suggest carbyne as a possible candidate molecule. There are also unidentified emission features in the infrared (3.3–11.3 μm) (Cohen *et al.* 1975; Tokunaga & Young 1980; Russell, Soifer & Willner 1978; Bregman & Rank 1975; Russell *et al.* 1982) which do not appear to be of simple molecular origin and the infrared excess, which is relatively flat from 2–30 μm, cannot be characterized by even several blackbody temperatures (Russell *et al.* 1978).

Polarization maps (Perkins *et al.* 1981) reveal a centrosymmetric pattern which is consistent with the illumination of a biconical distribution of dust by a central source.

A ninth magnitude B8–A0 III star HD 44179 (BD $-10°$ 1476) is present at the centre of the Red Rectangle. This was discovered visually by Aitken in 1915 to be double (ADS 4954) with $\simeq 0.3$ arcsec separation. Cohen *et al.* 1975, (see their table 7 and references therein) list many observations of this binary since that date and these are summarized here in Fig. 1. Attempts to observe this binary in 1948 and 1975 (see Cohen *et al.* 1975) failed

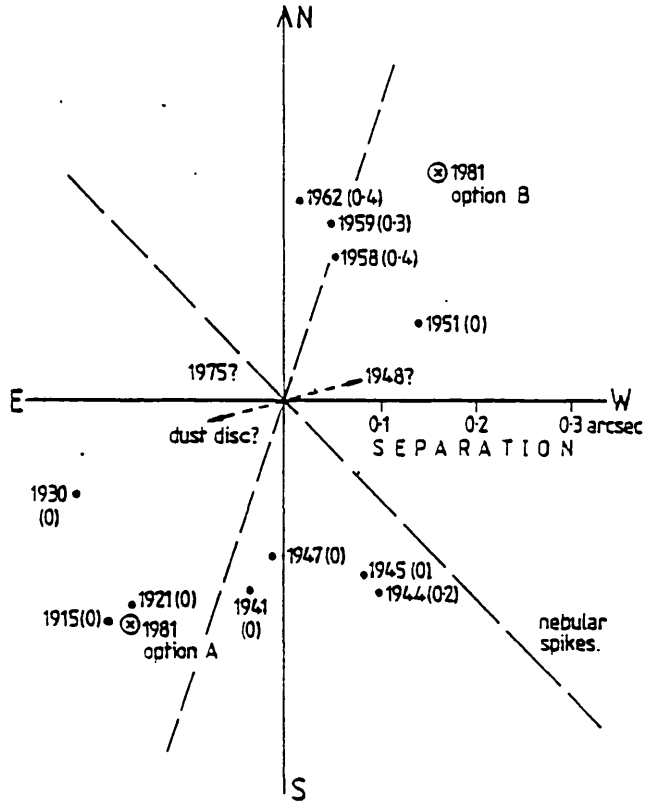

Figure 1. The position angles and separations for the two stars in the central binary of the Red Rectangle are given from previous visual observations from 1915 to 1962. In brackets is the magnitude difference between components. As these are nearly equal in brightness the most plausible option for position angles are depicted. These are all ambiguous by 180°. Also shown as circled crosses are the two options for the present speckle observations.

either because the separation on these two occasions was < 0.1 arcsec or because one component became heavily obscured by dust. The difference in magnitude of the components (given in brackets after the date in Fig. 1) has varied from 0 to 0.5, though this variability may again be caused by absorption by patchy concentrations of dust.

A consequence of this near equality in brightness of the two components is that the values of all the visual measurements of position angle could differ by 180° from those shown in Fig. 1. However, the most plausible progression of position angle with time, in an anticlockwise direction, is illustrated. Possible positions for the components during the unsuccessful 1948 and 1975 observations are suggested.

In view of the peculiar nature of this object and the recent lack of observational evidence for a double star, speckle observations have now been made which are capable of resolving stellar sources separated by > 0.03 and ≤ 0.9 arcsec.

2 Observations

The observations were made on 1981 November 11 with the speckle interferometer of the Imperial College of Science and Technology combined with the 3.9-m Anglo-Australian telescope. The technical details of this system and the analysis of the data with a two-dimensional hard-wired autocorrelator, are exactly those described by Meaburn *et al.* (1982).

Altogether 9.4×10^4 exposures of the central object HD 44179 in the Red Rectangle were obtained and autocorrelated. These were through a 220 Å bandwidth interference filter centred on 5000 Å and each was 1/25 s in duration. A similar number was also obtained of a nearby reference star for comparison.

For the two-dimensional autocorrelations of HD 44179 the 'seeing pedestal' was approximated by a best-fit Gaussian and then subtracted. Fig. 2 shows a radial cut through these summed two-dimensional autocorrelations of HD 44179 at a position angle (north to south through east) of $146 \pm 3°$. The presence of a secondary peak indicates a definite binary component at a separation of 0.29 ± 0.02 arcsec. At present the magnitude difference between the primary and secondary component is uncertain but experience with systems of known magnitude difference suggest that it is probably no more than one magnitude. Since this analysis is by autocorrelation there is an automatic ambiguity of 180° in the position angle of any binary source and consequently the two possible positions and their uncertainties are compared in Fig. 1 with all the separations and values of position angle measured previously (Cohen *et al.* 1975).

3 Discussion

The width of the secondary maximum in Fig. 2 is $\lesssim 3$ pixels ($\lesssim 0.04$ arcsec) which is near the limiting resolution of the AAT, then it must be a consequence of two stellar sources whose individual extents are unresolved. Cohen *et al.* (1975) had raised the possibility that some variable reflection from concentrations of dust could have been mistakenly identified as a binary star.

If the progression of position angles and separations for the visual observations from 1915 to 1962 is as depicted in Fig. 1 then option A for these 1981 speckle measurements is most probably correct. In this case the large spread of values for both 1915–30 and 1941–47 must be a consequence of the uncertainties associated with the visual technique for stars separated by less than 0.3 arcsec. These results are then consistent with an orbital period of 60 ± 5 yr with an orbital angular diameter of 0.29 ± 0.02 arcsec. In this case the major axis of the projected ellipse (eccentricity $\simeq 0.33$) of a circular orbit for two equal components could be at $150 \pm 10°$. With this configuration the failure of the 1948 and 1975 observations can easily be explained by the separation becoming < 0.1 arcsec in which case obscuration by dust need not be invoked. Though a disc of dust may be present on the 'equator' of the Red Rectangle along the dashed line in Fig. 1.

Incidentally, a very much faster ($\simeq 15$ yr) orbital period, in a clockwise direction, could give, though less plausibly, many of the values (or their 180° counterparts) shown in Fig. 1.

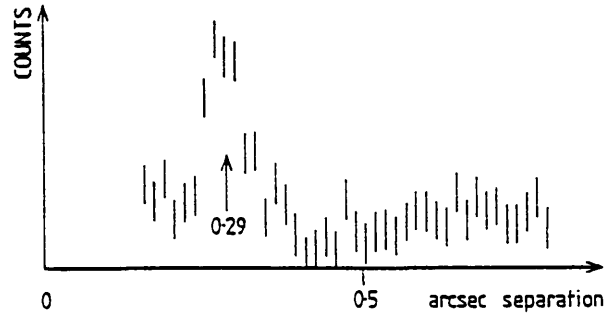

Figure 2. A cut through the integrated two-dimensional autocorrelation in which the 'seeing' pedestal approximate by a best-fit Gaussian, has been subtracted. The strong maximum with position angle 146° and separation 0.29 arcsec indicates that this is a binary star.

Cohen *et al.* (1975) from spectroscopy and photometry of the central binary suggest a distance of 330 pc. For two equal stars separated by 4.6×10^{-4} pc ($\equiv 0.29$ arcsec or 96 AU) with an orbital period of $\simeq 60$ yr then their total mass would be $\simeq 31\,M_\odot$. For a period of $\simeq 15$ yr this would become $\simeq 492\,M_\odot$. This creates a difficulty since if the spectral type of B9 III (Cohen *et al.* 1975) is correct for both stars, and the total visual magnitude is 8.8, then the implied total mass, using the approximate mass–luminosity relation from Allen (1973) and a value of $A_v = 1.2$ (Cohen *et al.* 1975), is $\sim 7\,M_\odot$. Alternatively the derived bolometric luminosity of HD 44179 is $1050\,L_\odot$ (Cohen *et al.* 1975), implying a mass $\sim 7.5\,M_\odot$. Both these values are very different from the two possible values suggested by the binary system.

It is also interesting to note from Fig. 1 that there appears to be no close correlation between the plane of the orbit of the central binary and the geometry of the nebulosity. Theories which predict the creation of planetary or proto-planetary nebulae by mass ejection from a binary star usually consider the ejection of mass either perpendicular or parallel to the orbital plane (Morris 1981).

Speckle observations of the orbital parameters of close binary stars improve on the accuracy by about 10 times over previous visual techniques and do not require particularly good 'seeing' to perform a successful observation (Morgan *et al.* 1978, 1980, 1982). Consequently, further speckle observations of this binary even over as few as the next 5 yr should permit its orbital parameters to be defined more precisely. If these are combined with high-dispersion spectroscopic measurements, which should lead to a knowledge of the orbital velocities of each component, an accurate distance to the Red Rectangle and the individual masses of the stars could be obtained.

References

Allen, C. W., 1973. *Astrophysical Quantities*, 3rd edn, Athlone Press, London.

Bregman, J. D. & Rank, D. M., 1975. *Astrophys. J.*, **195**, L125.

Cohen, M., Anderson, C. M., Cowley, A., Coyne, G. V., Fawley, W. M., Gull, T. R., Harlan, E. A., Herbig, G. H., Holden, F., Hudson, H. S., Jakoubek, R. O., Johnson, H. M., Merrill, K. M., Schiffer, F. H., Soifer, B. T. & Zuckerman, B., 1975. *Astrophys. J.*, **196**, 179.

Greenstein, J. L. & Oke, J. B., 1977. *Publ. astr. Soc. Pacific*, **89**, 131.

Meaburn, J., Hebden, J. C., Morgan, B. L. & Vine, H., 1982. *Mon. Not. R. astr. Soc.*, **200**, 1P.

Morgan, B. L., Beddoes, D. R., Scaddan, R. J. & Dainty, J. C., 1978. *Mon. Not. R. astr. Soc.*, **183**, 701.

Morgan, B. L., Beckmann, G. K. & Scaddan, R. J., 1980. *Mon. Not. R. astr. Soc.*, **192**, 143.

Morgan, B. L., Beckmann, G. K., Scaddan, R. J. & Vine, H. A., 1982. *Mon. Not. R. astr. Soc.*, **198**, 817.

Morris, M., 1981. *Astrophys. J.*, **249**, 572.

Perkins, H. G., Scarrott, S. M., Murdin, P. & Bingham, R. G., 1981. *Mon. Not. R. astr. Soc.*, **196**, 635.

Russell, R. W., Gull, G., Beckwith, S. & Evans, N. J., 1982. *Publ. astr. Soc. Pacific*, **94**, 97.

Russell, R. W., Soifer, B. T. & Willner, S. P., 1978. *Astrophys. J.*, **220**, 568.

Schmidt, G. D., Cohen, M. & Margon, B., 1980. *Astrophys. J.*, **239**, L133.

Tokunaga, A. T. & Young, E. T., 1980. *Astrophys. J.*, **237**, L93.

Warren-Smith, R. F., Scarrott, S. M. & Murdin, P., 1981. *Nature*, **292**, 317.

Mon. Not. R. astr. Soc. (1984) **206**, 669–672

Speckle interferometry of *Hipparcos* link stars

A. N. Argue *Institute of Astronomy, University of Cambridge, The Observatories, Madingley Road, Cambridge CB3 0HA*

J. C. Hebden, B. L. Morgan and H. A. Vine
The Blackett Laboratory, Imperial College of Science and Technology, Prince Consort Road, London SW7 2BZ

Received 1983 June 15

Summary. Speckle interferometry has been carried out on 39 stars that had been selected as provisionally suitable for linking *Hipparcos* positional measurements to an extragalactic reference frame by *Space Telescope*. We used the Imperial College, London, speckle interferometer and autocorrelator on the Anglo-Australian 3.9-m telescope. The result is that about 30 per cent of the stars selected turned out to be confirmed or suspected multiple stars in the range 0.03–0.7 arcsec.

1 Introduction

Our object was to test whether certain stars are suitable candidates for linking astrometric measurements made by the *Hipparcos* and *Space Telescope* astrometric satellites.

Hipparcos will establish a stellar reference frame based on 100 000 stars brighter than $B = 13$ mag (ESA 1979). Too few extragalactic objects of suitable quality brighter than this limit are known which could provide a direct link to an extragalactic reference frame and indirect methods will have to be applied: that with which we are concerned here is based on the *Space Telescope*. The fine guidance sensor (FGS) of *ST* ought to function astrometrically to a limit of 17 mag: it will measure the angular separation between an extragalactic object and a *Hipparcos* star provided this separation is smaller than 18 arcmin, the field of the FGS. The accuracy of this measurement is hoped to be ±0.002 arcsec (Duncombe *et al.* 1982); this is of the same order as the accuracy of a mean positional measurement by *Hipparcos* (Kovalevsky 1982; *Hipparcos* 1982, p. 259). To achieve this accuracy in the angular-separation measurement it is necessary that neither of the objects shall display structure down to the *ST* resolution limit of 0.05 arcsec. For most of the stars tested here the telescope used was the Anglo-Australian 3.9-m which has a diffraction-limited resolution limit of 0.03 arcsec. The upper limit of binary detection was 0.7 arcsec. A small number had previously been observed with the Perkins 1.9-m telescope at Lowell Observatory, and for these the range was 0.1–1.0 arcsec (Argue *et al.* 1982). The technique of speckle inter-

ferometry employed has been described by Morgan *et al.* (1978), Beddoes *et al.* (1976) and Hebden, Morgan & Vine (1984).

2 Selection of objects

(i) The extragalactic objects were selected mainly from the latest and probably final list drawn up by the working group of IAU Commission 24. This group had been set up to select objects with suitable radio and optical properties to act as benchmarks for establishing an extragalactic reference frame (the IAU 1982 'Patras' List: Argue *et al.* 1983).

(ii) Link stars within 18 arcmin of their respect sources were selected by inspection of ESO and SRC Sky Survey prints as described by Argue & Baxter (1982). The stars measured here have B magnitudes ranging from 7.1 to 11.2. A companion star within 15 arcsec would be included in the instantaneous field of view of *Hipparcos* and would perturb the measurement unless fainter by at least 3.5 mag. Such companions can be detected by eye on the charts for separations down to about 2 arcsec. Using the AAT we are confident that we can detect a companion to a star of magnitude 10 if it is no more than three magnitudes fainter and if its separation lies in the range 0.03–0.7 arcsec. Separations between 0.7 and 2 arcsec will be the subject of a special investigation by de Vegt at Hamburg.

Table 1. Stars that showed no indication of multiplicity. The 1981 measurements were made on the Perkins 1.9-m telescope, Lowell Observatory; those of 1982 on the Anglo-Australian 3.9-m telescope.

Star	Date	*UT* (h m)	Scale (arcsec)
SAO 129060	82 Oct 28	13 02	0.03–0.7
SAO 215376	82 Oct 28	13 08	0.03–0.7
SAO 109741	82 Oct 28	13 38	0.03–0.7
SAO 109727	82 Oct 28	13 45	0.03–0.7
	81 Nov 13	10 52	0.03–1.0
SAO 147712	82 Oct 28	13 59	0.03–0.7
SAO 130631	82 Oct 28	14 56	0.03–0.7
	81 Dec 8	03 43	0.1 –1.0
SAO 194728	82 Oct 28	15 02	0.03–0.7
SAO 149494	82 Oct 28	15 16	0.03–0.7
SAO 131160	82 Oct 28	15 21	0.03–0.7
	81 Dec 8	04 24	0.1 –1.0
AGK–0°0524	82 Oct 28	15 33	0.03–0.7
BD–0°0759	82 Oct 28	15 38	0.03–0.7
SAO 170477	82 Oct 28	15 45	0.03–0.7
SAO 170501	82 Oct 28	15 50	0.03–0.7
SAO 217442	82 Oct 28	15 55	0.03–0.7
SAO 132447	82 Oct 28	16 09	0.03–0.7
BD–15°1291	82 Oct 28	16 26	0.03–0.7
SAO 256316	82 Oct 28	16 48	0.03–0.7
AGK3–0°1083	81 Dec 8	09 04	0.1 –1.0
SAO 154846	82 Oct 28	17 45	0.03–0.7
SAO 164461	82 Oct 28	10 40	0.03–0.7
SAO 164452	82 Oct 28	10 50	0.03–0.7
BD–12°6025	82 Oct 28	10 56	0.03–0.7
SAO 164787	82 Oct 28	11 29	0.03–0.7
SAO 214107	82 Oct 28	12 13	0.03–0.7
SAO 191517	82 Oct 28	12 20	0.03–0.7
SAO 231636	82 Oct 28	12 35	0.03–0.7
SAO 165890	82 Oct 28	12 52	0.03–0.7

Table 2. Stars showed that some evidence of multiplicity. The 1981 measurements were made on the Perkins 1.9-m telescope; those of 1982 on the Anglo-Australian 3.9-m telescope.

Star	Date	*UT* (h m)	Scale (arcsec)
SAO 166102	82 Oct 28	12 56	0.03–0.7
CD–44°2164	82 Oct 28	16 02	0.03–0.7
SAO 151166	82 Oct 28	16 20	0.03–0.7
CD–41° 14398	82 Oct 28	10 13	0.03–0.7
SAO 146680	82 Oct 28	12 27	0.03–0.7
AGK3–0°1085	81 Dec 8	08 51	0.1 –1.0
AGK3–0°1082	81 Dec 8	08 42	0.1 –1.0

Table 3. Stars that showed a binary component. The position angle is measured from north through east at the epoch of date with an ambiguity of 180°. All were observed on the Anglo-Australian 3.9-m telescope.

Star	Date	*UT* (h m)	Separation (arcsec)	Position angle (°)
AGK3+6°0778	82 Oct 28	16 34	0.298	196
AGK3+22°0834	82 Oct 27	17 24	0.244	224
SAO 230558	82 Oct 28	10 20	0.179	142
SAO 126934	82 Oct 28	11 11	0.256	235
SAO 165283	82 Oct 28	12 05	0.262	245

3 Observations

We observed on the night of 1982 October 28/9 (a few observations were made on the previous night through the kind cooperation of J. Meaburn). The Imperial College speckle interferometer was set up at the R-C focus and operated there by one of us (HAV). The speckle exposures, of duration 0.02 s (increased to 0.04 s for four stars at the end of the night because of poor seeing), were recorded on video tape for analysis in the laboratory in London, but a quick-look integrated autocorrelation was displayed in real time to allow a decision to be made about the next step: if the indication was that the object had structure, then another star to link the same source was selected (by ANA); if single, then generally we moved to another source field. This interactive facility was a most valuable one.

About half the night was lost due to cloud.

4 Reduction and results

The video tapes were run and the autocorrelation curves analysed by one of us (JCH) at Imperial College.

Our results are given in Tables 1–3. The two AGK3 stars in Table 3 are previously known binaries and had been included in the programme at the request of G. E. Taylor of the Royal Greenwich Observatory for another purpose: these two stars ought to be omitted from any discussion on the frequency of multiple stars among a population of supposedly 'clean' stars selected by eye from Sky Survey prints. The indications here are that about 30 per cent are in fact suspected or proven multiples.

Acknowledgments

We are grateful to our night assistant at the AAT, Mr S. Lee, whose dexterity in operating the telescope was an important factor in our making the most of difficult weather conditions. Costs were covered by a travel grant from SERC which is gratefully acknowledged.

References

Argue, A. N. & Baxter, R. D., 1982. *Abh. Hamburger Sternw.*, X, Heft 3, 111.

Argue, A. N., Baxter, R. D., Morgan, B. L. & Vine, H., 1982. *Scientific Aspects of the* Hipparcos *Mission*, p. 53, eds Perryman, M. A. C. & Guyenne, T. D.

Argue, A. N., de Vegt, Chr., Elsmore, B., Fanselow, J. L., Harrington, R. S., Hemenway, P. D., Johnston, K. J., Kumkova, I. I., Walter, H. G. & Witzel, A., 1983. *Report of Working Group of IAU Commission 24 on Opitcal/Radio Astrometric Sources for the Establishment of an Inertial Reference Frame, Astr. Astrophys.*, in press.

Beddoes, D. R., Dainty, R. C., Morgan, B. L. & Scaddan, R. J., 1976. *J. Opt. Soc. Am.*, 66, 1247.

Duncombe, R. L., Benedict, G. F., Hemenway, P. D., Jefferys, W. H. & Shelus, P. D., 1982. Astrometric Observations with Space Telescope. In *The Space Telescope Observatory*, ed. Hall, D. N. B., NASA.

ESA, 1979. SC1(79)10 Hipparcos *Space Astrometry, Report of the Phase A Study.*

Hebden, J. C., Morgan, B. L. & Vine, H., 1984. *Proc. SPIE*, 445, *Instrumentation in Astronomy V*, ed. Crawford, D. L., in press.

Hipparcos, 1982. *Compilation of the Input Catalogue.* Paris-Meudon and Jean Grou-Radenez.

Kovalevsky, J., 1982. *Scientific Aspects of the* Hipparcos *Mission*, p. 15, eds Perryman, M. A. C. & Guyenne, T. D.

Morgan, B. L., Beddoes, D. R., Scaddan, R. J. & Dainty, J. C., 1978. *Mon. Not. R. astr. Soc.*, 183, 701.

References

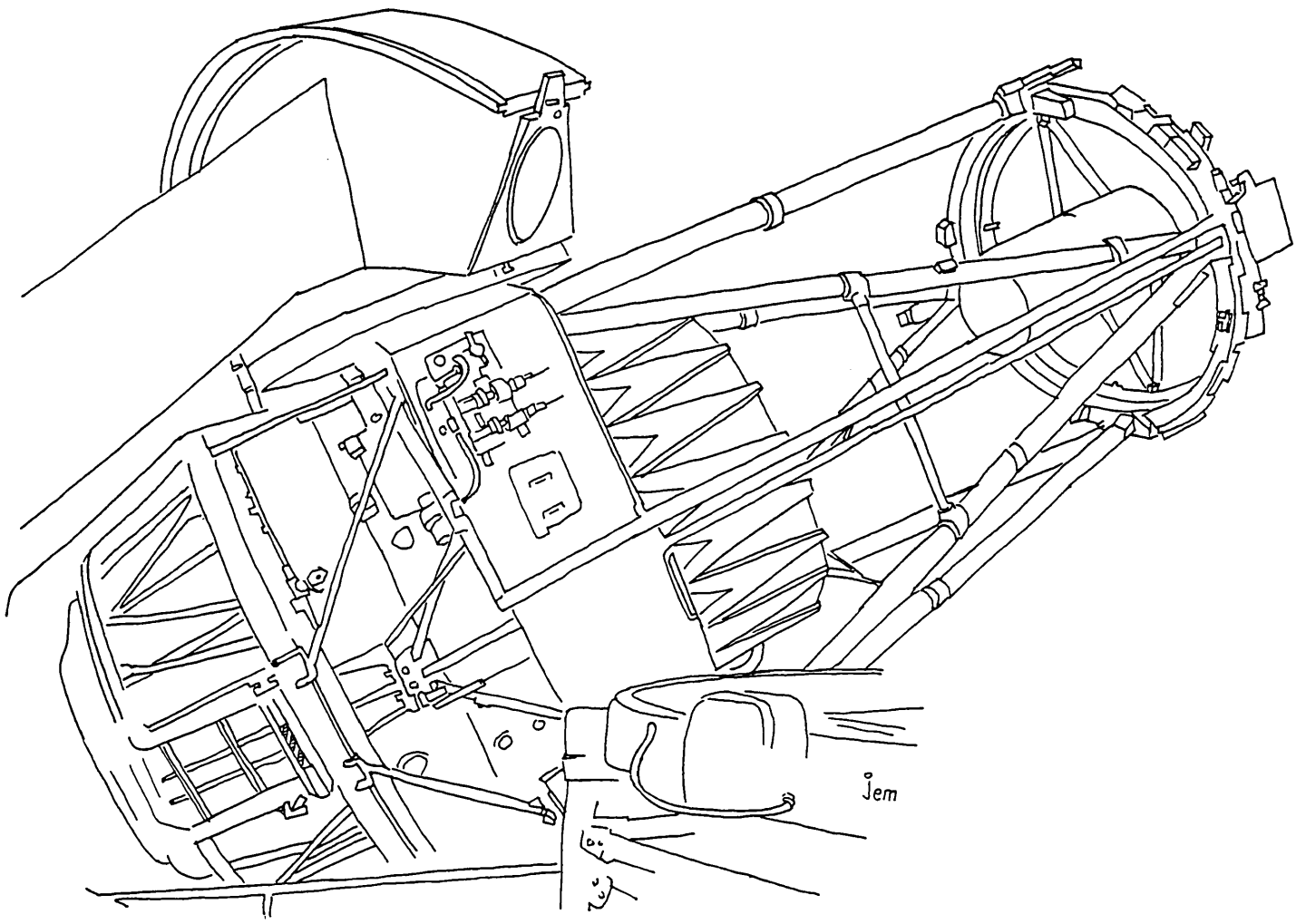

References

[1] Labeyrie,A.,Astron.Astrophys.,6,85. 1970

[2] Dainty,J.C.,In "Laser speckle and related phenomena" ed. Dainty,J. C., Springer-Verlag, 2nd Edition. 1984

[3] Worden,S.P.,Vistas.Astr.,20,301. 1977

[4] Labeyrie,A.,In "Progress in Optics" vol.14 p.47 ed. Wolf,E., North -Holland. 1976

[5] Roddier,C. and Roddier,F.,J.Opt.Soc.Am.,65,664. 1975

[6] Scaddan,R.J. and Walker,J.G.,Appl.Opt.,17,3779. 1978

[7] Dainty,J.C.,Opt.Commun.,7,129. 1973

[8] Korff,D.,J.Opt.Soc.Am.,63,971. 1973

[9] Gezari,D.Y.,Labeyrie,A. and Stachnik,R.V.,Astrophys.J.,173,L1. 1972

[10] Beddoes,D.R.,Dainty,J.C.,Morgan,B.L. and Scaddan,R.J.,J.Opt.Soc. Am.,66,1247. 1976

[11] Hecht,E. and Zajac,A.,"Optics",Addison-Wesley. 1979

[12] Dainty,J.C.,Mon.Not.R.Astr.Soc.,183,223. 1978

[13] Morgan,B.L.,Beddoes,D.R.,Scaddan,R.J. and Dainty,J.C.,Mon.Not.R. Astr.Soc.,183,701. 1978

[14] Beddoes,D.R.,Ph.D. Thesis,Imperial College,Univ. of London. 1979

[15] Airy,G.B.,Mon.Not.R.Astr.Soc.,30,57. 1870

[16] Parry,G.,Walker,J.G. and Scaddan,R.J.,Opt.Acta,26,563. 1979

[17] Woolf,N.J.,Ann.Rev.Astron.Astrophys.,20,367. 1982

[18] Korff,D.,Dryden,G. and Leavitt,R.P.,J.Opt.Soc.Am.,65,1321. 1975

[19] Welter,G.L. and Worden,S.P.,J.Opt.Soc.Am.,68,1271. 1978

[20] Worden,S.P.,Stein,M.K.,Schmidt,G.D. and Angel,J.R.P.,Icarus,32, 450. 1977

[21] Arnold,S.J.,Boksenberg,A. and Sargent,W.L.W.,Astrophys.J.,234, L159. 1979

[22] Walker,J.G.,Appl.Opt.,21,3132. 1982

[23] Liu,Y.C. and Lohmann,A.,Opt.Commun.,8,372. 1973

[24] Bates,R.H.T.,Gough,P.T. and Napier,P.J.,Astron.Astrophys.,22, 319. 1973

[25] Gough,P.T. and Bates,R.H.T.,Opt.Acta,21,243. 1974

[26] Stachnik,R.V.,Nisenson,P. and Noyes,R.W.,Astrophys.J.,271,L37. 1983

[27] Knox,K.T. and Thompson,B.J.,Astrophys.J.,193,L45. 1974

[28] Weigelt,G.P.,Appl.Opt.,17,2660. 1978
[29] Nisenson,P. and Papaliolios,C.,Opt.Commun.,45,311. 1983
[30] Sherman,J.W.,J.Opt.Soc.Am.,66,175. 1976
[31] Lynds,C.R.,Worden,S.P. and Harvey,J.W.,Astrophys.J.,207,174. 1976
[32] Welter,G.L. and Worden,S.P.,Astrophys.J.,242,673. 1980
[33] Bates,R.H.T. and Cady,F.M.,Opt.Commun.,32,365. 1980
[34] Hunt,B.R.,Fright,W.R. and Bates,R.H.T.,J.Opt.Soc.Am.,73,456. 1983
[35] Weigelt,G.P.,Opt.Commun.,21,55. 1977
[36] Weigelt,G.P. and Wirnitzer,B.,Opt.Lett.,8,389. 1983
[37] Fienup,J.R.,Opt.Lett.,3,27. 1978
[38] Walker,J.G.,Opt.Acta,28,1017. 1981
[39] Schneiderman,A.M. and Karo,D.P.,Opt.Eng.,16,72. 1977
[40] Breckinridge,J.B.,McAlister,H.A. and Robinson,W.G.,Appl.Opt.,18, 1034. 1979
[41] Simon,G.W.,Astronom.J.,71,190. 1966
[42] "Image Intensifier Systems" ,E.M.I Ltd. 1983
[43] Mullard Technical Handbook, Book2,part2A. 1981
[44] Blazit,A.,Koechlin,L. and Oneto,J.L.,"Image processing in astronomy", eds.de Jager/Nieuwenhuijen. 1975
[45] Blazit,A.,Bonneau,D.,Koechlin,L. and Labeyrie,A.,Astrophys.J.,214, L79. 1977
[46] Vokac,P.R.,"Applications of digital image processing",SPIE.vol 119 (IOCC). 1977
[47] Walker,J.G.,Opt.Acta,28,885. 1981
[48] McAlister,H.A.,Astrophys.J.,215,159. 1977
[49] McAlister,H.A.,Sky and Telescope,53,346. 1977
[50] Hege,E.K.,Hubbard,E.N.,Strittmatter,P.A. and Worden,S.P., Astrophys.J.,248,L1. 1981
[51] Morgan,B.L.,Beckmann,G.K. and Scaddan,R.J.,Mon.Not.R.Astr.Soc.,192 ,143. 1980
[52] Morgan,B.L.,Beckmann,G.K.,Scaddan,R.J. and Vine,H.A.,Mon.Not.R. Astr.Soc.,198,817. 1982
[53] Davies,C.L.,Ph.D. Thesis,Imperial College,Univ. of London. 1980
[54] Fried,D.L.,J.Opt.Soc.Am.,56,1372. 1966
[55] Roddier,F.,In "Progress in Optics" vol.19 p.281 ed. Wolf,E., North -Holland. 1981
[56] Roddier,C. and Roddier,F.,J.Opt.Soc.Am.,63,661. 1973
[57] Kelsall,D.,J.Opt.Soc.Am.,63,1472. 1973

[58] Dainty,J.C. and Scaddan,R.J.,Mon.Not.R.Astr.Soc.,170,519. 1975

[59] King,J.R.,Pub.Astr.Soc.Pac.,83,199. 1971

[60] Chelli,A.,Lena,P.,Roddier,C.,Roddier,F. and Sibille,F.,Opt.Acta,26 ,583. 1979

[61] Aime,C.,Kadiri,S.,Ricort,G.,Roddier,C. and Vernin,J.,Opt.Acta,26, 575. 1979

[62] Born,M. and Wolf,E.,"Principles of Optics", Pergamon Press, 5th Edition. 1975

[63] Bruck,Y.M. and Sodin,L.G.,Astron.Astrophys.,87,188. 1980

[64] Stone,E.C. and Lane,A.L.,Science,206,925. 1979

[65] Fante,R.L.,J.Opt.Soc.Am.,69,1394. 1979

[66] Fizeau,H.,Compt.Rend.Acad.Sci.,66,932. 1868

[67] Michelson,A.A.,Nature,45,160. 1891

[68] Hanbury Brown,R. and Twiss,R.Q.,Proc.Roy.Soc.A,248,199. 1958

[69] Hanbury Brown,R.,Davis,J. and Allen,L.R.,Mon.Not.R.Astr.Soc.,167, 121. 1974

[70] McAlister,H.A.,Astrophys.J.,212,459. 1977

[71] Meaburn,J.,Morgan,B.L.,Vine,H.,Pedlar,A. and Spencer,R.,Nature,296 ,331. 1982

[72] McCarthy,D.W.,Low,F.J.,Kleinmann,S.G. and Gillett,F.C.,Astrophys. J.,257,L7. 1982

[73] Pease,F.G.,Ergebn.Exakten Naturwiss,10,84. 1931

[74] Labeyrie,A.,Ann.Rev.Astron.Astrophys.,16,77. 1978

[75] Beckers,J.M.,Opt.Acta,29,361. 1982

[76] Blazit,A.,Bonneau,D.,Josse,M.,Koechlin,L.,Labeyrie,A. and Oneto,J. L.,Astrophys.J.,217,L55. 1977

[77] Sibille,F.,Chelli,A. and Lena,P.,Astron.Astrophys.,79,315. 1979

[78] McCarthy,D.W.,Astrophys.J.,257,L93. 1982

[79] Chelli,A.,Perrier,C. and Biraud,Y.G.,Astron.Astrophys.,117,199. 1983

[80] Michelson,A.A. and Pease,F.G.,Astrophys.J.,53,249. 1921

[81] Duncombe,R.L.,Benedict,G.F.,Hemenway,P.D.,Jefferys,W.H. and Shelus ,P.D.,"The Space Telescope Observatory", ed. Hall,D.N.B.,NASA. 1982

[82] ESA,Hipparcos Space Astrometry,Report of the Phase A study,SC1(79) 10. 1979

[83] Argue,A.N.,Baxter,R.D.,Morgan,B.L. and Vine,H.,Scientific aspects of the Hipparcos mission,ESA SP-177,p.53. 1982

[84] Hanbury Brown,R.,Ann.Rev.Astron.Astrophys.,6,13. 1968

[85] Kovalevsky,J.,Scientific aspects of the Hipparcos mission,ESA SP-177,p.15. 1982

[86] Bowell,E.,Morgan,B.L.,Lumme,K.,Dainty,J.C.,Vine,H and Poutanen,H. ,Bull.Am.Astron.Soc.,13,3. 1981

[87] Van Flandern,T.C.,Tedesco,E.F. and Binzel,R.P.,In "Asteroids" p.443 ed. Gehrels,T.,Univ. of Arizona Press. 1979

[88] Seyfert,C.K.,Astrophys.J.,97,28. 1943

[89] Bertola,F.,Astronom.J.,73,861. 1968

[90] Glaspey,J.W.,Eilek,J.A.,Fahlman,G.G. and Auman,J.R.,Astrophys.J., 203,335. 1976

[91] Pedlar,A.,Booler,R.V.,Spencer,R.E. and Stewart,O.J.,Mon.Not.R. Astr.Soc.,202,647. 1983

[92] Telesco,C.M. and Harper,D.A.,Astrophys.J.,235,392. 1980

[93] Van Breugel,W.J.M.,Schilizzi,R.T.,Hanmel,E. and Kapahi,V.K., Astron.Astrophys.,96,310. 1981

[94] Angel,J.R.P.,Stockman,H.S.,Woolf,N.J.,Beaver,E.A. and Martin,P.G. ,Astrophys.J.,206,L5. 1976

[95] Young,P.J.,Westphal,J.A.,Kristian,J.,Wilson,C.P. and Landauer,F. P.,Astrophys.J.,221,721. 1978

[96] Van der Hulst,J.M.,Hummel,E. and Dickey,J.M.,Astrophys.J.,261,L59 . 1982

[97] Neugebauer,G.,Garmire,G.,Rieke,G.H. and Low,F.J.,Astrophys.J.,166 ,L45. 1971

[98] Feitzinger,J.V.,Schlosser,W.,Schmidt-Kaler,T. and Winkler,C., Astron.Astrophys.,84,50. 1980

[99] Cassinelli,J.P.,Mathis,J.S. and Savage,B.D.,Science,212,1497. 1981

[100] Airey,R.W.,Lees,D.J.,Morgan,B.L. and Traynar,M.J.,Proc.Eighth Symposium on Photoelectronic Image Devices, SPIE. 1983

[101] Meaburn,J.,Hebden,J.C.,Morgan,B.L. and Vine,H.,Mon.Not.R.Astr. Soc.,200,1P. 1982

[102] Meaburn,J.,Walsh,J.R.,Hebden,J.C.,Morgan,B.L. and Vine,H.,Mon. Not.R.Astr.Soc.,204,41P. 1983

[103] Meaburn,J.,Walsh,J.R.,Hebden,J.C.,Morgan,B.L. and Vine,H.,Mon. Not.R.Astr.Soc.,205,53P. 1983

[104] Argue,A.N.,Hebden,J.C.,Morgan,B.L. and Vine,H.,Mon.Not.R.Astr. Soc.,206,669. 1984

[105] Meaburn,J.,Mon.Not.R.Astr.Soc.,196,19P. 1981
[106] Vreux,J.M.,Dennefeld,M. and Andrillat,Y.,Astron.Astrophys.,113, L10. 1982
[107] Panagia,N.,Tanzi,E.G. and Tarenghi,M.,Astrophys.J.,272,123. 1983
[108] Innes,R.T.A.,Ann.Cape.Obs.,9,75B. 1903
[109] Feinstein,A. and Marraco,H.G.,Astron.Astrophys.,30,271. 1974
[110] Aller,L.H. and Dunham,T.,Astrophys.J.,146,126. 1966
[111] Thackeray,A.D.,Mon.Not.R.Astr.Soc.,135,51. 1967
[112] Davidson,K.,Mon.Not.R.Astr.Soc.,154,415. 1971
[113] Walborn,N.R.,Astrophys.J.,179,517. 1973
[114] Westphal,J.A. and Neugebauer,G.,Astrophys.J.,156,L45. 1969
[115] Harvey,P.M.,Hoffmann,W.F. and Campbell,M.F.,Astron.Astrophys.,70, 165. 1978
[116] Aitken,D.K. and Jones,D.,Mon.Not.R.Astr.Soc.,172,141. 1975
[117] Hyland,A.R.,Robinson,G.,Mitchell,R.M.,Thomas,J.A. and Becklin,E. E.,Astrophys.J.,233,145. 1979
[118] Chelli,A.,Perrier,C. and Biraud,Y.G.,Astron.Astrophys.,117,199. 1983
[119] Walborn,N.R.,Blanco,B.M. and Thackeray,A.D.,Astrophys.J.,219,498. 1978
[120] Warren-Smith,R.F.,Scarrott,S.M.,Murdin,P. and Bingham,R.G.,Mon. Not.R.Astr.Soc.,187,761. 1979
[121] Bowell,E.,McMahon,J.,Horne,K.,A'Hearn,M.F.,Dunham,D.W.,Penhallow, W.,Taylor,G.E.,Wasserman,L.H. and White,N.M.,Bull.Am.Astron.Soc., 10,594. 1978
[122] Aller,L.H.,"Astrophysics. The Atmospheres of the Sun and the Stars", p.29, Ronald Press. 1963
[123] Walborn,N.R.,Gull,T.R. and Davidson,K.,Sky and Telescope,63,16. 1982
[124] Hege et al.,Bull.Am.Astron.Soc.,12,662. 1980
[125] Cohen,M.,Anderson,C.M.,Cowley,A.,Coyne,G.V.,Fawley,W.M.,Gull,T.R. ,Harlan,E.A.,Herbig,G.H.,Holden,F.,Hudson,H.S.,Jakoubek,R.O., Johnson,H.M.,Merrill,K.M.,Schiffer,F.H.,Soifer,B.T. and Zuckerman ,B.,Astrophys.J.,196,179. 1975
[126] Perkins,H.G.,Scarrott,S.M.,Murdin,P. and Bingham,R.G.,Mon.Not.R. Astr.Soc.,196,635. 1981
[127] Schmidt,G.D.,Cohen,M. and Margon,B.,Astrophys.J.,239,L133. 1980
[128] Greenstein,J.L. and Oke,J.B.,Pub.Astr.Soc.Pac.,89,131. 1977

[129] Russell,R.W.,Gull,G.,Beckwith,S. and Evans,N.J.,Pub.Astr.Soc. Pac.,94,97. 1982

[130] Warren-Smith,R.F.,Scarrott,S.M. and Murdin,P.,Nature,292,317. 1981

[131] Morris,M.,Astrophys.J.,249,572. 1981

[132] Mendez,R.H. and Niemela,V.S.,Astrophys.J.,250,240. 1981

[133] Mendez,R.H.,Gathier,R. and Niemela,V.S.,Astron.Astrophys.,116,L5. 1982

[134] Kohoutek,L.,Mon.Not.R.Astr.Soc.,204,93P. 1983

[135] Kohoutek,L.,IAU Inf.Bull.Var.Stars,2113. 1982

[136] Koppen,J.,Astron.Astrophys.,56,189. 1977

[137] Aitken,D.K. and Roche,P.F.,Mon.Not.R.Astr.Soc.,200,217. 1982

[138] Feibelman,W.A. and Aller,L.H.,Astrophys.J.,270,150. 1983

[139] Savage,B.D.,Fitzpatrick,E.L.,Cassinelli,J.P. and Ebbets,D.C., Astrophys.J.,273,597. 1983

[140] Stachnik,R. and Labeyrie,A.,Sky and Telescope,67,205. 1984

[141] Schweizer,F.,Astrophys.J.,233,23. 1979

[142] Schweizer,F.,Astronom.J.,85,801. 1981

[143] King,I.R.,Astrophys.J.,222,1. 1978

[144] Ovenden,M.W.,Nature,239,508. 1972

[145] Safronov,V.S.,In "Asteroids" p.975 ed. Gehrels,T.,Univ. of Arizona Press. 1979

[146] Allen,C.W.,"Astrophysical Quantities",Athlone Press, 3rd Edition. 1973